Towards Continuous Crystallization-based Separation, Chiral Resolution and Deracemization of Chiral Compounds

Johannes Hoffmann

Supervisor: Prof. Joop H. ter Horst

International CORE Training Network for Continuous Resolution and Deracemization of Chiral Compounds by Crystallization

Thesis submitted in satisfaction with the requirements of the Strathclyde Institute of Pharmacy and Biomedical Sciences at the University of Strathclyde for the Degree of Doctor of Philosophy.

March 2020

Declaration

I declare that this thesis is entirely my own work and has not been submitted previously to this or any other university. Where the work of others is utilized this is acknowledged and cited in the proper manner.

Laakdal, 16.03.2020

Johannes Hoffmann — Place, Date

List of Publications

The experimental chapters of this thesis are based on three publications:

1. **Total Spontaneous Resolution using Continuous Antisolvent Crystallization**
   Authors: Johannes Hoffmann, Charline J.J. Gerard, Joop H. ter Horst

2. **Chiral Separation at the Eutectic Point: A Case Study of Mandelic Acid**
   Authors: Johannes Hoffmann, Raghunath Venkatramanan, Charline J. J. Gerard, Heike Lorenz, Andreas Seidel-Morgenstern, Joop H. ter Horst

3. **Separation, Resolution and Deracemization in Chiral Eutectic Solutions**
   Authors: Johannes Hoffmann, Raghunath Venkatramanan, Charline J. J. Gerard, Heike Lorenz, Andreas Seidel-Morgenstern, Joop H. ter Horst

Abstract

A large number of modern active pharmaceutical ingredients (API) are chiral molecules. In most cases only one enantiomer has the desired effect in the human body, while the other enantiomer can have no effect or be harmful. Therefore the pharmaceutical industry aims for the direct production of the only the target enantiomer through asymmetric catalyzed chiral synthesis. However the asymmetric syntheses route is not always available and the racemate is produced instead, therefore chiral separation techniques are needed. Crystallization based chiral separation techniques have shown to be a selective and efficient tool for the separation, resolution and deracemization of chiral racemates. As there is a drive in the pharmaceutical industry towards continuous processes, the aim of this thesis is to demonstrate a number of new resolution and deracemization process configurations easily adaptable to continuous operation.

In chapter 3, a batch and continuous antisolvent deracemization process is introduced, to investigate if and to which extend control over secondary nucleation can be preserved during an antisolvent crystallization. As antisolvent crystallization causes a fast drop in solubility and causes high local supersaturations, often thought to trigger chrially unselective primary nucleation, it is usually not selected for chiral separation. In this chapter the objective is to extend the scope of existing deracemization processes with antisolvent crystallization.

Preferential crystallization has been used to successfully separate chiral conglomerate forming systems. However conglomerate systems are rather rare with racemic compound forming systems being the majority. While direct separation through preferential crystallization is not possible at racemic composition for compound forming systems, at the eutectic the pure enantiomer and racemic compound can be separated. This can be used in a hybrid process, where a primary method is used to enrich a racemic solution to eutectic composition, followed by a preferential crystallization. The objective of chapter 4 is to investigate and compare a semi-batch parallel and serial process configuration for the separation of racemic compound and pure enantiomer at eutectic solution composition, with regards to feasibility and process operating conditions.

While crystallization based chiral separation processes provide a selective and efficient method for separation, there are a large number of process configurations for different compound types. The objective of chapter 5 is to develop and validate a general process design configuration which allows for the crystallization based separation, resoltution and deracemization for racemic compound, as well as conglomerate forming systems with and without racemization.

The findings in this thesis, together with work found in literature are used in chapter 6 to construct industrially relevant guidelines and criteria, based on process specifications such as productivity, yield and enantiomeric excess, to choose continuous crystallization-based chiral separation processes.

Table of Content

1 Introduction

1.1 Chirality

The term chirality is derived from the ancient Greek word for hands and refers to an object which is not superimposable over its mirror image by translation or rotation [1]. An example is a right hand and its non-superimposable mirror image, the left hand. This is also why chirality often is referred to as handedness. As objects can be chiral so can molecules, often caused by an asymmetric carbon atom which serves as the chiral centre of a molecule. Chirality is a phenomenon which is commonly observed in nature, for example in amino acids which are always found in the left-handedness.

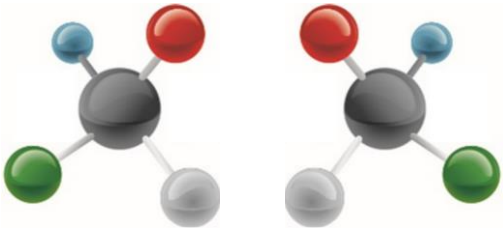

Figure 1: Schematic representation of a chiral molecule with an asymmetric carbon atom at its centre, surrounded by four substituents.

Single-handed molecules of chiral compounds are called enantiomers. They can be separated into D (+) and L (-) handedness by the direction at which they rotate under polarised light, where D refers to dextro- (clockwise rotation) and L to levororotatory (counter-clockwise rotation). If both enantiomers are present at equimolar ratio they are called racemates, which show no rotation in either direction [2].

Both enantiomers show the same physical properties like solubilities, melting points, density and growth kinetic [3]. Furthermore, their chemical structure and morphology are the same [2, 4, 5]. However, the way the enantiomers interact with the human body, for instance in the case of drug substance, is vastly different. While one handedness has the desired interaction with the body, the other handedness can be harmful or have no effect at all. There are several examples of chiral drugs [6], where only one enantiomer has the desired effect and the counter enantiomer is inactive or harmful.

1.2 Chirality in life

The reason why different enantiomers of chiral drugs interact differently with the body could be due to the phenomenon that chirality can also be found in nature and life. Most amino acids found in nature are levorotatory, while sugars occurring in RNA and DNA are dextrorotatory [7]. Studies have also shown that using the other handedness not found naturally for sugars involved in the RNA and DNA multiplication or amino acids disrupted naturally occurring processes in cells and bodies [7]. Therefore chirality plays an important part in naturally occurring processes, giving indications for the interaction of the human body with chiral molecules.

1.3 Importance of Chiral Separation in Industry

The separation of chiral molecules in the industry is of importance, where the different effects of the enantiomers with the human body can have an impact on the product properties and effects. One sector where the separation of chiral compounds is especially important is the pharmaceutical industry where a lot of drug substances are chiral and regulatory requirements of the products are especially as shown by the US Food and Drug Administration (FDA) regulations [8, 9]. For a chiral drug to be marketed, the toxicity or inactivity of the counter enantiomer has to be investigated. If the counter enantiomer shows to have side effects, chiral separation or asymmetric syntheses resulting in the chirally pure product are required. However, as the latter is not always available, processes for chiral separation needs to be investigated and improved as the demands on the product and production capabilities change. The pharmaceutical industry is known to manufacture most of the drugs in a batch configuration as the product masses are rather low (kg-t) in comparison with large scale industrial products, where hundreds of kilotons are produced in a single plant each year. But there is a drive in the pharmaceutical industry toward continuous manufacturing as it has usually lower upkeep costs than batch processes and allows for more consistent product quality.

Not just the pharmaceutical industry deals with chiral products, also for the food and agrochemical industry this is an important topic. In the food industry, some flavours are chiral molecules where the taste we perceive can change with the enantiomer. One example of this is the carvone molecule, where the L-carvone is known as spearmint and is used in essential oils and refreshing products while the D-carvone results in a cumin aroma [10]. While the side effects may not be as severe as in the drug substances, for the product properties such as taste, the use of the correct enantiomer is important. In the agrochemical industry, many pesticides are also chiral molecules. Studies have shown that in the case of pesticides also only one enantiomer has the desired effect on the plant, while the counter enantiomer has often none. If the active ingredient in a pesticide, however, can be reduced to the active enantiomer, the exposure of chemicals on fields could be reduced by half, which can contribute to the environmental impact of the agricultural industry.

These examples show that there is an interest of industry in chiral separation. Therefore chirality is an important topic not just for pharmaceutical but also agricultural and food industry. As most chiral compounds are crystalline [11-13], crystallization based separation processes are a key technology in the production of chirally pure products.

There are several chiral resolution techniques available such as crystallization, chiral chromatography [14], as well as deracemization, which combines a racemization reaction of a chiral compound in solution with preferential crystallization (Classical Resolution) and a number of other techniques [13]. In general chiral resolution refers to the separation of the enantiomers of a chiral compound, which does not include asymmetric synthesis which refers to an enantioselective catalysed process [15, 16] resulting in the synthesis of only one handedness. Chiral resolution techniques can be applied to racemic compound forming systems as well as conglomerates.

1.4 Racemic compound, Conglomerate

There are two major types of equilibria between enantiomers, the less common conglomerate and frequently occurring racemic compound forming systems [13]. In the case of conglomerates, the enantiomers of both handedness form enantiomerically pure crystals which are physically mixed at an equal ratio in the racemic composition [1, 4] as shown in the right-hand graph in Figure 2. Racemic conglomerate mixtures can be separated directly through preferential crystallization as both enantiomers form only pure crystals and have the same physical properties [4, 13]. On the other hand, the enantiomers of the racemic compound forming systems form crystals with enantiomers from both handedness being incorporated into the crystal lattice at the racemic composition, forming a racemic compound as shown in Figure 2 (left). The racemic compound and its pure enantiomers crystals have different physical properties such as melting point and solubilities. Due to this, the enantiomers of the racemic compound cannot be separated directly through crystallization based separation techniques at the racemic composition. However, they can be separated at the eutectic composition, which follows from the phase diagram discussed in section 1.5.

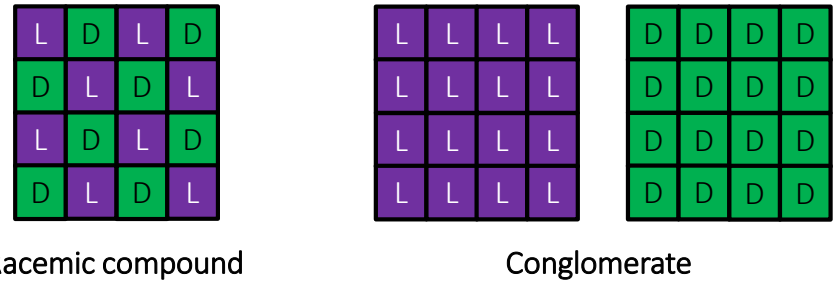

Figure 2: Schematic of a racemic compound- (left) and conglomerate (right) forming crystal lattice at the racemic composition with the enantiomer molecules D and L.

In order to perform a crystallization experiment on a crystalline compound, a number of preliminary investigations like solvent and polymorphism screening will have to be conducted. Where polymorphs have the same chemical composition, but different spatial arrangements of the constituents [17], resulting in them having varying solubilities and melting points. Once a solvent and the stable polymorph have been determined, solubility experiments need to be performed. Two types of solubility experiments can be differentiated: isothermal and clear-point methods, which will be discussed in detail in chapter 2. The temperature dependent solubility of a compound in a solvent system can thus be determined and plotted in a binary phase diagram.

1.5 Binary and ternary phase diagrams of chiral compounds

1.5.1 Binary phase diagrams of chiral compounds

One way of representing chiral compounds is through a binary melting point phase diagram, where mass based mixtures of solid D and L molecules are plotted against their melting temperatures. In general binary melting point phase diagrams represent the solid-liquid equilibria of a two component system as a function of temperature at a constant pressure.

Figure 3 shows a melting point diagram of a conglomerate forming system (Figure 3, left), with the melting points of the pure enantiomers T_E on each end of the diagram. From the melting point of the pure enantiomers, the melting temperature reduces with increasing mass fraction of the counter enantiomer, represented by the liquidus line until the eutectic point *eu* is reached. At the eutectic point, both enantiomers are mixed at an equimolar composition with the lowest melting temperature T_{Rac}. In conglomerate systems, the point where both enantiomers are present at an equal amount is referred to as racemic mixture. Below the liquidus line, both enantiomers start to melt so a two phasic domain is reached at which the pure enantiomer and the liquid are present. Once the melting temperature of the racemic mixture is reached only one solid phase remains, with a composition of D and L following the starting composition in the melt respectively, indicated my a mixing point M (Figure 3, left). The line representing the temperature after which only solid remains are referred to as solidus line [2].

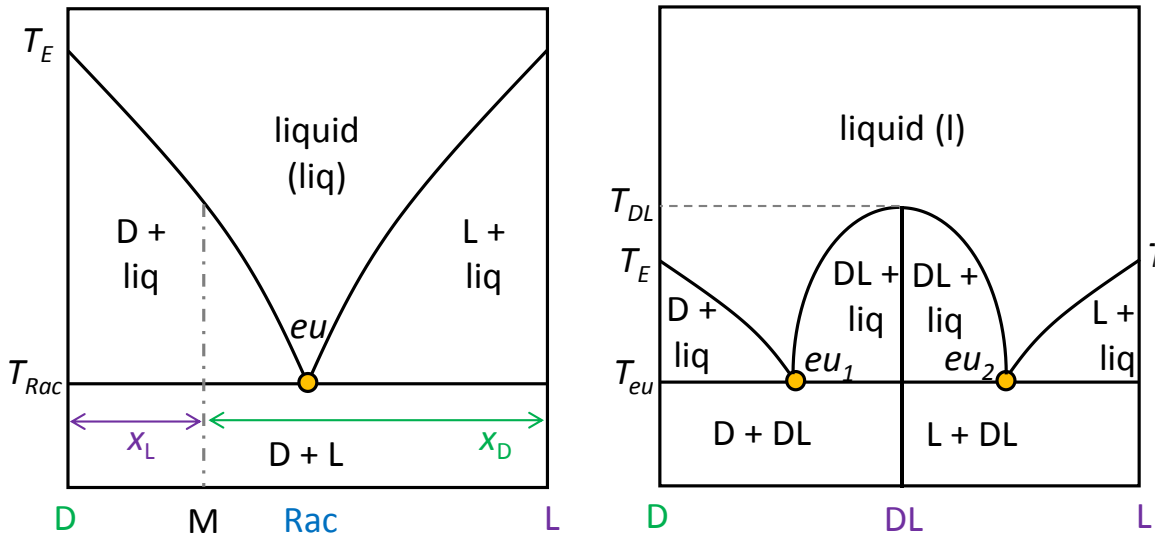

Figure 3: Melting point phase diagrams (temperature over mass fraction) of a conglomerate forming system (left) and racemic compound forming system (right) with pure enantiomers D, L, Racemic mixture Rac, Racemic compound DL, eutectics eu and their respective melting points indicated.

On the right hand side in Figure 3 the melting point phase diagram of a racemic compound forming system [4] is represented. The melting points of the pure enantiomers are represented at each side of the phase diagram, with the melting temperature reducing with increasing counter enantiomer fraction until the eutectic pint is reached. Racemic compound forming systems form a racemic compound, here represented by DL (Figure 3, right), if both enantiomers are mixed at the racemic composition between the solidus and liquidus line. The racemic compound behaves like a pure compound in the melting point phase diagram and has a different melting point than the pure enantiomers, which can be higher or lower. The racemic compound and pure enantiomer are in equilibrium with the melt at the eutectic composition, at the eutectic temperature in the eutectic point. The eutectic melting point is the lowest melting temperature of the system and marks the solidus line. The solid composition between pure enantiomer and racemic compound which corresponds to the composition of the eutectic point is system specific.

In resolution processes, the enantiomers to be separated are usually dissolved in a solvent. Another way of representing chiral compounds in a binary phase diagram is the solubility of the enantiomers and racemic mixture for conglomerates or racemic compound for racemic compound forming systems in a solvent against a dependent variable such as temperature. Figure 4 shows a binary phase diagram of a chiral conglomerate forming (left) and racemic compound forming (right) system in a solvent against temperature. In general, binary phase diagrams used for solubility only show a certain magnification of the full binary phase diagram which also includes the liquid and solid phase borders of the solvent. However, as the solvent usually solidifies at temperature ranges which are not aligned with the compound to be produced only the solid phase border of the solid compound can be seen.

In the case of a conglomerate forming chiral compound (Figure 4, left) the solubility *C* of the racemic mixture is double of the solubility of the pure enantiomer at the same temperature.

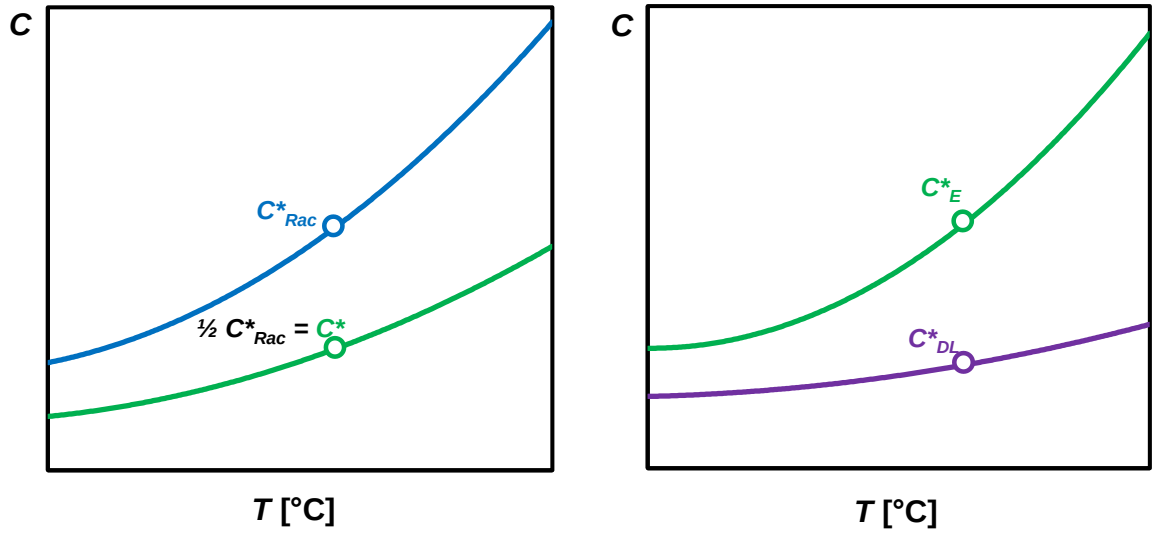

Figure 4: Solid-Solvent phase diagram of: a conglomerate (left) with the temperature dependent solubility of the racemic mixture (blue), as well as pure enantiomer (green) and a racemic compound forming system (right) with the temperature dependent solubility of the pure enantiomer (green) and racemic compound (purple)

As shown in Figure 3 (left), at the racemic mixture both enantiomers are present at an equimolar ratio. Therefore the solubility of the racemic mixture at a certain temperature is saturated with respect to both enantiomers. For racemic compound forming systems (Figure 4, right) the solubility of the racemic compound and pure enantiomer cannot be related in this way. The racemic compound and pure enantiomer have different melting points as shown in Figure 3 (right), which also results in different solubilities in a solvent. As the melting points of the racemic compound can be higher or lower than the pure enantiomers so can the solubility. This is due to the crystal structure of racemic compounds which differs from their pure enantiomers resulting in different physical properties. The representation of solubilities in a solvent of enantiomers, racemic mixtures and racemic compounds is often used for crystallization processes, as the starting and end concentration of a process depending on the dependent variable can be directly extracted based on the range in which the process is to be run. However, it does not clarify the interaction between the solvent and the solid phases and what solid form is in equilibrium with the solution at a certain composition. To that end, ternary phase diagrams of a chiral compound in a pure solvent can be used.

1.5.2 Ternary Conglomerate and Racemic Compound Phase Diagrams

Ternary phase diagrams are a good way to represent the behaviour of chiral compounds in a pure solvent, as all solid and liquid phases can be observed. In comparison to binary phase diagrams which only show an overall solubility, ternary phase diagram can distinguish between pure enantiomer and racemic compound solubilities, as well as the solubility of mixed compositions. Conglomerate and racemic compound forming compounds form different phase diagrams as shown in Figure 5.

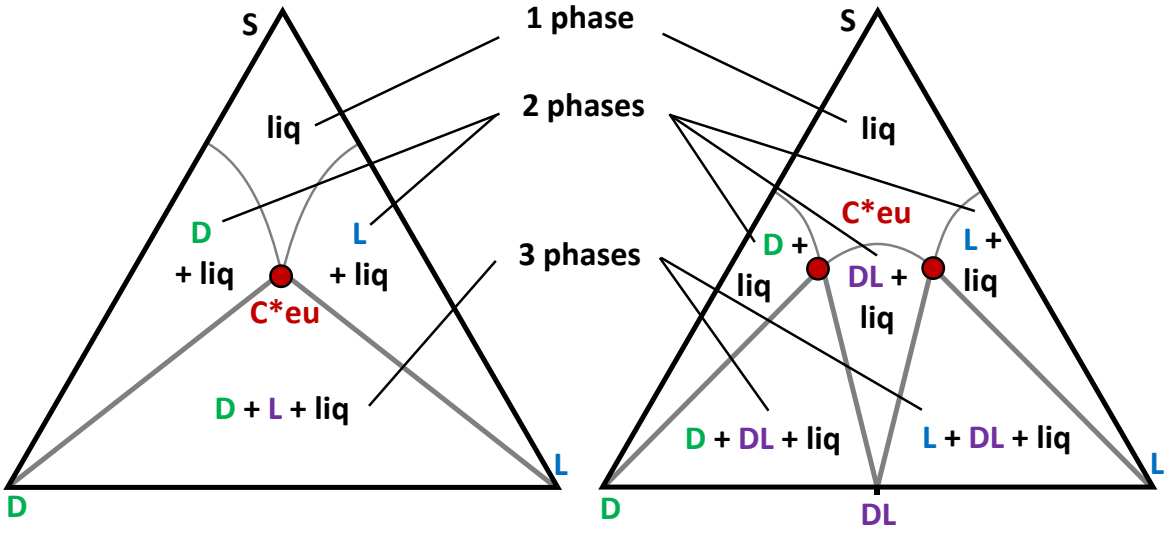

Figure 5: Schematic of ternary phase diagrams of a conglomerate (left) and racemic compound (right) forming chiral molecule, with the number and composition of phases indicated.

Ternary phase diagrams (TPD) are isothermal cuts of a temperature dependent prism, representing the equilibrium compositions at that temperature [4]. Each corner of a phase ternary phase diagram represent the pure compound indicated, in this case, the solvent S, the D and L enantiomers. Along the outer lines of the triangle, a binary mix of the two components of the end of each line is represented. Within the triangle, the coexisting phases and their phase borders are represented at the respective compositions. The TPD shown in Figure 5 indicates the solid phases in equilibrium with the solution. In the one phasic domain (Figure 5), only a clear solution is present. If the solution is saturated, the solid-liquid phase border is reached, indicated by a thin grey line. In the two phasic domain (Figure 5), solid pure enantiomers D/L or the racemic compound DL are coexisting with the saturated solution. While in the two phasic domain, only the indicated compound can be crystallized if a process were to be conducted with a solution composition in this domain. The three phasic domain is the last shown in the TPD in Figure 5. In this domain, two solid crystalline phases are coexisting with the saturated solution, which also means that within this domain two enantiomer compounds can be separated [1, 4]. In the case of a conglomerate forming system, the D- and L-enantiomer are in equilibrium with the solution, which allows them to be separated. For the racemic compound forming system, one pure enantiomer and the racemic compound are in equilibrium with the solution in the triphasic domain allowing for the stable enantiomer to be crystallized. To reach the three phasic domain from the liquid, the saturated solution has to reach the eutectic composition indicated by C^*_{eu} (red circles in Figure 5). At the eutectic point,

the solution is fully saturated with respect to both solid phases in equilibrium. For conglomerates, the eutectic composition is equal to the racemic composition with both enantiomers present in an equal ration in equilibrium with the solution. Racemic compound forming systems form two eutectic compositions, where the solution of a mixed suspension, containing the racemic compound and one enantiomer, is saturated in equilibrium with respect to both solid phases, at a certain temperature. This liquid composition is specific for the racemic compound forming system and its solvent at a certain temperature. To apply preferential crystallization to racemic compound forming systems, a saturated solution at eutectic composition has to be used as starting solution as both the racemic compound and the pure enantiomer are in equilibrium with the solution at this point.

With the knowledge of ternary and binary phase diagrams, suitable crystallization processes for the individual physical properties and crystallization behaviour of the solute can be applied.

1.6 Crystallization

There are several processes to achieve chirally pure product such as fermentation, where the natural metabolism of microorganisms is used to produce enantiopure amino acids for the food industry [13]. Another way of producing target enantiomers is asymmetric catalyzed synthesis, where enantiomerically pure catalysts such as metal-ligand complexes from chiral ligands or biocatalysts are used to selectively synthesis chirally enriched or pure compounds [13, 18, 19]. However selective production of the target enantiomer is often not available so that techniques for chiral separation are needed. One effective method is chiral chromatography [14] which has been well investigated [13]. The enantiomers of chiral molecules are separated, as one enantiomer interacts with the chiral stationary phase in the chromatography column, while the other does not interact or interacts less and is, therefore, leaving the column at a different time than the other enantiomer. While this method is highly efficient and widely applicable, the chiral molecules needed for the stationary phase can be expensive and depending on the enrichment large quantities of solvent are needed making chiral chromatography an expensive method only applied for high-value chiral molecules for example in the pharmaceutical industry. The most frequently applied chiral separation techniques are crystallization based processes as they are highly selective, widely applicable and cost-efficient. The applicability of crystallization for chiral molecules follows from the phase diagrams, as they form domains in a solution where one or two solid phases are in equilibrium with the solution allowing for the separation of the enantiomers. Besides chiral molecules often show solubility in a solvent which depends on a latent variable such as temperature which allows for induction of supersaturation, which can be used for the separation of one enantiomer. There are several crystallization based techniques available for the separation of chiral compounds depending on the compound type, which will be discussed in detail in section 1.9.

1.7 Driving force of Crystallization and Supersaturation

The state of equilibrium for a system can be described as the state with the lowest free Gibbs energy. In the case of crystallization, the fundamental driving force can then be described as

the difference of the chemical potentials of a solution μ and its corresponding solution in a saturated state μ^*. Therefore if a saturated solution is in thermodynamic equilibrium the difference in chemical potential is zero.

$$\Delta\mu = \mu - \mu^* \quad (1)$$

If the difference in chemical potential is positive, the solution is supersaturated, allowing for crystallization to occur. In the case of negative chemical potential, the solution is undersaturated, allowing for dissolution from the solid to the liquid phase. The chemical potential can be defined with the standard potential μ_0, activity a of the solution and a^* of its saturated solution, using the universal gas constant R and absolute temperature T:

$$\mu = \mu_0 + RT * \ln(a) \quad (2)$$

$$\mu^* = \mu_0 + RT * \ln(a^*) \quad (3)$$

Both equations can be combined to express the dimensionless fundamental driving force of crystallization:

$$\frac{\Delta\mu}{RT} = \ln\left(\frac{a}{a^*}\right) = \ln(S) \quad (4)$$

Where S is the supersaturation of a solution.

$$S = \exp\left(\frac{\Delta\mu}{RT}\right) \quad (5)$$

As the activities are unpractical and often unknown, the difference of concentration ΔC between an actual solution concentration C and its saturated equilibrium concentration C* (i.e. solubility of compound A in a solvent) are used to describe the driving force.

$$\Delta C = C - C^* \quad (6)$$

Following this, the supersaturation S can also be expressed as a difference between the solution and its equilibrium concentration.

$$S = \frac{C}{C^*} \quad (7)$$

The equilibrium concentration in this work can be described as the solubility of a solid at a constant temperature and solvent composition.

1.8 Nucleation Mechanisms

Crystal nucleation can be divided into primary and secondary nucleation. Primary nucleation is a spontaneous and stochastic event, where new crystals are generated by transporting solid building blocks from the liquid to the solid phase [20-22]. There are two major nucleation theories as to how the mechanism exactly works: classical nucleation theory and two steps nucleation theory [23, 24] which will not be discussed here. As primary nucleation is not chirally selective but stochastic and can generate crystals of either handedness (usually both) it is not a suited mechanism for crystallization based chiral separation processes and must, therefore, be prevented.

Secondary nucleation, on the other hand, occurs only in the presence of parent or seed crystals in the suspension. If a supersaturated solution is seeded, the excess in concentration with regards to the equilibrium concentration for this solution will crystallize on the seed crystals. There are several major mechanisms which can produce secondary nuclei commonly described in literature [2, 22, 25]: seeding, contact nucleation, fluid shear and attrition.

While seeding [2] is technically not nucleation mechanism but rather an addition of seeds of the target crystalline product, providing the necessary surface area for the crystal growth to occur, it is standardised practise in crystallization processes to initiate the crystallization in a supersaturated solution. In the case of processes described in this thesis, the initial seeding provides the crystals which serve as bases for all following secondary nucleation mechanisms. Fluid shear and contact nucleation occur from the removal of material, loosely absorbed at the surface of the crystal by mechanical forces [23, 26]. Studies on contact nucleation have been conducted by Agrawal and Person [23], where they found no evidence of mechanical attrition on parent seed crystals yet secondary nucleation was observed. Higher supersaturations enable the production of more secondary nuclei [22, 23] as the adsorption layer thickness increases with supersaturation, providing more material which can be scraped off the surface for contact nucleation. For the fluid shear to occur, higher stirring rates are required, enabling the removal of the adsorbed layers. Such conditions with high supersaturations and high fluid shear can be found in Chapter 3 during antisolvent deracemization.

The more important secondary nucleation mechanism reported by ter Horst, Schmidt and Ulrich [22] is attrition. Attrition occurs in the presence of larger crystals in the suspension and can be described as the removal of small crystal fragments from the parent crystal which then serve as seed crystals themselves. The cause of attrition can be collisions between the crystals, crystals and stirrer or crystallizer wall. A number of factors like suspension density or stirring speed [27] play an important role in attrition. As the same crystals are grown as those present in the suspension during secondary nucleation, it is chirally selective. Therefore, this mechanism is the desired nucleation mechanism for the processes described in this work.

1.9 Crystallization based Techniques for Resolution

For the separation of chiral compounds in industry, the most common approach is asymmetric synthesis allowing for the production of the target compound only, however, this often requires the use of toxic catalysts [28] and is not always available and the racemate is produced instead. Crystallization based separation is used to produce the pure target compound, while the impurities remain in solution. While there is a broad range of industrially applied crystallization processes, not all are suitable for chiral resolution. For example, evaporative crystallization, where the solvent is removed to concentrate the solution, causing crystallization to occur, is often applied in the production of salt and sugar [22] which do not have a strong temperature dependence of solubility. However, solvent evaporation is challenging to control to not crystallize the counter enantiomer, as mixing effects and heat capacities have to be considered. Another example is precipitation or reactive crystallization, where two components in solution remixed and undergo a reaction, resulting in a sparingly soluble solid, which subsequently crystallizes. Also, this technique is not very well suited for

chiral separation as the process is chirally unselective. However, there are a large number of crystallization processes available, allowing a selective separation of enantiomers. As the variety of physical properties such as solubility and crystallization behaviour due to for example crystals shape of chiral compounds vastly differ, there are several techniques available for chiral separation. Examples such difference in physical properties can be found in several publications investigating different compounds [13, 19, 29-41] The by far most common technique for chiral separation is classical resolution, where a racemate is combined with an enantiopure coformer, creating two diastereomeric salts with different solubilities which can be separated by crystallization (1.9.1). Some rather recent crystallization techniques are Viedma ripening [34, 35, 38, 42-46] and temperature cycling [35, 47-49] which can be categorized as deracemization processes offer new approaches towards chiral resolution, which are discussed in section 1.9.3. A more commonly applied technique, especially in the pharmaceutical industry, is antisolvent crystallization [50-53]. While applied commonly in the pharmaceutical industry, its main use is crystallizing as much compound from the solution as possible due to the large decrease in solubility with antisolvent addition, rather than chiral resolution. A detailed introduction to antisolvent crystallization and its opportunities for new applications are discussed in section 1.9.5. The most commonly applied technique for the separation of conglomerate forming systems is preferential crystallization (1.9.2), which has been studied intensively [13, 33, 37, 54-67], where cooling crystallization is among the most frequent one found also in industrial application.

1.9.1 Classical Resolution

Classical resolution is the most frequently applied technique for the separation of chiral compounds on an industrial scale especially in the pharmaceutical industry [13] and is especially suited for the direct separation of racemic compound forming systems. As shown in the ternary phase diagram of a racemic compound forming system (1.5.2) at the racemic composition only the racemic compound can be crystallized. In classical resolution, a racemate is coupled with an enantiopure coformer resulting in the formation of two diastereomeric salts with different solubilities, which can then be subsequently separated through crystallization

1.9.2 Preferential cooling Crystallization

As a large number of crystallizable compounds show a temperature dependent solubility, this technique has been used in many process configuration for its scalability and flexibility. For preferential cooling crystallization, batch stirred tank or plug flow crystallizers [67, 68], semi-batch configurations [61, 64, 67], as well as hybrid processes [57, 63, 69] can be found. A preferential crystallization is a kinetically driven process, where through the addition of seeds of the target enantiomer, the crystallization rate of one enantiomer with regards to the other is increased [13].

The general procedure of a preferential cooling crystallization for a chiral conglomerate can be seen in Figure 6, with its corresponding ternary phase diagram in Figure 7. In the first step, a racemic starting solution at the temperature T_1 is supersaturated by cooling to a crystallization temperature T_2, creating the starting point 0, indicated in Figure 7. Seeds of the desired enantiomer are then added to the supersaturated racemic solution, initiating the

crystallization process of in this case the L enantiomer (blue squares, Figure 6). While the target enantiomer is crystallized, it is removed from the solution, shifting the solution composition towards an excess of the undesired handedness as shown by the blue line in Figure 7 going from point 0 towards point 1 (grey). Once the enrichment of the undesired handedness is reached it will start to primary nucleate, as indicated by the green cycle in Figure 7 and the crystallizer on the right hand side in Figure 6. The counter enantiomer will crystallize until an equimolar ratio of both enantiomers at the crystallization temperature is reached as shown in point 2 (Figure 7).

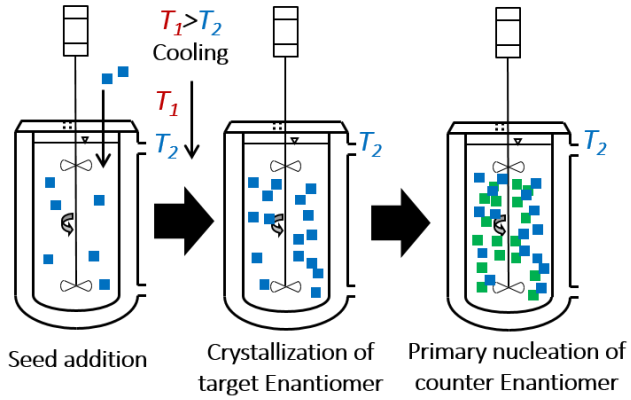

Figure 6: Schematic of preferential cooling crystallization in batch configuration with target enantiomer (blue) and counter enantiomer (green), starting temperature T_1 and crystallization temperature T_2.

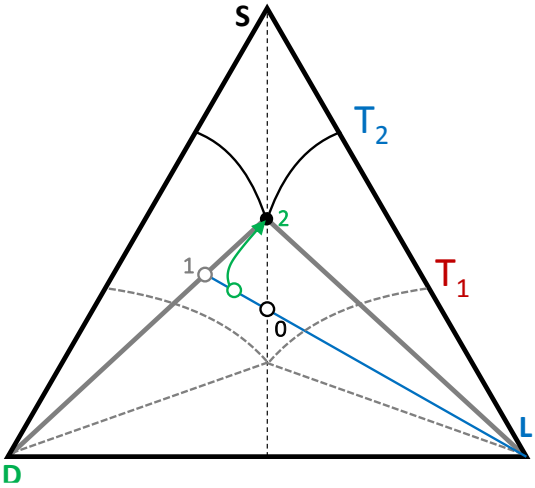

Figure 7: Schematic of a ternary phase diagram showing a preferential cooling crystallization with starting concentration 0, theoretical end concentration with respect to the L enantiomer and racemic equilibrium concentration at crystallization temperature T_2.

In order to prevent the primary nucleation of the counter enantiomer, the solution composition must remain at racemic composition. In many preferential cooling process configurations, both enantiomers are crystallized simultaneously, while the clear solutions are mixed, preventing the enrichment of one handedness in the solution respectively [19].

By ensuring that the solution composition in the crystallizers remains close to or at the racemic composition, semi-batch and continuous preferential cooling crystallization processes can be designed.

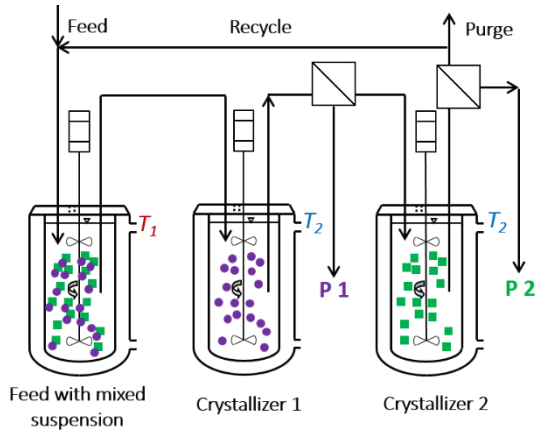

Figure 8: Schematic of a serial preferential cooling crystallization in continuous configuration with target enantiomer P2 (green) and counter enantiomer P1 (purple), starting temperature T_1 and crystallization temperature T_2.

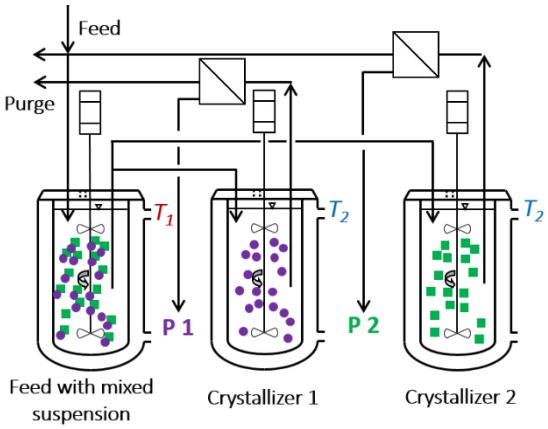

Figure 9: Schematic of a parallel preferential cooling crystallization in continuous configuration with target enantiomer P2 (green) and counter enantiomer P1 (purple), starting temperature T_1 and crystallization temperature T_2.

Figure 8 shows a continuous serial process for preferential cooling crystallization. In such a process a racemic feed at a high temperature T_1 is transferred to one crystallizer, saturated at a lower temperature T_2, with seeds of the undesired enantiomer which is crystallized first, enriching the counter enantiomer in solution. The enriched solution is then transferred to crystallizer 2 (Figure 8), where the target product P2 is crystallized. By crystallizing the products sequentially, the risk of unselectively crystallizing the undesired handedness in the product vessel is reduced. The desaturated solution from crystallizer 2 is recycled to the feed vessel, where it is re-enriched by dissolving the racemic solid excess. Such a process can be run in a number of modifications [37], the one shown in Figure 8 is one representation of a process used in this work.

Another more commonly used approach for the separation of conglomerates using preferential crystallization is a parallel crystallization processes as shown in Figure 9. From a feed with a racemic composition, saturated solution at a high temperature is transferred simultaneously to two crystallizers, at lower temperature, each containing seeds of respectively one enantiomer to be crystallized. At the same time suspension is continuously removed from the crystallizers and filtered for product removal, where a fraction equal to the feed flow is recycled to the feed vessel, while the rest of the solution is recycled back into the crystallizer. By remixing the solution of both crystallizers in the feed the solution is re-enriched ensuring a racemic composition in the feed throughout. In addition, the solution between the crystallizers can be exchanged, to crystallize the build-up enrichment of the respective counter enantiomer in each vessel, in order to prolong the process and prevent primary nucleation as demonstrated by Lorenz [19]. Also for the parallel processes, there are a number of process designs using different configurations of this process as mentioned at the beginning of this section.

As chiral compounds each have different physical properties, solubilities and crystallization kinetics, there are several process designs for the separation of these compounds. In this work, we investigate a serial process to be used as a generalized process configuration to

separate different chiral conglomerate forming compounds by only altering the process parameters.

1.9.3 Crystallization-based deracemization

One way of preventing the build-up of one enantiomer in the solution while the other is crystallized is inducing a racemization reaction. A racemization reaction in a chiral molecule allows for the reversible conversion of one enantiomer into the other [13, 70]. Figure 10 illustrates racemization for the case of a preferential crystallization. If in this case, the D enantiomer is preferentially crystallized, the counter enantiomer enriches in solution, which will lead to its primary nucleation after sufficient enrichment is reached. Through the racemization, the enantiomer in excess in the solution is converted to the other handedness until an equimolar ration is reached. In theory, this allows for all the crystallisable racemic material to be produced as target enantiomer. The conditions at which a racemization reaction can be conducted vary for each compound. In some cases, they auto racemize in a certain solvent or require a racemization catalyst, usually a strong base. In addition, some compounds only racemize at high temperatures.

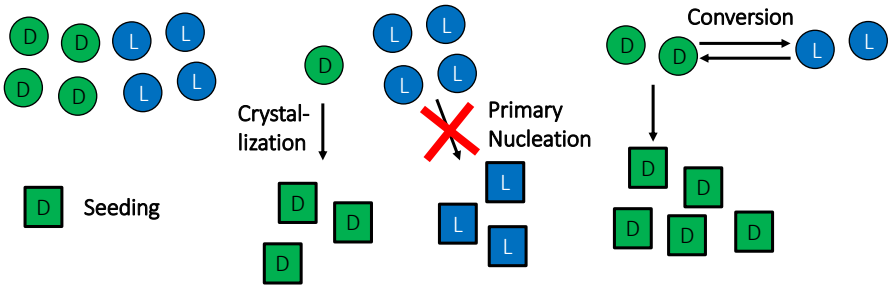

Figure 10: Schematic of a racemization reaction in solution while one enantiomer is preferentially crystallized, with rectangles being solid crystals of enantiomers and circles representing the enantiomers in solution.

If racemization reaction is performed in combination with a preferential crystallization, it can be defined as deracemization process [48, 71]. Processes like Viedma ripening and temperature cycling require a racemization reaction in solution. Some processes having a very fast racemization reaction while the preferential crystallization is performed are referred to as SOAT [72] (Second Order Asymmetric Synthesis). Viedma ripening and temperature cycling are recently discovered processes for chiral separation, where a slightly enriched suspension is brought to enantiopurity by grinding or oscillating the temperature. This kind of processes involve dissolving the undesired enantiomer, racemization in solution and then recrystallization of the target enantiomer. In addition to that, both Viedma ripening and temperature cycling are dynamic processes with changing solid compositions and temperatures.

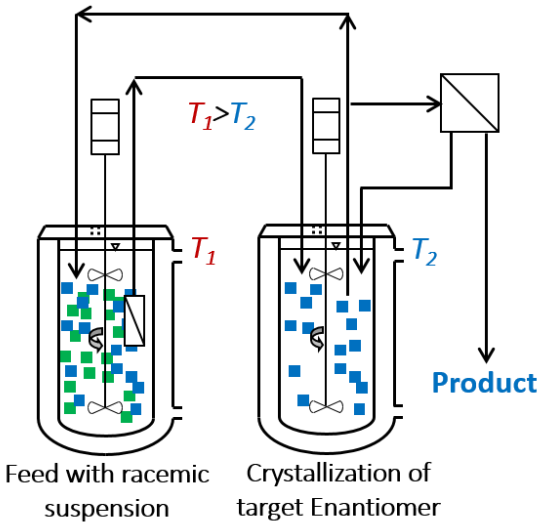

Figure 11: Schematic of a deracemization process in CSTR configuration using a cooling crystallization for driving force induction; with the target enantiomer (blue) and the counter enantiomer (green).

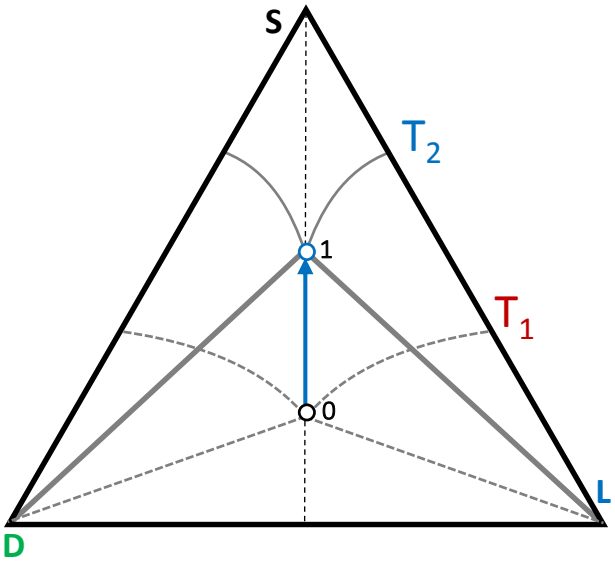

Figure 12: Schematic of a ternary phase diagram showing a deracemization process with the feed concentration 0 and the end concentration 1 in the crystallizer.

An alternative deracemization process as investigated in this work can be conducted which prevents the transformation of solids by avoiding the presence of the solid counter enantiomer in the product crystallizer. In such deracemization process, performed in a continuously stirred tank reactor (CSTR), a feed with a mixed racemic suspension and a crystallizer with product extraction, as shown in Figure 11, are used. Seeds of the desired handedness will be prepared in the crystallizer and solid excess at racemic composition in a feed vessel. Both vessels contain a saturated solution at racemic composition, at the respective temperatures and the racemization catalyst to ensure racemic composition in solution. Upon starting the process, a hot saturated solution is transferred to the crystallizer, where it is cooled and supersaturated as shown in Figure 12, at point 0. The Target enantiomer is then crystallized while the solution composition remains racemic due to the racemization reaction. This process can be continued until the solid excess in the feed has been depleted. This kind of deracemization process allows for steady-state operation, as both the feed and crystallizer are operated at a constant temperature and residence time.

While this kind of process allows for high yields and high purities, it can only be applied to conglomerate systems for direct crystallization as otherwise the racemic compound would be produced. As the conditions at which a racemization reaction can be conducted are compound specific, this kind of process cannot be applied to all conglomerates in this manner but sometimes requires the racemization to take place decoupled from the crystallization step [73].

1.9.4 Hybrid processes

While crystallization based separation is an efficient method for chiral separation it cannot always be directly applied. In general hybrid processes in crystallization refers to a combination of a crystallization process with another technique for purification to achieve a better overall separation result or enable the crystallization step in the first place. One

example of this is, for instance, combining a preferential crystallization for conglomerates with racemization of the solution in a second vessel [62]. Another example of the application of hybrid processes is the separation of racemic compound forming systems through preferential crystallization after an enrichment step with respect to one enantiomer. In this case, a primary separation technology is used to enrich a racemic starting solution to the eutectic composition, enabling the preferential crystallization of the pure enantiomer and racemic compound in the triphasic domain. This has been demonstrated by Gou [57] by using membrane separation to enrich racemic mandelic acid to its eutectic follow by a coupled batch crystallization. Another primary separation technology, which is efficient for chiral separation is chromatography, but it has increased costs with increasing chiral enrichment as more eluent and separation steps are required. One hybrid process was reported by Kaemmerer [74], where the enantiomer was enriched using a simulated moving bed (SMB) until the twophasic domain is reached and then the pure enantiomer is subsequently crystallized using antisolvent crystallization. The extent of enrichment is always dependent on the phase diagram of the compound, however, if the phase diagram of the compound shows to have a eutectic which is below 85-90 % enrichment with respect to one enantiomer, the chromatography can be used for initial enrichments until the eutectic composition is reached, from where the pure enantiomer and racemic compound can be separated in the triphasic domain. Such a combination has been demonstrated by Polenske and Lorenz [58, 69] using mandelic acid.

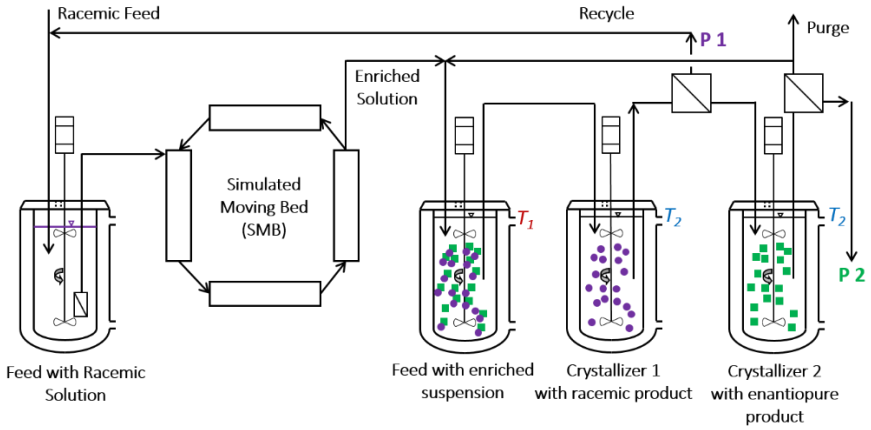

Figure 13: Schematic of a hybrid process with a racemic feed solution, initial enrichment in a simulated moving bed chromatography followed by a serial crystallization with a feed containing enriched suspension, crystallizer 1 for racemic product 1 including recycle and crystallizer 2 with target enantiopure product 2.

What all of the above mentioned examples in literature have in common is that the crystallization step is a batch process. Figure 13 shows the combination of a serial crystallization process and an SMB for the possible separation of racemic compound forming systems. In this example a racemic solution is prepared in a feed vessel and enriched to the eutectic composition in and SMB, followed by a concentration of the solid excess in a feed vessel used for the crystallization step. From there the racemic compound is crystallized first, in crystallizer 1, which is recycled to be re-enriched in the SMB, while the target enantiomer is crystallized in crystallizer 2. By using recycles for the racemic compound and depleted

solution back into the crystallization feed vessel, the overall yield of the hybrid process can be improved.

1.9.5 Antisolvent Crystallization

Antisolvent crystallization is a process which uses solubility differences of a crystalline compound in two different solvents with the compound being soluble in one solvent while having a very low solubility in the other. The solvent in which the compound is not soluble in is referred to as antisolvent. A binary phase diagram of an antisolvent crystallization process is shown in Figure 14 with a corresponding process configuration in Figure 15. A saturated solution with concentration C_0 (Figure 14) is prepared in the saturated solution feed vessel (Figure 15) and transferred to a crystallizer. At the same time, antisolvent (purple circle, Figure 14) is transferred from a second feed vessel (Figure 15) to the crystallizer, where the two streams are mixed. By mixing antisolvent with the saturated solution the overall concentration at the mixing point C_M (Figure 15) is reduced by dilution [21, 22, 39] in comparison to the starting concentration C_0. At the same time, the solubility C^* of the solute in the solvent mix is reduced much further than the mixing concentration C_M. This induces a supersaturation $\Delta C = C_M - C^*$ between solubility and mixing point concentration on the operating line, leading to crystallization. The operating line, which is also called dilution line, indicates the overall concentration in the solvent mix after mixing saturated solution with a concentration C_0 at a given antisolvent fraction.

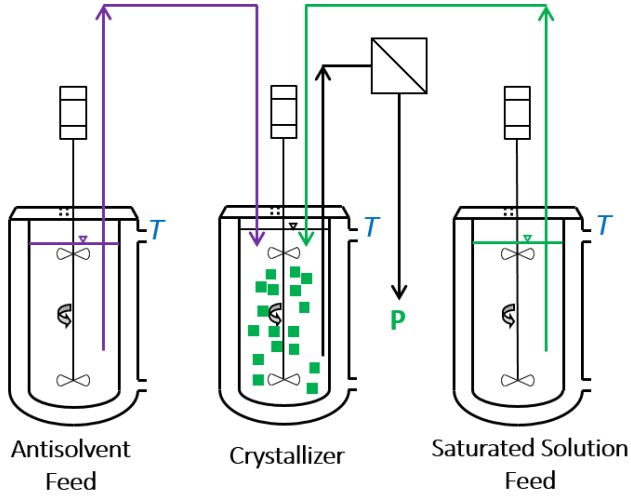

Figure 14: Schematic of a binary antisolvent phase diagram with the antisolvent dependent solubility line (blue), the dilution line from mixing the saturated solution with antisolvent, the mixing point at concentration C and the equilibrium solubility of the compound at a certain antisolvent fraction C*.

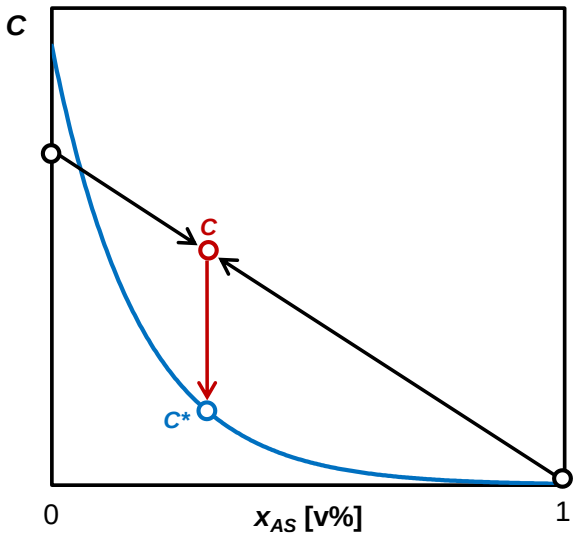

Figure 15: Schematic of an antisolvent crystallization process with antisolvent feed vessel (left), saturated solution feed vessel (right) and crystallizer (middle) containing solid crystals (green rectangles) and product removal.

Antisolvent crystallization often shows an initial large drop in concentration with small fractions of antisolvent, allowing for large concentration differences between operating line and solubility, with small amount of solid remaining in the solution after larger antisolvent fractions (typically higher than 50v%). Antisolvent crystallization processes typically have high yields and allow for almost all of the solid to be removed from the solution, making it a

frequently applied crystallization process in the pharmaceutical industry [11, 12, 50, 51, 75, 76].

Despite its many benefits, the large concentration differences between operating line and solubility, as well as high local supersaturations at the mixing point between antisolvent and crystallizer solution, caused by larger concentrations of antisolvent at the local mixing point then in the rest of the crystallizer suspension, it would seem chirally unselective primary rather than selective secondary nucleation would be dominant in such a process. Therefore they are typically not applied for chiral separation and so far it has not yet been investigated if under which conditions secondary nucleation in an antisolvent process can be preserved. In chapter 3 of this work, it is investigated if the preferred handedness in a chiral separation process can be obtained.

1.10 Benefits of continuous crystallization

Continuous chiral resolution and deracemization techniques allow for steady-state production of the desired handedness at constant process conditions such as temperature, antisolvent fraction and solution concentration, permitting a reproducible process with constant product properties such as enantiopurity and particle size. In addition, continuous processes allow for solution recycling and therefore a higher overall yield in comparison to batch processes

1.11 Aim and Objectives

While predominantly batch processes for crystallization are used in the pharmaceutical industry, due to their low production volumes and heavy regulation, there is a drive towards continuous manufacture [75] as it has many advantages (1.10) over batch configurations especially with regards to reproducibility and product purity. As an increasing fraction of new pharmaceutical compounds are chiral [6, 8, 9, 12, 77] (1.3) and asymmetric synthesis routes are not always available, crystallization based chiral separation techniques are needed (ref. section 1.6 and 1.9).

As there are a vast variety of chiral molecules having different physical properties and crystallization behaviours (1.9), there are a number of crystallization based techniques and process designs depending on the compound type (1.4), phase diagram (1.5) and crystallization behaviour (1.9) While preferential crystallization processes can be efficient for conglomerate forming systems, many processes are specifically tailored to their compounds to be separated, depending on their solubilities and compound type, where sometimes more than one crystallization technique can be used for the separation. Deracemization processes such as Viedma ripening and temperature cycling-induced deracemization are dynamic processes and require the subsequent dissolution of the unwanted enantiomer, directed racemization of the unwanted enantiomer into the preferred enantiomer in the solution and the crystallization of the preferred enantiomer crystal product. Considering the number of steps needed in such a process, as well as the means to induce them (temperature changes, grinding, racemization catalysts), scaling such processes is challenging as each step and means of induction have to be scaled accordingly in addition to mixing effects and temperature

control. Antisolvent crystallization processes have high yields but also high local supersaturations, which enables unselective primary rather than selective secondary nucleation, so they have not been substantially investigated regarding their applicability towards chiral separation and control over secondary nucleation. Hybrid processes allow for preferential crystallization to be used to separate chiral compound forming systems in an enriched chiral solution while increasing overall process efficiency in comparison of just using one separation technique. While they can be an efficient technique for chiral separation the examples shown in section 1.9.4 involve a batch process for the crystallization step. Therefore, finding suitable process configurations, also with regards to yield and productivity desired, can be challenging.

The aim of this thesis is to demonstrate a number of new resolution and deracemization process configurations easily adaptable to continuous operation. This will culminate in a guideline to choose a suitable crystallization-based resolution or deracemization process based on the design information and specifications given, putting the separation processes developed in this thesis into perspective in the final chapter 6. Towards this aim, four objectives are investigated in their respective chapters, as illustrated in Figure 16, to contribute towards developing new crystallization based chiral resolution and deracemization techniques towards continuous manufacturing.

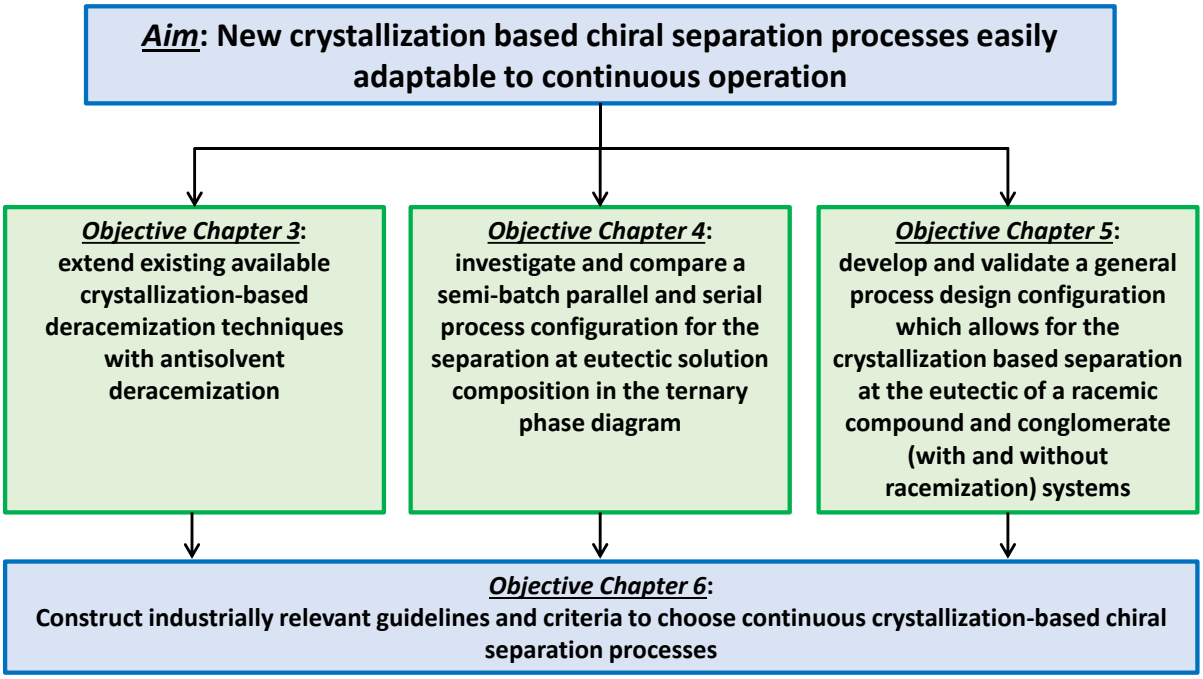

Figure 16: Overview of **Aim** and **Objective** in this thesis.

1.11.1 Chapter 3: Total Spontaneous Resolution using Antisolvent Crystallization

Antisolvent crystallization is a widely applied process in the pharmaceutical industry [11, 18, 50]due to its high yields and short process duration. However, as far as we know, it has not been reported to be used for chiral resolution or deracemization. This is due to the process producing high supersaturations, especially at the mixing points, leading to chirally aselective primary nucleation rather than chirally selective secondary nucleation. However, combining

antisolvent crystallization with a racemization reaction can potentially be beneficial as this would reduce the supersaturation for the counter enantiomer, possibly already in the mixing point. In addition, this process might allow for high productivities, while removing almost all solid material from the solution. If control over selective secondary nucleation can be achieved this could also lead to implication for polymorphism control in antisolvent crystallization processes. **Therefore, the objective in this chapter is to extend existing available crystallization-based deracemization techniques with antisolvent deracemization**. In chapter 3 the extent with which control over chirally selective secondary nucleation and with it over the produced handedness can be preserved, despite the high local supersaturations of antisolvent crystallization processes, it is investigated.

1.11.2 Chapter 4: Chiral Separation at the Eutectic Point: a Case Study for Mandelic Acid

In racemic compound forming systems, the enantiomers cannot be directly separated by preferential crystallization (1.9.2), which follows from the phase diagram (1.5.2) . They are most commonly resolved by Classical Resolution or by a primary separation method like chiral chromatography or Hybrid processes to increase process efficiency. While the benefits of hybrid processes have been highlighted in section 1.9.4, the crystallization step of the processes discussed in section 1.9.4 have been reported to be batch processes. Following from the ternary phase diagram (1.5.2), racemic compound forming systems can be separated through preferential crystallization in the triphasic domain. This requires an initial enrichment step, using a primary separation method, to reach the eutectic point (1.5.2). At the eutectic composition in the triphasic domain, the solid racemic compound and pure enantiomer phase are in equilibrium with the solution. However the pure enantiomer and racemic compound have different growth kinetics and solubilities, making separation challenging. Therefore a simple and simple robust process configuration is needed to separate the pure enantiomer and racemic compound and prevent the primary nucleation of the undesired solid form in the crystallizer. **The objective of this chapter is to investigate and compare a semi-batch parallel and serial process configuration (1.9.2) for the separation of racemic compound and pure enantiomer at eutectic solution composition in the ternary phase diagram, to determine if either of these configurations allows for feasible separation of the pure enantiomer and racemic compound to be used as crystallization step in a hybrid process.** The resulting process, if validated for its robustness in a semi-batch configuration can easily be extended to a continuous configuration.

1.11.3 Chapter 5: Resolutions, Separation and Deracemization in Chiral Eutectic Solutions

In section 1.9 a range of process designs and techniques for the crystallization based separation of chiral compounds, depending on their compound type, solubility and racemizability, are discussed. Following the results of chapter 4, the serial process configuration is investigated for its applicability in the separation of conglomerate forming systems and as deracemization process. The similarity for the diverse chiral compounds lies in the phase diagram (1.5.2): all conglomerate and racemic compound forming systems have triphasic domains enabling separation in the eutectic. In the case of conglomerate systems, when adding racemization it becomes deracemization in the eutectic. **The objective of this chapter is to develop and validate a general process design configuration which allows for**

the crystallization based separation in the eutectic of a racemic compound system as well as a conglomerate system and allows for the deracemization of a conglomerate system. As process specifications such as enantiopurity, productivity and yield are of high importance for industrial application, it is investigated if the serial configuration can reach similar values for the specifications as process designs reported in literature using the same model compounds.

1.11.4 Chapter 6: A guideline to choose continuous crystallization based chiral separation processes

As there is a drive towards continuous processes for crystallization in the pharmaceutical industry **the objective of this chapter is to construct industrially relevant guidelines and criteria, based on process specifications such as productivity, yield and enantiomeric excess, to choose continuous crystallization-based chiral separation processes.** To those end aspects of batch, semi-batch and continuous process design are discussed in this chapter, followed by an overview of the range of applicability of crystallization based processes for chiral separation, comparing the work done in this thesis to work found in literature. By using basic design approaches, chosen process specifications like productivity, product purity and yield can be validated against compound information like growth kinetics, in order investigate the feasibility of the chosen specifications and produce realistic predictions for the process design. The chapter presents a workflow to choose continuous crystallization based chiral separation process.

1.12 References

[1] G. Coquerel, Chiral Discrimination in the Solid State: Applications to Resolution and Deracemization, (2015) 393-420.

[2] J.W. Mullin, Crystallization, in: J.W. Mullin (Ed.), Crystallization (Fourth Edition), Butterworth-Heinemann, Oxford, 2001, pp. 536-575.

[3] C.A. Jacques Jean, & Wilen Samuel H., Enantiomers, racemates, and resolutions, (1981).

[4] A.C. J. Jacques, S. H. Wile, Enantiomers, Racemates and Resolutions, Krieger, Malabar1994.

[5] W.L.M.C.N. Hurley, Chemistry : principles and reactions, Australia : Cengage Learning, Australia, 2016.

[6] L.A. Nguyen, H. He, C. Pham-Huy, Chiral drugs: an overview, Int J Biomed Sci 2(2) (2006) 85-100.

[7] W.A. Bonner, Chirality and life, Origins of Life and Evolution of the Biosphere 25(1) (1995) 175-190.

[8] W.H. De Camp, The FDA perspective on the development of stereoisomers, Chirality 1(1) (1989) 2-6.

[9] W.H. De Camp, Chiral drugs: The FDA perspective on manufacturing and control, Journal of Pharmaceutical and Biomedical Analysis 11(11) (1993) 1167-1172.

[10] S. Chemat, A. Lagha, H. AitAmar, P.V. Bartels, F. Chemat, Comparison of conventional and ultrasound-assisted extraction of carvone and limonene from caraway seeds, Flavour and Fragrance Journal 19(3) (2004) 188-195.

[11] J. Chen, B. Sarma, J.M.B. Evans, A.S. Myerson, Pharmaceutical Crystallization, Crystal Growth & Design 11(4) (2011) 887-895.

[12] B.Y. Shekunov, P. York, Crystallization processes in pharmaceutical technology and drug delivery design, Journal of Crystal Growth 211(1) (2000) 122-136.

[13] H. Lorenz, A. Seidel-Morgenstern, Processes to separate enantiomers, Angew Chem Int Ed Engl 53(5) (2014) 1218-50.

[14] K.G. Feitsma, B.F.H. Drenth, Chromatographic separation of enantiomers, Pharmaceutisch Weekblad 10(1) (1988) 1-11.

[15] G.S. A. Collins, J. Crosby (Eds.), Chirality in Industry: The Commercial Manufacture and Applications of Optically Active Compounds, John Wiley & Sons, Chichester, 1992.

[16] G.S. A. Collins, J. Crosby (Eds.), Chirality in Industry II: Developments in the Manufacture and Applications of Optically Active Compounds, John Wiley & Sons,, Chichester 1997.

[17] R. Hilfiker, Polymorphism of Crystalline Systems, in: W. Beckmann (Ed.), Crystallization: Basic Concepts and Industrial Applications, Wiley-VCH Verlag GmbH & Co. KGaA2013, pp. 85-103.

[18] I.R. Baxendale, R.D. Braatz, B.K. Hodnett, K.F. Jensen, M.D. Johnson, P. Sharratt, J.-P. Sherlock, A.J. Florence, Achieving Continuous Manufacturing: Technologies and Approaches for Synthesis, Workup, and Isolation of Drug Substance May 20–21, 2014 Continuous Manufacturing Symposium, Journal of Pharmaceutical Sciences 104(3) (2015) 781-791.

[19] H. Lorenz, A. Perlberg, D. Sapoundjiev, M.P. Elsner, A. Seidel-Morgenstern, Crystallization of enantiomers, Chemical Engineering and Processing: Process Intensification 45(10) (2006) 863-873.

[20] D. Acevedo, Y. Yang, D.J. Warnke, Z.K. Nagy, Model-Based Evaluation of Direct Nucleation Control Approaches for the Continuous Cooling Crystallization of Paracetamol in a Mixed Suspension Mixed Product Removal System, Crystal Growth & Design 17(10) (2017) 5377-5383.

[21] A.S. Myerson, Handbook of Industrial Crystallization, in: A.S.E.D.L.A.Y. Myerson (Ed.), Handbook of Industrial Crystallization (Third Edition), Cambridge University Press, Woburn, 2019, p. xi.

[22] J.H. ter Horst, C. Schmidt, J. Ulrich, Fundamentals of Industrial Crystallization, Elsevier B.V.2015.

[23] S.G. Agrawal, A.H.J. Paterson, Secondary Nucleation: Mechanisms and Models, Chemical Engineering Communications 202(5) (2015) 698-706.

[24] R.J. Davey, S.L. Schroeder, J.H. ter Horst, Nucleation of organic crystals--a molecular perspective, Angew Chem Int Ed Engl 52(8) (2013) 2166-79.

[25] A. Ranodolph, Theory of Particulate Processes 2e: Analysis and Techniques of Continuous Crystallization, 2012.

[26] P. Cruz, F. Rocha, A. Ferreira, Determination of the critical mixing intensity for secondary nucleation of paracetamol in an oscillatory flow crystallizer, CrystEngComm 20(6) (2018) 829-836.

[27] M.A.L. Aland D. Randolph, Theory of Particulate Processes, Academic Press Inc., San Diego, 1988.

[28] T. Köllges, T. Vetter, Model-Based Analysis of Continuous Crystallization/Reaction Processes Separating Conglomerate Forming Enantiomers, Crystal Growth & Design 17(1) (2017) 233-247.

[29] E. Temmel, M.J. Eicke, F. Cascella, A. Seidel-Morgenstern, H. Lorenz, Resolution of Racemic Guaifenesin Applying a Coupled Preferential Crystallization-Selective Dissolution Process: Rational Process Development, Crystal Growth & Design 19(6) (2019) 3148-3157.

[30] E. Temmel, J. Gänsch, H. Lorenz, A. Seidel-Morgenstern, Measurement and Evaluation of the Crystallization Kinetics of l-Asparagine Monohydrate in the Ternary l-/d-Asparagine/Water System, Crystal Growth & Design 18(12) (2018) 7504-7517.

[31] K. Petruševska-Seebach, A. Seidel-Morgenstern, M.P. Elsner, Preferential Crystallization ofl-Asparagine in Water, Crystal Growth & Design 11(6) (2011) 2149-2163.

[32] H. Lorenz, D. Sapoundjiev, A. Seidel-Morgenstern, Enantiomeric Mandelic Acid SystemMelting Point Phase Diagram and Solubility in Water, Journal of Chemical & Engineering Data 47(5) (2002) 1280-1284.

[33] H. Lorenz, A. Seidel-Morgenstern, Binary and ternary phase diagrams of two enantiomers in solvent systems, Thermochim. Acta 382 (2002) 129.

[34] R.M. Kellogg, Practical Stereochemistry, Acc Chem Res 50(4) (2017) 905-914.

[35] G.M. Maggioni, M.P. Fernández-Ronco, M.W. van der Meijden, R.M. Kellogg, M. Mazzotti, Solid state deracemisation of two imine-derivatives of phenylglycine derivatives via high-pressure homogenisation and temperature cycles, CrystEngComm 20(27) (2018) 3828-3838.

[36] R.J. Davey, G. Sadiq, C.C. Seaton, R.G. Pritchard, G. Coquerel, C. Rougeot, Racemic compound versus conglomerate: concerning the crystal chemistry of the triazoylketone, 1-(4-chlorophenyl)-4,4-dimethyl-2-(1H-1,2,4-triazol-1-yl)pentan-3-one, CrystEngComm 16(21) (2014) 4377.

[37] C. Rougeot, J.E. Hein, Application of Continuous Preferential Crystallization to Efficiently Access Enantiopure Chemicals, Org. Process Res. Dev. 19(12) (2015) 1809-1819.

[38] R.R. Steendam, M.C. Brouwer, E.M. Huijs, M.W. Kulka, H. Meekes, W.J. van Enckevort, J. Raap, F.P. Rutjes, E. Vlieg, Enantiopure isoindolinones through Viedma ripening, Chemistry 20(42) (2014) 13527-30.

[39] R.R.E. Steendam, J.H. ter Horst, Continuous Total Spontaneous Resolution, Crystal Growth & Design 17(8) (2017) 4428-4436.

[40] C. Xiouras, A.A. Fytopoulos, J.H. Ter Horst, A.G. Boudouvis, T. Van Gerven, G.D. Stefanidis, Particle Breakage Kinetics and Mechanisms in Attrition-Enhanced Deracemization, Crystal Growth & Design 18(5) (2018) 3051-3061.

[41] C. Xiouras, E. Van Cleemput, A. Kumpen, J.H. Ter Horst, T. Van Gerven, G.D. Stefanidis, Towards Deracemization in the Absence of Grinding through Crystal Transformation, Ripening, and Racemization, Crystal Growth & Design 17(2) (2016) 882-890.

[42] A.H.J. Engwerda, H. Meekes, B. Kaptein, F.P.J.T. Rutjes, E. Vlieg, Speeding up Viedma ripening, Chemical Communications 52(81) (2016) 12048-12051.

[43] L.-C. Sögütoglu, R.R.E. Steendam, H. Meekes, E. Vlieg, F.P.J.T. Rutjes, Viedma ripening: a reliable crystallisation method to reach single chirality, Chemical Society Reviews 44(19) (2015) 6723-6732.

[44] C. Xiouras, J.H. Ter Horst, T. Van Gerven, G.D. Stefanidis, Coupling Viedma Ripening with Racemic Crystal Transformations: Mechanism of Deracemization, Crystal Growth & Design 17(9) (2017) 4965-4976.

[45] W.L. Noorduin, B. Kaptein, H. Meekes, W.J.P. van Enckevort, R.M. Kellogg, E. Vlieg, Fast Attrition-Enhanced Deracemization of Naproxen by a Gradual In Situ Feed, Angewandte Chemie International Edition 48(25) (2009) 4581-4583.

[46] M.L. Maarten W. van der Meijden, Edith Gelens, Wim L. Noorduin, Hugo Meekes, Willem J. P. van Enckevort, Bernard Kaptein, Elias Vlieg and Richard M. Kellogg, Attrition-Enhanced Deracemization in the Synthesis of Clopidogre l - A Practical Application of a New Discovery, Org. Process Res. Dev. 13(6) (2009) 1195-1198.

[47] F. Breveglieri, G.M. Maggioni, M. Mazzotti, Deracemization of NMPA via Temperature Cycles, Crystal Growth & Design 18(3) (2018) 1873-1881.

[48] W.W. Li, L. Spix, S.C.A. de Reus, H. Meekes, H.J.M. Kramer, E. Vlieg, J.H. ter Horst, Deracemization of a Racemic Compound via Its Conglomerate-Forming Salt Using Temperature Cycling, Crystal Growth & Design 16(9) (2016) 5563-5570.

[49] K. Suwannasang, A.E. Flood, G. Coquerel, A Novel Design Approach To Scale Up the Temperature Cycle Enhanced Deracemization Process: Coupled Mixed-Suspension Vessels, Crystal Growth & Design 16(11) (2016) 6461-6467.

[50] A.J. Alvarez, A.S. Myerson, Continuous Plug Flow Crystallization of Pharmaceutical Compounds, Crystal Growth & Design 10(5) (2010) 2219-2228.

[51] Q. Su, Z.K. Nagy, C.D. Rielly, Pharmaceutical crystallisation processes from batch to continuous operation using MSMPR stages: Modelling, design, and control, Chemical Engineering and Processing: Process Intensification 89 (2015) 41-53.

[52] Y. Yang, Z.K. Nagy, Combined Cooling and Antisolvent Crystallization in Continuous Mixed Suspension, Mixed Product Removal Cascade Crystallizers: Steady-State and Startup Optimization, Industrial & Engineering Chemistry Research 54(21) (2015) 5673-5682.

[53] G.X. Zhou, M. Fujiwara, X.Y. Woo, E. Rusli, H.-H. Tung, C. Starbuck, O. Davidson, Z. Ge, R.D. Braatz, Direct Design of Pharmaceutical Antisolvent Crystallization through Concentration Control, Crystal Growth & Design 6(4) (2006) 892-898.

[54] M.P. Elsner, G. Ziomek, A. Seidel-Morgenstern, Efficient separation of enantiomers by preferential crystallization in two coupled vessels, AIChE Journal 55(3) (2009) 640-649.

[55] M.P. Elsner, G. Ziomek, A. Seidel-Morgenstern, Simultaneous preferential crystallization in a coupled batch operation mode. Part II: Experimental study and model refinement, Chemical Engineering Science 66(6) (2011) 1269-1284.

[56] K. Galan, M.J. Eicke, M.P. Elsner, H. Lorenz, A. Seidel-Morgenstern, Continuous Preferential Crystallization of Chiral Molecules in Single and Coupled Mixed-Suspension Mixed-Product-Removal Crystallizers, Crystal Growth & Design 15(4) (2015) 1808-1818.

[57] L. Gou, S. Robl, K. Leonhard, H. Lorenz, M. Sordo, A. Butka, S. Kesselheim, M. Wolff, A. Seidel-Morgenstern, K. Schaber, A hybrid process for chiral separation of compound-forming systems, Chirality 23(2) (2011) 118-27.

[58] M.D.D. Heike Lorenz, E.D.L.K. Polenske, M.D. Andreas, M.D. Seidel-Morgenstern, METHOD FOR SEPARATION OF RACEMIC COMPOUND-FORMING CHIRAL SUBSTANCES BYA CYCLIC CRYSTALLIZATION PROCESS AND A CRYSTALLIZATION DEVICE, in: U.P. Office (Ed.) United States, 2012.

[59] G. Levilain, M.J. Eicke, A. Seidel-Morgenstern, Efficient Resolution of Enantiomers by Coupling Preferential Crystallization and Dissolution. Part 1: Experimental Proof of Principle, Crystal Growth & Design 12(11) (2012) 5396-5401.

[60] H. Lorenz, D. Polenske, A. Seidel-Morgenstern, Application of preferential crystallization to resolve racemic compounds in a hybrid process, Chirality 18(10) (2006) 828-40.

[61] K. Petruševska-Seebach, A. Seidel-Morgenstern, M.P. Elsner, Preferential Crystallization of l-Asparagine in Water, Crystal Growth & Design 11(6) (2011) 2149-2163.

[62] K. Petruševska-Seebach, K. Würges, A. Seidel-Morgenstern, S. Lütz, M.P. Elsner, Enzyme-assisted physicochemical enantioseparation processes—Part II: Solid–liquid equilibria, preferential crystallization, chromatography and racemization reaction, Chemical Engineering Science 64(10) (2009) 2473-2482.

[63] D. Polenske, H. Lorenz, A. Seidel-Morgenstern, Potential of different techniques of preferential crystallization for enantioseparation of racemic compound forming systems, Chirality 21(8) (2009) 728-737.

[64] J.H. Chaaban, K. Dam-Johansen, T. Skovby, S. Kiil, Separation of Enantiomers by Continuous Preferential Crystallization: Experimental Realization Using a Coupled Crystallizer Configuration, Org. Process Res. Dev. 17(8) (2013) 1010-1020.

[65] M.P. Elsner, G. Ziomek, A. Seidel-Morgenstern, Simultaneous preferential crystallization in a coupled, batch operation mode—Part I: Theoretical analysis and optimization, Chemical Engineering Science 62(17) (2007) 4760-4769.

[66] A.G. Jones, Crystallization Process Systems, in: A.G. Jones (Ed.), Crystallization Process Systems, Butterworth-Heinemann, Oxford, 2002, pp. 1-25.

[67] D. Binev, A. Seidel-Morgenstern, H. Lorenz, Continuous Separation of Isomers in Fluidized Bed Crystallizers, Crystal Growth & Design 16(3) (2016) 1409-1419.

[68] T. McGlone, N.E.B. Briggs, C.A. Clark, C.J. Brown, J. Sefcik, A.J. Florence, Oscillatory Flow Reactors (OFRs) for Continuous Manufacturing and Crystallization, Org. Process Res. Dev. 19(9) (2015) 1186-1202.

[69] H. Lorenz, D. Polenske, A. Seidel-Morgenstern, Application of preferential crystallization to resolve racemic compounds in a hybrid process, Chirality 18(10) (2006) 828-840.

[70] J.L. Bada, S.L. Miller, Racemization and the origin of optically active organic compounds in living organisms, Biosystems 20(1) (1987) 21-26.

[71] D.B. Amabilino, R.M. Kellogg, Spontaneous Deracemization, Israel Journal of Chemistry 51(10) (2011) 1034-1040.

[72] R. Oketani, C. Brandel, P. Cardinaël, G. Coquerel, Optimization of SOAT: Example of Naphthamide deracemization, Summer School on Chiral Crystallization, Resolution & Deracemization, Nijmegen, Netherlands, 2017.

[73] A.H.J. Engwerda, R. Maassen, P. Tinnemans, H. Meekes, F.P.J.T. Rutjes, E. Vlieg, Attrition-Enhanced Deracemization of the Antimalaria Drug Mefloquine, Angewandte Chemie International Edition 58(6) (2019) 1670-1673.

[74] H. Kaemmerer, Z. Horvath, J.W. Lee, M. Kaspereit, R. Arnell, M. Hedberg, B. Herschend, M.J. Jones, K. Larson, H. Lorenz, A. Seidel-Morgensten, Separation of Racemic Bicalutamide by an Optimized Combination of Continuous Chromatography and Selective Crystallization, Org. Process Res. Dev. 16(2) (2012) 331-342.

[75] K. Plumb, Continuous Processing in the Pharmaceutical Industry: Changing the Mind Set, Chemical Engineering Research and Design 83(6) (2005) 730-738.

[76] S. Veesler, F. Puel, 21 - Crystallization of Pharmaceutical Crystals, in: T. Nishinaga (Ed.), Handbook of Crystal Growth (Second Edition), Elsevier, Boston, 2015, pp. 915-949.

[77] N. Chhabra, M. Aseri, D. Padmanabhan, A review of drug isomerism and its significance, International Journal of Applied and Basic Medical Research 3(1) (2013) 16-18.

2 Methods

In this work, a variety of process configurations and designs has been investigated. As the processes look into different approaches towards continuous chiral separation, a variety of model compounds have been used, depending on the applicability of the crystallization processes.

As crystallization is a purification process, the overall objective of each process is to produce enantiopure product material. Therefore the produced crystalline product obtained during the experiments was investigated for its purity using offline and online techniques. In addition, the crystallization processes have to be monitored, where in situ techniques were used.

This chapter targets to provide some theoretical background to the chiral compounds, as well as the offline and online analysis techniques which were used in the different chapters throughout the thesis.

2.1 Chiral crystals of achiral Compounds

Most chiral crystals are formed by molecules of chiral compounds but there are also molecules of achiral compounds that can form chiral crystals. These achiral compounds crystallize in a specific chiral space group, which gives the resulting crystals the ability to rotate linear polarized light.

2.1.1 Sodium Bromate

Sodium bromate was the compound used for the antisolvent experiments in this work. It is a water-soluble salt which is achiral in solution but crystallizes as chiral crystals (thanks to the chiral space group $P2_13$ [1]) which exhibit rotation in plane-polarized light (Polarized Light Microscopy) [1]. Also, sodium chlorate crystals show such behaviour as shown by Kondepudi [2] who investigated the effects of stirring on the chirality of sodium chlorate. Achiral molecules such as sodium chlorate and sodium bromate have since been used in deracemization experiments to investigate under which conditions the transformation of a mixture of enantiomers to single handedness can be achieved. One famous experiment was conducted by Viedma, where a suspension of sodium chlorate in water with glass beads was ground, leading to a transformation of a racemic mix of crystals into a single handedness [3]. In other experiments, a reliable method for determining the chirality by counting the crystals under a polarised light microscope was explained [4] and also applied in a total spontaneous resolution experiment of sodium bromate [5]. Being achiral in solution but crystallizing in distinguishable handedness mimics a conglomerate forming systems with very fast racemization kinetic in a solvent, making it an ideal compound for antisolvent deracemization studies. The Sodium bromate (>99.5%) was purchased from Alfa Aesar. De-Ionized water purified by a Milli-Q gradient system was used as a solvent, while pure ethanol (99%) purchased by VWR served as antisolvent. Sodium Bromate has a very high solubility in water while being highly insoluble in most alcohols, as shown in the binary phase diagram in chapter 3, which allows nontoxic solvents and antisolvent to be used.

2.2 Chiral Crystals of chiral compounds

2.2.1 Mandelic Acid

Mandelic Acid (MA) is a chiral compound classified as a racemic compound forming systems. It is often used as a resolving agent for racemates in the production of certain chiral drugs [6]. The structure of the MA enantiomers with the chiral center of the molecule can be found in Figure 17. The racemic compound DL-MA, as well as the pure enantiomer D-MA used in this work, were purchased by Tokyo Chemicals International (TCI) with a purity of >99 %. Deionized water, purified by a Milli-Q gradient system was used as the solvent for this compound.

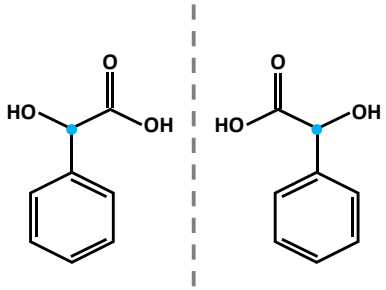

Figure 17: Enantiomers of Mandelic Acid with chiral center indicated (blue); D-MA (left) and L-MA (right).

Mandelic acid as a reported solid eutectic composition of 69 % mole fraction of one enantiomer in the other [7]. The solubilities in water, as well as the ternary phase diagram of mandelic acid, have been investigated [6, 7] and it was used as a model compound in several publications with hybrid processes, making it an ideal model compound for the work in this thesis.

2.2.2 Asparagine Monohydrate

Asparagine monohydrate (ASN) is a chiral molecule and non-essential amino acid which crystallizes as a conglomerate forming system. The structure of the enantiomers of ASN is shown in Figure 18. The racemic mixture DL-ASN and the pure enantiomers D- and L-ASN were purchased from Sigma Aldrich (>99%). Deionized Milli-Q water was used as a solvent for this compound during this work.

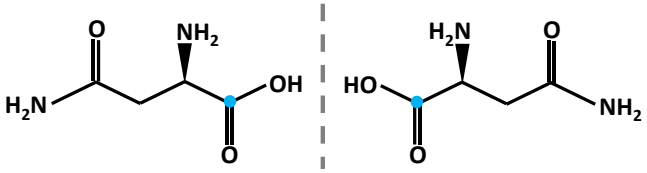

Figure 18: Enantiomers of Asparagine monohydrate with the chiral center indicated, with D-ASN (left) and L-ASN (right).

ASN has been used very frequently in literature [8-11] as a model compound for conglomerate forming systems. The solubility in water for this compound has been previously investigated [12, 13]. It is commercially available in large quantities, is safe to handle and has comparably low costs.

2.2.3 Clopidogrel-Imine

Another compound used in this work is clopidogrel-imine (CPG) which is a precursor of clopidogrel, a drug used as a blood thinner to reduce the risk of heart attacks. It crystallizes as a conglomerate and undergoes a racemization reaction in the presence of 1,8-Diazabicyclo[5.4.0]undec-7-ene (DBU). DBU is a strong base that has been used as a racemization catalyst in previous publications using this compound [14, 15] and was procured by sigma aldritch (99%). The structure of the enantiomers can be found in Figure 19. Acetonitrile (VWR, 99%) was used as a solvent for this compound and 1 w% DBU was added for it to undergo racemization reaction in solution.

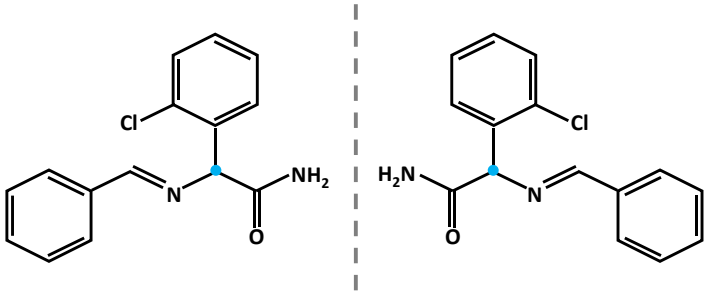

Figure 19: Enantiomers of Clopidogrel-Imine with the chiral center indicated; S-CPG (left) and R-CPG (right).

Although not very much investigated, due to its fast racemization, the compound has been used in deracemization experiments for Viedma ripening [14, 15], where a suspension with a low enantiomeric excess was enriched to enantiopurity through grinding. The racemic mix RS-CPG and pure enantiomer R-CPG were procured from Syncom B.V (>99%). Due to the compound racemizing quickly in solution in the presence of DBU, it was the ideal compound to be used in deracemization experiments in this work.

2.3 Material Characterization Methods

2.3.1 Solubility Determination and Gravimetric Analysis

The knowledge of the solubility of a crystalline compound in a solvent, forming a solution, is the basis of every crystallization process and can be represented in a phase diagram. The phase diagram describes at which temperature a specific solution composition is in equilibrium with a specific crystalline phase [16]. Solubility measurements allow determining the overall maximum concentration of a crystalline phase in a solvent in equilibrium at a given temperature. To determine solubility, an isothermal or clear point method can be used. In an isothermal solubility determination, a suspension of the crystalline solid and the solvent is created in a small isolated vessel to prevent evaporation. The stirred suspension is held at a certain constant temperature for at least 24 h to allow for equilibration. Afterward, a solution sample of the suspension can be taken and analyzed to determine the concentration, for instance through gravimetric analysis. Gravimetric analysis allows determining the solid content in a solvent through a mass balance. The weight of the solution sample is determined and the solvent evaporated. Afterward, the weight of the solid is determined which allows calculating the concentration of the solution at the time the sample was taken.

For the clear point method, a suspension of known concentration and composition is heated until all solid is dissolved. The temperature at which no more solid is present in the vial is then considered to be the solubility temperature. This technique is employed in the commercial equipment of Technobis (Netherland) with Crystal16 and Crystalline. The Crystalline consists of 8 independent blocks for one 8 ml vial each and the Crystal16 of 4 independent blocks which can hold four 1.5 ml vials each. In the blocks, the temperature profile can be set to determine the solubility or clear point temperatures for the samples. The detailed experimental procedure for the Crystalline can be found in chapter 3 and for the Crystal16 it is described in the appendix of chapter 5.

2.4 Analysis techniques of chiral compounds

2.4.1 Polarized Light Microscopy

Chiral molecules and chiral crystals of chiral molecules can rotate plane-polarized light [17], where the direction of the rotation depends on the enantiomer. This can be used to distinguish crystals of two enantiomers in a sample by exposing them to plane-polarized light under a microscope.

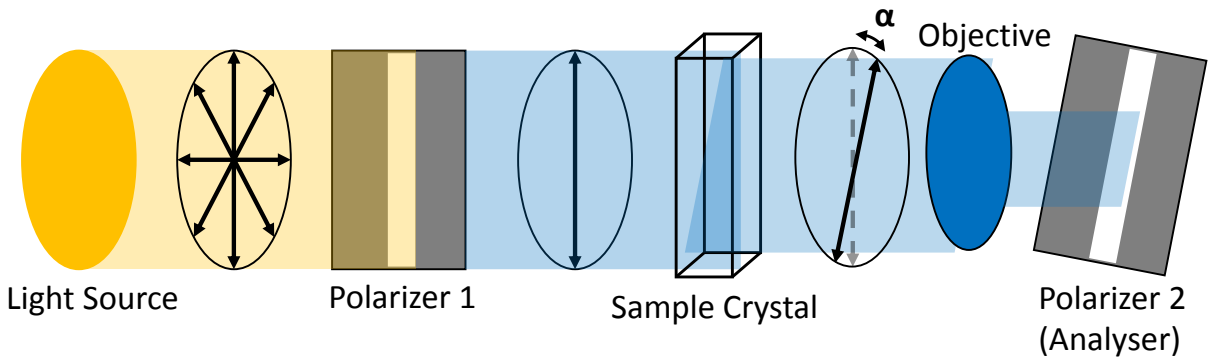

Figure 20: Schematic of the principle of a polarized light microscope.

Figure 20 shows a schematic of the principle of polarised light microscopy. The normal light from a light source is sent through a polarization filter (Polarizer 1, Figure 20), which only allows linear polarized light to pass through. The light is then sent through a chiral crystal sample. Depending on the handedness of the crystals, the light is rotated clock or counterclockwise passing through the crystals. Afterward, the rotating light passes through the objective for magnification and is then passed through a second polarization filter (Polarizer 2, Figure 20) which can be rotated in order to match the angle of the polarized light passing through the sample. If crystals of both handednesses are present in the sample they appear in a different colour depending on the position of the second polarizer, which allows distinguishing the handedness of the crystals. An example of this can be found in chapter 3 where a polarized light microscope was used to determine the enantiomeric excess of sodium bromate crystals.

2.4.2 High-Performance Liquid Chromatography (HPLC)

HPLC is an offline analytical technique that is used to separate components in a sample mixture and determine their quantity. During an HPLC measurement a mobile phase, consisting of a sample dissolved in a solvent, is transported through a column filled with a

stationary phase, consisting of solid adsorbent material, using a high-pressure pump. When the mobile phase passes through the column, the dissolved components interact with the stationary phase, resulting in the dissolved components passing through the column at a different time called retention time. The composition of the mobile and stationary phase depends on the sample which is being measured. Components that have a stronger interaction with the stationary phase will remain in the column for a longer time, while components with a stronger preference for the mobile phase pass through quickly. The retention time depends on the length of the column, where longer columns have a better separation result, as the components have more opportunities for interaction. After the components of the sample have passed through the column they are detected usually through a UV detector.

In this work, chiral HPLC [18, 19] was used to determine the chiral purity of crystallized products after a crystallization based chiral separation process. In a chiral column, chiral substances are used for the stationary phase which interacts with one enantiomer only or stronger than with the other, resulting in a separation of both enantiomers. The interaction is specific for the enantiomers, and material used for the stationary phase results in constant retention times for each enantiomer in a specific column, allowing for the handedness to be identified. The resulting peaks are represented in a chromatogram with a surface area A_i of each peak, which can be used to calculate the enantiomeric excess $E = (A_1\text{-}A_2)/(A_1+A_2)$. All the HPLC measurements in this work were conducted with Agilent HPLC instrument, where the method was adapted to the compound.

2.4.3 Raman Spectroscopy

Raman spectroscopy is based on inelastic scattering of light during an energy transfer of incident light and illuminated target molecules [20]. Laser light at 532 nm or 785 nm (near-infrared) [21] is used to bring molecules from a ground state to a higher vibration state as indicated in Figure 21, by using more energy than required for this step. Due to the excess energy used, most of the incident light is scattered by the sample molecules at the same wavelength, which is called Raleight scattering [21] as shown in Figure 21.

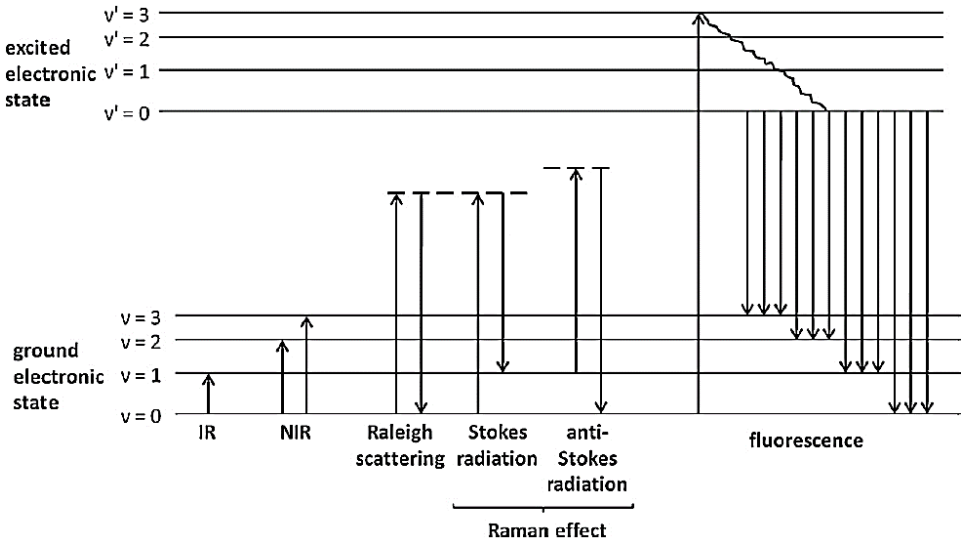

Figure 21: IR and NIR absorption, the Raman effect and fluorescence [21].

Only a very small fraction (10^{-8}) is scattered inelastically by the molecule, which indicates the exchange of energy between light and molecule, transferring it to an excited state. The inelastic scattering is called the Raman effect (Figure 21). It is shown in Figure 21 that the inelastically scattered light has a lower or higher energy level than the incident light. In case of a lower energy level, it is called Stokes radiation, while the inelastically scattered light on a higher energy level is called anti-Stokes radiation. Stokes radiation mainly occurs at lower temperatures around 20°C, while anti-Stokes is more common at much higher temperatures.

The Raman spectrum of a compound shows the difference between incident and scattered radiation in wavenumbers versus the intensity of the scattered radiation. The intensity of the Raman spectra is proportional to the wavelength of the laser and as the inelastic scattering is low a laser with a higher wavelength of around 700 nm, as in this work, is preferred. Furthermore, the intensity of Raman spectra depends on the concentration of the material, particle size and sampling volume. The amount of energy that is exchanged between the light and molecule depends on the structure of the material, the kind of bonds between the molecules and the type of material. Therefore Raman can be used to discriminate between different crystals structures of the same chemical compound for instance in distinguishing polymorphs. This also allows differentiating between crystal structures of pure enantiomers and the corresponding racemic compound, as Raman is chirally blind and does not allow do distinguish between the handedness of pure enantiomers of one compound.

Raman is a useful process analytical tool for monitoring solids or suspensions in-situ as Raman probes are very robust and allow to monitor multicomponent systems [20]. They are also highly flexible as solids, gases, and liquids can be monitored.

2.4.4 ATR-UV Spectroscopy

An Attenuated total internal reflection UV probe was used to measure the overall solution concentration in a crystallizer. This technique is based on the behaviour of incident ration which hits an interface between a transparent material with a high refractive index and a transparent medium with a lower refractive index. If the angle of the light beam hits the interface at a certain angle, an evanescent wave penetrates a path length into the solution [22] and is then fully reflected into the crystal, which is called total internal reflection. As the evanescent wave penetrates the solution a portion of the light is absorbed. This is used in ATR UV probes by placing a sapphire crystal at the top of the probe with a certain prismatic geometry to ensure the light beam hits the crystal at a right angle so attenuated total internal reflection occurs. A schematic of such a probe is shown in Figure 22, where a light beam with intensity I_0 goes into the sapphire crystal so an evanescent wave is created which interacts with the solution and the light with an intensity I, is fully reflected into the crystal. The intensities are related to the absorbance A at a given wavelength λ, which can be related to the concentration C, with the adsorption coefficient ε, using the Beer Lamberts law $A(\lambda) = \varepsilon(\lambda)Czd_P$. The number of reflections is expressed as z and the d_P is the penetration depths of the evanescent wave into the solution, which is depending on the angle of incidence, the wavelength, the temperature-dependent refractive index of the sapphire and

the solution. As the incidence angle is specific to the probe used and the wavelength is chosen from the spectra, the temperature of the solution plays an important role.

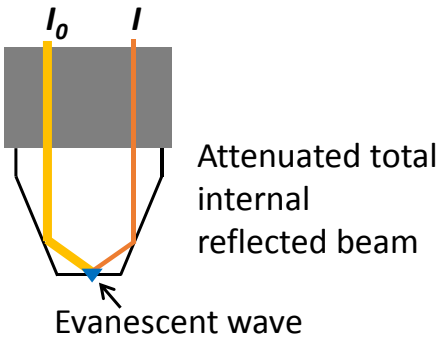

Figure 22: Schematic of an ATR UV probe head.

The ATR UV probe allows for in situ measurement of a solution property during a crystallization process and is not affected by the presence of solids due to the evanescent wave which interacts with the solution at a small penetration depth.

2.5 Application of Methods and Materials

2.5.1 Chapter 3

In chapter 3 of this thesis, antisolvent crystallization experiments are conducted with sodium bromate. The solubility of sodium bromate in water/ethanol mixtures is conducted using the clear point method, while the concentration of the solution during the experiments is determined with gravimetric analysis. The solid enantiomeric excess of the produced sodium bromate crystal samples is measured with polarized light microscopy.

2.5.2 Chapter 4

In chapter 4, enantiopure and racemic mandelic acid are separated at the eutectic point. A submergible Raman probe (RXN2, Kaiser Instruments) is used to monitor the suspension density and solid enantiomeric excess of the enantiopure and racemic mandelic acid crystals in the product crystallizer during the crystallization processes, while ATR UV is used to monitor the solution concentration. The purity of the produced product is confirmed using chiral HPLC.

2.5.3 Chapter 5

In chapter 5 a serial process configuration is investigated with regards to its general applicability for separating chiral compounds at the eutectic composition by testing the separation of enantiomers on mandelic acid, asparagine monohydrate and clopidogrel-imine at eutectic composition. For mandelic acid, the Raman was used to monitor the suspension density, while for the other two compounds suspension samples are taken and the solids are analyzed with chiral HPLC for their purity. The solubility of CPG in acetonitrile is determined using crystal 16.

2.6 References

[1] R.M. Pagni, R.N. Compton, Asymmetric Synthesis of Optically Active Sodium Chlorate and Bromate Crystals, Crystal Growth & Design 2(4) (2002) 249-253.

[2] D.K. Kondepudi, R.J. Kaufman, N. Singh, Chiral Symmetry Breaking in Sodium Chlorate Crystallizaton, Science 250(4983) (1990) 975-976.

[3] C. Viedma, Selective Chiral Symmetry Breaking during Crystallization: Parity Violation or Cryptochiral Environment in Control?, Crystal Growth & Design 7(3) (2007) 553-556.

[4] C. Xiouras, J. Van Aeken, J. Panis, J.H. Ter Horst, T. Van Gerven, G.D. Stefanidis, Attrition-Enhanced Deracemization of NaClO3: Comparison between Ultrasonic and Abrasive Grinding, Crystal Growth & Design 15(11) (2015) 5476-5484.

[5] R.R.E. Steendam, J.H. ter Horst, Continuous Total Spontaneous Resolution, Crystal Growth & Design 17(8) (2017) 4428-4436.

[6] H. Lorenz, A. Seidel-Morgenstern, A contribution to the mandelic acid phase diagram, Thermochimica Acta 415(1) (2004) 55-61.

[7] H. Lorenz, D. Sapoundjiev, A. Seidel-Morgenstern, Enantiomeric Mandelic Acid SystemMelting Point Phase Diagram and Solubility in Water, Journal of Chemical & Engineering Data 47(5) (2002) 1280-1284.

[8] D. Binev, A. Seidel-Morgenstern, H. Lorenz, Continuous Separation of Isomers in Fluidized Bed Crystallizers, Crystal Growth & Design 16(3) (2016) 1409-1419.

[9] T. Carneiro, S. Bhandari, E. Temmel, H. Lorenz, A. Seidel-Morgenstern, Shortcut Model for Describing Isothermal Batch Preferential Crystallization of Conglomerates and Estimating the Productivity, Crystal Growth & Design 19(9) (2019) 5189-5203.

[10] E. Temmel, J. Gänsch, H. Lorenz, A. Seidel-Morgenstern, Measurement and Evaluation of the Crystallization Kinetics of l-Asparagine Monohydrate in the Ternary l-/d-Asparagine/Water System, Crystal Growth & Design 18(12) (2018) 7504-7517.

[11] K. Wurges, K. Petrusevska-Seebach, M.P. Elsner, S. Lutz, Enzyme-assisted physicochemical enantioseparation processes-Part III: Overcoming yield limitations by dynamic kinetic resolution of asparagine via preferential crystallization and enzymatic racemization, Biotechnol Bioeng 104(6) (2009) 1235-9.

[12] K. Petruševska-Seebach, A. Seidel-Morgenstern, M.P. Elsner, Preferential Crystallization of l-Asparagine in Water, Crystal Growth & Design 11(6) (2011) 2149-2163.

[13] A.S. Dunn, V. Svoboda, J. Sefcik, J.H. ter Horst, Resolution Control in a Continuous Preferential Crystallization Process, Org. Process Res. Dev. 23(9) (2019) 2031-2041.

[14] M.L. Maarten W. van der Meijden, Edith Gelens, Wim L. Noorduin, Hugo Meekes, Willem J. P. van Enckevort, Bernard Kaptein, Elias Vlieg and Richard M. Kellogg, Attrition-Enhanced Deracemization in the Synthesis of Clopidogre l - A Practical Application of a New Discovery, Org. Process Res. Dev. 13(6) (2009) 1195-1198.

[15] W.L. Noorduin, P. van der Asdonk, A.A.C. Bode, H. Meekes, W.J.P. van Enckevort, E. Vlieg, B. Kaptein, M.W. van der Meijden, R.M. Kellogg, G. Deroover, Scaling Up Attrition-Enhanced Deracemization by Use of an Industrial Bead Mill in a Route to Clopidogrel (Plavix), Org. Process Res. Dev. 14(4) (2010) 908-911.

[16] J.H. ter Horst, C. Schmidt, J. Ulrich, Fundamentals of Industrial Crystallization, Elsevier B.V.2015.

[17] J.W. Mullin, Crystallization, in: J.W. Mullin (Ed.), Crystallization (Fourth Edition), Butterworth-Heinemann, Oxford, 2001, pp. 536-575.

[18] K.G. Feitsma, B.F.H. Drenth, Chromatographic separation of enantiomers, Pharmaceutisch Weekblad 10(1) (1988) 1-11.

[19] H. Lorenz, A. Seidel-Morgenstern, Processes to separate enantiomers, Angew Chem Int Ed Engl 53(5) (2014) 1218-50.

[20] K. Bakeev, Process Analytical Technology: Spectroscopic Tools and Implementation Strategies for the Chemical and Pharmaceutical Industries, 2nd Edition, 2010.

[21] T. De Beer, A. Burggraeve, M. Fonteyne, L. Saerens, J.P. Remon, C. Vervaet, Near infrared and Raman spectroscopy for the in-process monitoring of pharmaceutical production processes, International Journal of Pharmaceutics 417(1) (2011) 32-47.

[22] P. Billot, M. Couty, P. Hosek, Application of ATR-UV Spectroscopy for Monitoring the Crystallisation of UV Absorbing and Nonabsorbing Molecules, Org. Process Res. Dev. 14(3) (2010) 511-523.

3 Total Spontaneous Resolution using Continuous Antisolvent Crystallization

Antisolvent crystallization is a widely applied process in pharmaceutical industry due to its high yields and short process duration. However, it hardly has been reported to be used for chiral resolution or deracemization as it is generally thought that due to the high supersaturations produced during the process, especially at the mixing points, chirally unselective primary nucleation rather than enantioselective secondary nucleation would occur. Here, we demonstrate that enantioselective secondary nucleation is the dominant nucleation mechanism in seeded fed-batch and continuous antisolvent crystallization of sodium bromate, leading to a control over the produced handedness. In addition, seeded fed-batch antisolvent deracemization of Clopidogrel shows close to enantiopure crystalline product, retaining the chirality of the seed crystals.. This work reveals that, unlike generally thought, secondary rather than primary nucleation is dominant in antisolvent crystallization, even at such high local supersaturations usually occurring in this process. A dominance of secondary nucleation will strongly affect nucleation control strategies in industrial crystallization processes.

3.1 Introduction

A large fraction of pharmaceuticals is chiral. Two enantiomers of a chiral molecule have identical physico-chemical properties such as solubility and melting point, but may exhibit different pharmaceutical activities [1, 2]. While one enantiomer acts as an active pharmaceutical, the other could be inactive or even harmful [3, 4]. Control over the production of the desired enantiomer is therefore of importance for pharmaceutical industry. However, as industrial asymmetric synthesis routes are often unavailable, the synthesis process generally results in a racemic mixture containing both the preferred and unwanted enantiomers in equal amounts and enantiopurity must be achieved afterwards. Crystallization-based chiral separation is a highly selective method to achieve enantiopurity, where preferential crystallization is among the most common methods [5-7].

During a preferential crystallization process, seed crystals of the desired handedness are added to a supersaturated solution, leading to the formation of the desired handedness.

To increase the yield of preferential crystallization, simultaneously a racemization reaction can be applied in the solution, preserving the 50/50 ratio of both enantiomers in solution while selectively removing the preferred enantiomer from solution through crystallization. By using a racemization in solution the yield can be theoretically increased to 100% as all molecules of the undesired handedness can be converted into the desired one and crystalized [8]. Another appealing aspect of deracemization is that only a feed solution and one crystallizer are needed since the solution remains at racemic composition at all times. As the solution remains racemic, the risk of primary nucleating the undesired handedness is very low, making the process more robust against flowrate fluctuations or temperature changes [9-13]. If a continuous feed of fresh saturated solution and a product removal are added, continuous processing is achieved. Thus, deracemization processes are a good target to

implement continuous preferential crystallization processes. In order to induce the supersaturation in the crystallizer, usually a cooling crystallization is used, running the crystallizer at a lower temperature than that of the saturated feed solution. This way of inducing supersaturation is very commonly applied in industry [14]. Sodium Bromate as model compound, a continuous total spontaneous resolution using cooling crystallization has been reported [15]. There the sodium bromate was preferentially crystallized through cooling crystallization from a saturated solution in the presence of enantiopure seed crystals. Furthermore sodium bromate and sodium chlorate experiments have been conducted highlighting the importance of the secondary nucleation mechanism to crystallize a specific handedness [16]. However, depending on the growth rate of the compound, cooling crystallization can take long period of time and it requires the change of temperature which can become an issue especially for thermally sensitive compounds [17, 18].

A lot of research is currently conducted towards Viedma ripening and temperature cycling deracemization processes for chiral purification [10, 19-31]. However, to the best of our knowledge continuous configurations have not been reported for these processes. Considering the drive of the pharmaceutical industry towards continuous manufacturing, there is a strong demand for continuous deracemization processes. However, the problem with continuous antisolvent crystallization is that primary nucleation rather than secondary nucleation occurs during the crystallization process due to the high supersaturation achieved; especially at the mixing point. Since the primary nucleation mechanism is not chirally selective, crystals of both handedness are getting crystallized resulting in chirally impure product. In this work, we aim to determine whether the range of deracemization process configurations can be extended to include continuous antisolvent crystallization-enhanced deracemization. Antisolvent crystallization processes produce a high yield and enable a fast crystallization of the model compound. Furthermore can they be applied to thermally sensitive compounds, as the process can be performed isothermally at large concentration differences between feed and crystallizer vessels. The technique is commonly applied in pharmaceutical industry [32-34]. It will be investigated if and to which extend secondary nucleation from enantiomerically pure seed crystals can be achieved and controlled. The chosen model compound, sodium bromate, is chiral in the solid state but achiral in solution [35]. This behaviour mimics infinitely fast solution racemization [15] and therefore be used to investigate if the initial seed purity in a antisolvent crystallization can be preserved through secondary nucleation. A fast racemization ensures the enantiomers in solution remain at a racemic ratio during the crystallization process, which prevents primary nucleation of the undesired handedness and ensures pure product is produced. Combining this method with antisolvent crystallization, which allows for a fast isothermal process, would extend the range of existing deracemization processes and provide interesting applications in the pharmaceutical industry. Also deracemization processes using sodium bromate and sodium chlorate have been conducted in the past by Viedma [36], a suspension only containing 50/50 mix of each handedness was over time turned into an enantiopure suspension through grinding. The mechanism was then later shown to also work for organic compounds [10], where in this work the sodium bromate is used for an initial investigation to determine feasibility which can later be extended to organic compounds.

After determining the phase diagram for antisolvent crystallization of sodium bromate in water using the antisolvent ethanol, the performed fed-batch antisolvent crystallizations are tested on their feasibility for deracemization. Following the results of the fed-batch process a continuous process is designed, based on the experimental results of the fed-batch studies, to investigate the robustness of the process with regards to enantiomeric excess of the product at varying antisolvent fractions and residence times. This allows to investigate if and under which conditions the secondary nucleation mechanism in such a process can be maintained and controlled.

3.2 Experiments

For the sodium bromate (VWR, 99%) fed-batch and continuous experiments a solvent mixture of double filtered water (Milli-Q gradient, Millipore SAS, solvent) and ethanol (VWR, 99%, antisolvent) was used at different fractions of antisolvent x_{AS}. In order to confirm the process for organic substances, initial fed-batch studies are conducted using clopidogrel-imine (Syncom, 99%) with a solvent mixture of acetonitrile (VWR, 99%) and water with an initial 4 v% 1,8-Diazabicyclo[5.4.0]undec-7-ene (DBU) fraction which serves as racemization catalyst.

3.2.1 Solubility

The solubility of sodium bromate in solvent mixtures of water and ethanol, was determined using a crystalline (Technobis, the Netherlands). Vials with mass-based antisolvent fractions x_{AS} =10, 20, 30, 50 m% and various concentrations of sodium bromate between 30 to 300 mg/ml were prepared. Due to the high density of sodium bromate in comparison with an organic molecule, overhead stirrers with a stirring speed of 1200 rpm were used. Each vial then underwent 4 temperature cycles. At a high temperature for 30 minutes all solid was dissolved, after which the sample was cooled to a low temperature at a rate of 0.3 °C/min to allow the sample to crystallize out. Once the low temperature was reached the sample was held again for 30 minutes to allow for crystallization to proceed. Then, the sample was heated up to the high temperature with a heating rate of 0.3 °C/min and a new cycle begins. During the cycles, time stamped pictures of the samples were taken by the camera of the instrument every 5 seconds. Above a specific temperature during the heating step, no more crystals were visible on the pictures. This temperature is referred to as the clear point temperature and is a good estimation of the saturation temperature of the sample. For each sample of know concentration, 4 temperature cycles are run, leading to 4 clear points temperature measurements. If these clear point temperatures were within ± 3°C margin, an average clear point temperature was determined for the sample, otherwise the run was discarded and a new sample was prepared.

3.2.2 Fed-batch antisolvent crystallization experiments

The schematic of the fed-batch antisolvent crystallization set up is shown in Figure 23, where the black lines represent the batch set up consisting of a crystallizer (middle, Fig. 1) for the saturated starting solution and an antisolvent feed tank connected to the crystallizer through a peristaltic pump (Watson Marlow, 520u). Both vessels were jacketed and temperature

controlled at 20°C through a Pt100 probe (Radleys) connected to a heater chiller (Lauda pro line) .

An initial solution of 500 ml, containing water and 7 v% antisolvent (Ethanol), at a concentration of 274 mg/ml sodium bromate was prepared in the jacketed crystallizer (Figure 23, middle). The the initial antisolvent fraction was chosen to prevent a very steep decrease in concentration with very small antisolvent fractions starting from the pure solvent saturated solution. The solution was heated up to 30 °C and kept at that temperature for 20 minutes to ensure a clear solution. After cooling the clear solution back to the saturation temperature of 20.0 °C, a given mass m_S of seed crystals of a specific handedness (enantiomeric excess E_i = 96.1%) and were added. A constant suspension temperature throughout the process was ensured through a thermostat bath (Lauda proline) connected to a Pt100 probe submerged in the suspension. The added ethanol throughout the fed-batch process was kept at 20 °C in the antisolvent feed vessel through a heater chiller, in order to prevent local temperature changes through mixing effects.

The fed-batch antisolvent crystallization experiment was initiated by starting the flow of antisolvent F_{AS} into the crystallizer using a peristaltic pump (Watson Marlow, 520u). After reaching the target antisolvent fraction of x_{AS}=50 v%, the suspension was filtered and the solid product dried for analysis. During the experiment, suspension samples were filtered and the obtained crystals were analysed for their enantiomeric excess (see Purity Determination). The solute concentration in the suspension liquid phase of the sample was determined using a gravimetrical method. For this, the solvent was evaporated from the solution sample using an oven at 40 °C. From the remaining solid weight and the evaporated solvent weight, the solvent and solute masses were determined. The antisolvent fraction was determined through the pump calibration of the antisolvent feed pump at each point in time during the fed batch process.

In order to reduce possible primary nucleation due to local supersaturations at the point of antisolvent addition, the suspension was vigorously stirred at 800 rpm. To prevent fouling, the inlet tube of antisolvent was placed above the suspension with the antisolvent dropping into the stirred suspension at addition. Baffles were used to prevent the formation of a vortex and to ensure the suspension to be well-mixed. In addition, the particle size distribution of the product and seed crystals was determined (Mastersizer 3000, Malvern).

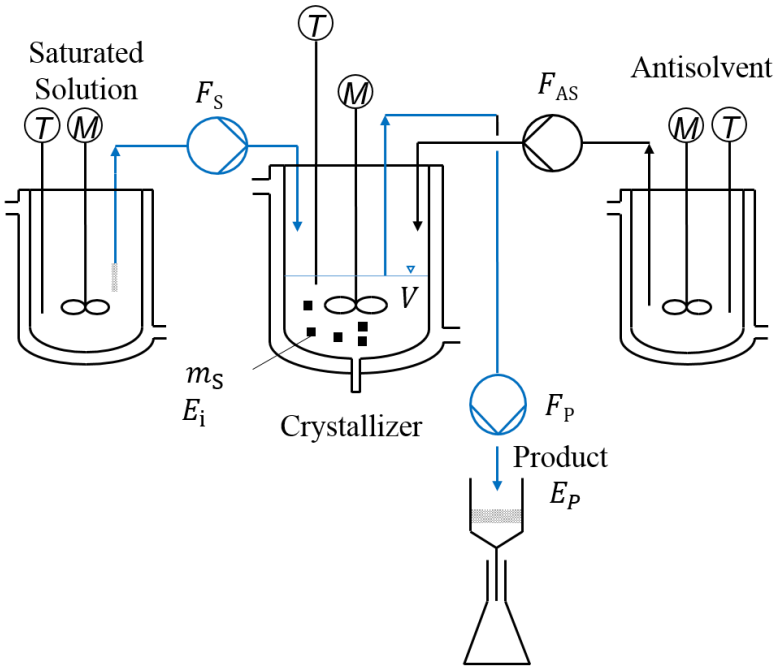

Figure 23: Schematic of the fed–batch (black lines) and continuous (black and blue lines) antisolvent crystallization set ups with saturated solution feed tank (left); crystallizer (middle), suspension removal and filtration (bottom), and antisolvent feed vessel (right). In the fed-batch configuration antisolvent is added with a feed flow rate F_{AS} to the crystallizer containing a suspension of crystals of a single handedness. In the continuous configuration both a solution feed flow rate F_S and an antisolvent feed flow rate F_A are continuously added to the crystallizer while a continuous suspension flow F_P is leaving the crystallizer.

The influence of antisolvent addition rate F_{AS}, seed crystal amount m_S and enantiomeric excess E_i of the seed crystals on enantiomeric excess E_P of the product crystals, productivity P and yield X was examined.

3.2.3 Continuous Antisolvent Crystallization experiments

The schematic of the continuous antisolvent crystallization set up (Figure 1) was realized by extending the fed-batch with a continuous solution feed and suspension outflow which are shown in blue. For the saturated solution feed, a 5 l feed vessel was added to the set up (Figure 23, left). A pump (Watson Marlow, 530) was used to pump the saturated solution into the crystallizer. The inlets in the crystallization vessel were positioned such that the incoming solution and antisolvent did not get in direct contact with the baffles or walls of the crystallizer before entering the suspension, preventing fouling. The continuous product outflow was realised as a level control by fixating the outflow tubing (MasterFlex, d_i = 6.4 mm) to a baffle at a defined height so that the suspension volume was 0.5 l under operating conditions. A peristaltic pump (MasterFlex, Pump Drive) at a high rotation rate was used to constantly extract slurry into the filter. During the crystallization process, high stirring rates of 800 rpm were used to prevent the accumulation of solids in the crystallizer. While a pump calibration is conducted for the pumps used, the resulting flowrate is affected by the position of the tubing which can change from one experiment to another. In order to account for the error and determine the flowrate for each experiment precisely the volume of saturated solution and antisolvent is measured prior to addition in the feed vessels. The duration of an

experiment is measured and the remaining volume in the vessels after it has concluded, which allows for the calculation of the flowrate during each experiment

For each experiment, 500 ml of a starting sodium bromate solution in water and antisolvent at a particular antisolvent fraction was prepared in the crystallizer at 30 °C after which it was cooled down to its saturation temperature of 20.0°C. Then, the saturated clear solution was seeded with seed crystals (enantiomeric excess E_i = 95.2%). A seed mass of 10 g/l of the same seeds was used for each experiment.

The continuous experiment was started by starting the pumps that controlled the ingoing feed flows of solution and antisolvent and the outgoing suspension flow. The feed flow rates were chosen in such a way that the antisolvent fraction of the initial solution in the crystallizer was maintained. A saturated sodium bromate solution at a concentration C_0 of 350 mg/ml at 20 °C was used as feed while pure ethanol was used as antisolvent. The experiment duration was at least 7 residence times. The residence time was determined by $\tau = V/F$ were V is the constant volume of the suspension in the crystallizer and F the overall incoming flow rate. During each experiment, suspension samples were taken with the same procedure as in the fed-batch antisolvent crystallization experiments.

The influence of the antisolvent fraction x_{AS} in the crystallizer suspension and residence times on enantiomeric excess of the product crystals were examined. For the experiments with different residence times, the overall flowrate was changed at constant ratio of feed solution and antisolvent flow rates. We estimated that the antisolvent fraction in the liquid phase of the suspension did not vary more than 1.5 v% from the target antisolvent fraction.

During the experiments C1-C3, the overall feed flow $F = F_S + F_{AS}$ is kept constant (20 ml/min) and with that the residence time (between 24-26 min), where the differences are due slight variations in the overall flowrates. At the same time the flow rate of the saturated solution F_S and antisolvent F_{AS} are changed respectively in each experiment to vary the antisolvent fraction (Table 2, experiments C1, C2 and C3) in each experiment.

For continuous experiments C4 and C5 the overall flowrate F is varied, while the overall antisolvent fractions x_{AS} = 20 v% is kept constant, investigating the influence of residence time on the process, as at a higher flow rate F the residence time $\tau = V/F$ becomes shorter.

3.2.4 Purity determination

Sodium bromate is achiral in solution and chiral in the solid state, thus standardised methods such as HPLC cannot be used for the determination of the handedness of the crystalline product. Sodium bromate crystals are sensitive to polarized light and therefore they can be analysed using a microscope equipped with polarized light. A slurry sample was taken from the crystallizer using a syringe and subsequently filtered and dried. The crystal sample was then suspended in a clear saturated solution of sodium bromate in water and left to grow overnight through slow evaporation of water under conditions at which no further nucleation occurred. Under polarized light, crystals of one handedness appeared orange, while those of the other handedness appeared blue. By changing the polarization angles, the colours of each handedness crystals are reversed (figure 2).

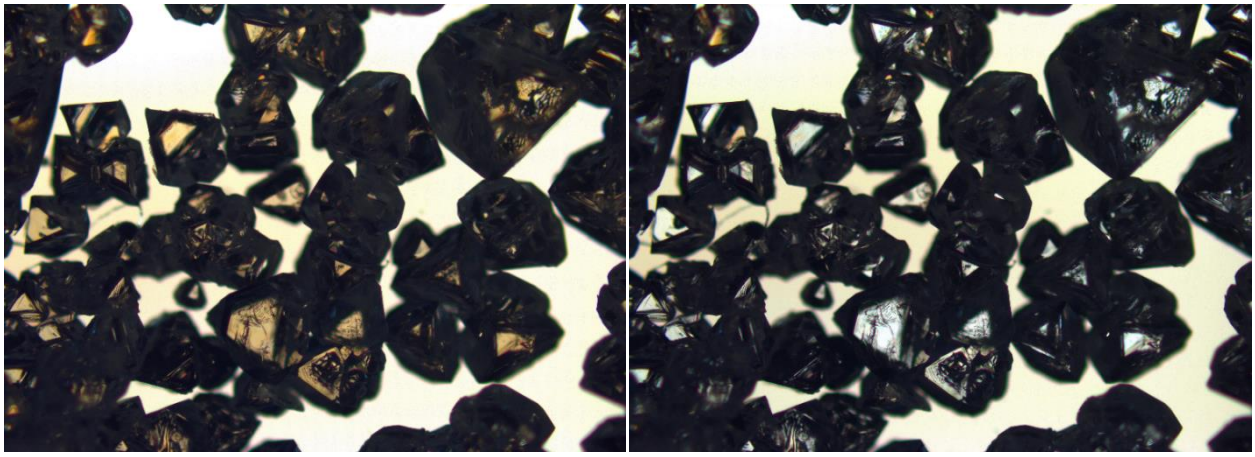

Figure 24: Sections of pictures of product crystals seen under a microscope with polarization angles of 100° (left) and 70° (right). The determined number-based enantiomeric excess of the product on the entire set of pictures was determined to be *E*=95%.

For all solid samples the same microscope (Leica DM6000M) was used at the polarization angles of 100° and 70° and pictures were taken with both polarizations. For both pictures, the crystals of each handedness were then counted. Each picture rendered a set of 200-400 crystals. For each purity sample, 2 to 3 sets of crystal pictures were analyzed resulting in 400-1000 crystals counted per solid sample to ensure a high statistical value. The crystals with an orange (N_O) and blue (N_B) colour are counted for one of the two polarization angles in all pictures to determine the enantiomeric excesses E_1 and E_2 through equation 1:

$$E = \frac{N_O - N_B}{N_O + N_B} * 100 \quad (1)$$

Although the crystals usually changed colour upon the inversion of the angle of polarized, typically 10-24 crystals did not, in a sample of at least 400 crystals. This results in a variation of around 2.5-6% in the enantiomeric excesses E_1 and E_2. Therefore, the average of E_1 and E_2 was used as the final enantiomeric excess of the solid sample.

3.3 Results

Sodium bromate is a water soluble salt which is achiral in solution but crystallizes as chiral crystals (thanks to the chiral space group $P2_13$ [37]) which exhibit rotation in plane polarized light (Figure 24) [37]. Being achiral in solution but crystallizing in distinguishable handedness mimics a conglomerate forming systems with a very fast racemization kinetic in a solvent, making it an ideal compound for antisolvent deracemization studies. Sodium Bromate has a very high solubility in water, while being highly insoluble in most alcohols.

3.3.1 Antisolvent crystallization phase diagram

Sodium bromate is known to be readily soluble in water while the solubility in ethanol is very low [15, 36]. Therefore, we identified ethanol as a potential antisolvent for the antisolvent crystallization of sodium bromate from solutions in water. Figure 3 shows the temperature dependent solubility of sodium bromate at various antisolvent fractions. These solubilities are obtained by measuring clear point temperatures using various concentrations of sodium bromate in the samples at a particular antisolvent fraction. The vertical dashed red line in

figure 3 at a temperature of 20°C indicates the corresponding solubilities of sodium bromate at various antisolvent fraction. While the solubility of sodium bromate in pure water at 20°C is C^* = 370.5 g/l, it reduces with increasing antisolvent fractions to C^* = 188.9 g/l (x_{AS} = 12.4 %), C^* = 97.7 g/l (x_{AS} = 24 %), C^* = 59.4 g/l (x_{AS} = 35.2 %), up to an almost tenfold decrease of C^* = 19.5 g/l in a solvent mixture with 35.2 v% ethanol, indicating a strong non-linear solubility decrease due to the antisolvent. These solubilities are used to construct a phase diagram showing an antisolvent fraction dependent solubility at a constant temperature (Figure 26).

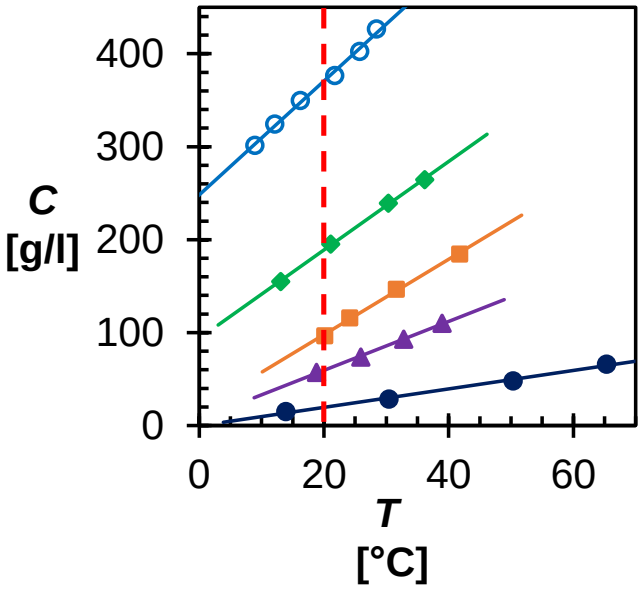

Figure 25: Temperature dependent solubilities of Sodium Bromate in water - ethanol mixtures with 0 (blue cycles), 12.4 (green diamonds), 24 (orange squares), 35.2 (purple triangles) and 55.8 v% ethanol (dark blue circles). Sodium Bromate solubility values at 20°C are highlighted by the intercept of the solubility lines with the red line.

Figure 4 shows that the sodium bromate solubility decreases strongly non-linearly with the antisolvent fraction. Using the phase diagram shown in Figure 25, isothermal antisolvent crystallization processes can be conducted with sodium bromate using ethanol as antisolvent.

3.3.2 Fed-batch antisolvent crystallization

It was chosen to perform a number of seeded fed-batch antisolvent crystallization experiments for sodium bromate, in order to determine product yield and enantiomeric excess. During such fed-batch antisolvent crystallizations the antisolvent is added with a certain flow rate to the saturated solution containing enantiopure seeds until a specific antisolvent fraction is reached. Fed batch experiment 1 is exemplified in Figure 26. The fed-batch process starts with a saturated solution in the crystallizer (C_0 = 273 mg/ml, x_{AS} = 7%, blue circle figure 4). Since the sodium bromate solubility in pure water is very high, we used a saturated solution with an antisolvent fraction of x_{AS} = 7% as initial solution. This antisolvent fraction allowed us to use an initially saturated solution containing 20 mg/ml sodium bromate crystal seeds of an almost single handedness (enantiomeric excess E = 96.1 %) while the suspension density towards the end of the process at x_{AS} = 50.1% remained sufficiently low around 200g/l or 17w%. Upon starting the process, a constant flow of antisolvent is pumped

into the crystallizer leading to a dilution of the initial concentration following the operating line in the direction of the blue arrow in Figure 26. At the same time the solubility is decreasing non-linearly, following the solubility line. As the solubility becomes lower than the overall concentration product immediately starts crystallizing. Experiment 1 is stopped when arriving at an antisolvent fraction of x_{AS} = 50.1 v%.

The maximum amount that can crystallize out at this antisolvent fraction is given by the concentration difference between the overall concentration C_M = 147 mg/ml (blue square, Figure 26) and the solubility C^* = 21.8 mg/ml. The actual concentration in the solution is measured to be C = 31 mg/ml (green cycle at 50.1 % x_{AS}, Figure 26), slightly higher than the solubility. Using the measured concentration, solubility, and the concentration at the operating line C_M (Figure 26, blue rectangle), the yield can be calculated as the actually obtained amount over maximum amount $X = C_M\text{-}C/C_M\text{-}C^*$ at the antisolvent fraction 50.1 %. For experiment 1 a close to maximum yield of X = 92.4% is obtained. Figure 5 shows the measured enantiomeric excess E of the crystals in the suspension remains high throughout the experiment. The process starts with an enantiomeric excess in the seed material of 96.1%, while the final is determined at E = 95.6%, showing that the handedness can be retained. The productivity of for a fed-batch process can be calculated using the process time t and the concentration difference between operating line C_M and solution C.

$$P = \frac{C_M(t) - C(t)}{t} \tag{2}$$

Figure 29 shows the productivities of the fed batch process with the overall productivity P (blue diamonds, Figure 29) and productivity of enantiopure product produced P_E (green diamonds, Figure 29) as a function of the antisolvent fraction during experiment 1. At small antisolvent fraction the change in solubility is very high as shown by the red solubility line in Figure 26, which leads to large concentration differences between operating and solubility line and therefore high productivities. As the antisolvent fraction over time increases the productivity goes down to a final value of 45 g/lh which is quite high in comparison to other processes like preferential crystallization where the values are between 2-8 g/lh for batch processes, as shown in a soon to be published book by Nima and Zoltan (chapter 12) . The high yield and productivity show that a large quantity of product could be produced, while the handedness of the seed crystals could be preserved throughout the process, leading to highly pure target product.

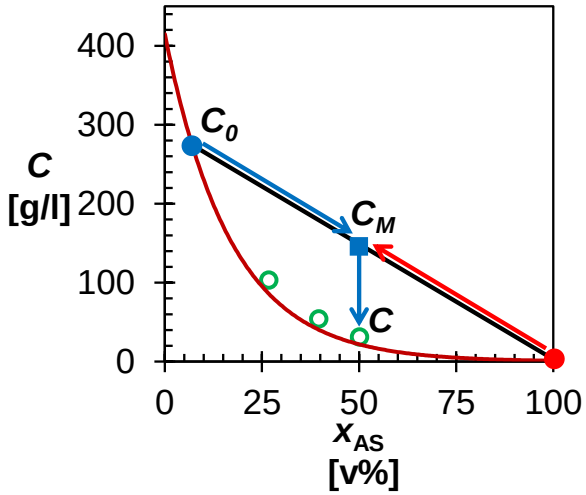

Figure 26: The solubility of sodium bromate at 20 °C (red line) as a function of the antisolvent fraction x_{AS} in water. The operating line (black line) of the fed-batch experiment 1 starts at a saturated solution at an antisolvent fraction x_{AS} = 7 v% (blue circle) to which 100% pure antisolvent (red circle) is added with a constant rate until an antisolvent fraction x_{AS} = 50.1 v% (blue square) is reached. The concentrations measured during the process are indicated by green circles.

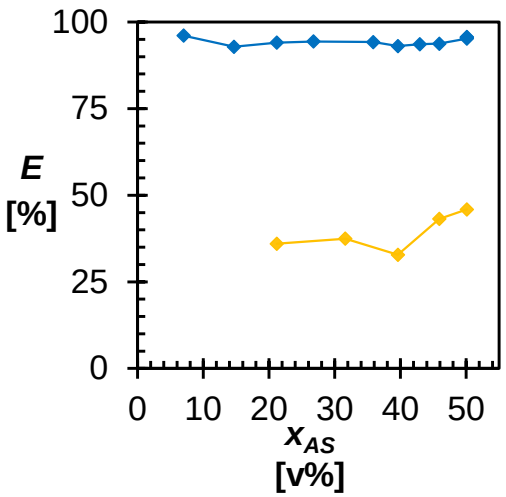

Figure 27: Product purity (blue) measured over the course of fed-batch antisolvent crystallization experiment 1 (blue) and of the unseeded experiment 5 (yellow).

Looking at the measured concentrations throughout the process shown in Figure 26 (green cycles) the yield remains high throughout the experiment as the concentration remains close to the solubility. This is represented through the overall bulk supersaturation ratio $S = C/C^*$ for each concentration measured in the crystallizer during the process at the respective antisolvent fraction. The ratio can be determined from the measured concentrations during the process and the equilibrium solubility at the prevailing antisolvent fractions (Figure 26, green circles). The bulk supersaturation ratios during the experiment are 1.2 (x_{AS} = 26.8%), 1.3 (x_{AS} = 39.6%) and 1.4 (x_{AS} = 50.1%). In comparison the largest metastable zone width during the solubility experiments reached, was at a clear point temperature of 65°C (66 mg/ml) and a cloud point temperature of 40°C (39 mg/ml) at a supersaturation of 1.7. Therefore the reached supersaturations in this experiments are not close to the supersaturation, where primary nucleation would be expected. In addition the measured enantiomeric excess during the experiment shown in Figure 27 also remains high throughout, also at the beginning of the process, where the local supersaturations are especially high due to the large drop in solubility at low antisolvent fractions shown in Figure 26 (red line). This shows that the secondary nucleation mechanism is dominant in this process allowing for the handedness to be retained. Throughout the experiment the overall productivity and that of the pure enantiomer produced remain very close to one another as shown in Figure 29. The orange line (Figure 29), represents the theoretical productivity $P_{th} = C_M(t)-C^*(t)/t$ as difference between operating line and solubility, dived by process time. While the overall productivity (blue diamonds, Figure 29) is close to the theoretical productivity especially at higher antisolvent fractions but diverges from the theoretical value at antisolvent fractions between 15-30 v%, indicating a

lower yield during this time of the process. The productivity represented by the red line (Figure 29) is the minimum productivity of pure enantiomer of this process if only racemate were to be produced. It is observed that the achieved productivities are much higher than the minimum value shown here.

While the productivity and yield are important values to analyse and compare processes with regards to their efficiency, loss of product $L = C(t)/t$ (green line, Figure 29), which can be determined as the remaining concentration of product in the solution, over process time, gives an important indication of the efficiency of the process. Initially at low antisolvent fractions the productivity is high but there is still a large amount of solids remaining in the solution. With increasing antisolvent fraction the loss decreases as more product is crystallized. A balance between loss and productivity must be found at which a process can be operated so that the productivity remains high, yet the loss is acceptable. This ration however also depends on the value of the product vs the cost of the antisolvent needed to reduce the loss.

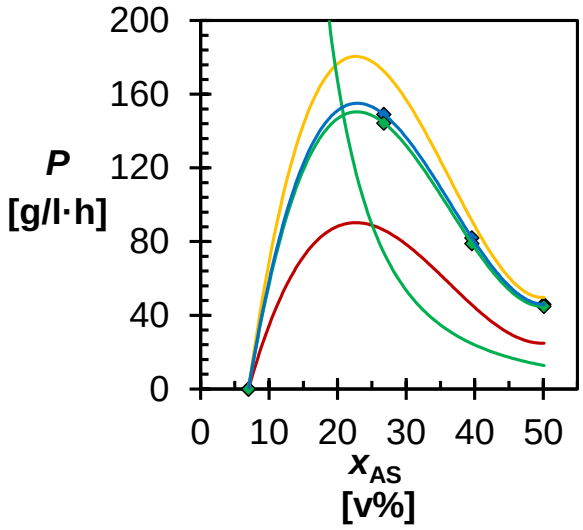

Figure 28: Overall process productivity P during the fed-batch antisolvent crystallization in experiment 1 (blue diamonds and solid line) compared to the theoretical productivity P_{th} (yellow line), the productivity the target enantiomer produced P_E (green rectangles and solid line) and the minimum productivity if all product where to be racemic (red line).

In order to determine the importance of seeding, an unseeded experiment is conducted and investigated. Even in an unseeded experiment no racemic product is obtained but rather a product with a substantial enantiomeric excess (E_P = 45 [illegible]) which is quite high considering no seeds are added. After a limited number of primary nucleation events at the start, enantioselective secondary nucleation very quickly takes over as the dominant nucleation mechanism, with the initially primary nucleated crystals serving as seeds for secondary nucleation. To exclude antisolvent addition rate a seeded fed-batch experiment is performed at the same process conditions (experiment 2, Table 1), yielding a high enantiomeric excess E = 86.6% and yield. In the unseeded experiment an overall yield X = 88 % is reached, similar to experiment 1. Enantiomeric excess is much lower in the unseeded experiment compared to the seeded once. As seen in Figure 27 the value for the enantiomeric excess in the

unseeded experiment (orange diamonds, Figure 27) is relatively stable, indicating that the enantiomeric excess of the first nucleated crystals is preserved.

The main parameter for control over the handedness of the crystals in the fed-batch experiments is the addition rate of antisolvent. If the antisolvent addition rate is increased, the local supersaturation at the mixing point is increased, which increases the likelihood of excessive primary nucleation of the undesired handedness. Additional fed-batch antisolvent crystallization experiments with antisolvent addition rates of F_{AS}= 6 and 20 ml/min (Table 1, experiment 2 and 3) were performed, with the results shown in Table 1 It is shown that beyond a certain threshold addition rate the local supersaturations becomes sufficiently high to induce primary nucleation resulting in a loss of control over the handedness of the crystalline product. This was shown in experiment 3 (Table 1) enantiomeric excess to E_P = 78.5 % in comparison to E_S =89.3 %.. However, all the conditions led to a significant increase in the final product purity compared to the unseeded experiment 4. As the total duration of experiment 3 is reduced to less than 30 min at the antisovlent additon rate shown in Table 1, further shortening the experimental duration is possible, but would make sampling difficult due to the short process time. The fed-batch experiments show that seeded fed-batch antisolvent crystallization processes can be used as a deracemization process to produce a desired handedness.

Table 1: Overview of experimental conditions (antisolvent addition rate F_{AS}, seed mass m_S, enantiomeric excess E_S of the seed material) and results (enantiomeric excess E_P of product crystals and the yield X) of the fed batch antisolvent crystallization experiments.

Experiment	Process conditions			Experimental results	
	F_{AS} [ml/min]	m_S [g]	E_S [%]	E_P [%]	X [%]
1	3	10	96.1	95.6	92.4
2	6	10	88.5	86.5	84.01
3	20	10	89.3	78.5	88.5
4	6	0	-	32.6	88.0

3.3.3 Continuous Antisolvent Crystallization

Following the results of the fed-batch experiments, continuous antisolvent crystallization experiments are conducted. In the continuous antisolvent crystallization experiment C1, the crystallizer initially contained a starting solution with x_{AS} = 50 v%, saturated at C^* = 21.7 mg/ml (4, Figure 29) and almost enantiopure seed crystals E = 95.2% at a suspension density of 10 g/l. With these starting conditions, the process quickly arrives at the steady state value of the concentration $C(t)$ as shown in Figure 30 (green circles). Upon starting the process, saturated solution (1, Figure 29) and antisolvent (2, Figure 29) are pumped into the crystallizer with flow rates of respectively F_{AS} = 9.9 and F_S = 9.4 ml/min resulting in an antisolvent fraction x_{AS} = 51.4 v% (target fraction: x_{AS} = 50 v%) and a residence

time τ = 26min. The antisolvent and saturated solutions, represented through the mixing point (3, Figure 29) on the dilution line of the phase diagram, are mixed with the suspension in the crystallizer. The concentration on the operating line at the mixing point is C_M = 170.3 mg/ml, from which the crystallization occurs leading to the concentration $C(t)$ = 29.4 mg/ml at the operating point (4, orange circle in Figure 29). The resulting yield of X = 93.9% aligns with the low bulk supersaturation of S = 1.45.

The enantiomeric excess measured during the process is plotted in Figure 30 (blue diamonds) and remains high throughout the process with a final value of E = 92.3%. The overall productivity of the experiment C1 is determined to be $P = (C_M\text{-}C)/\tau$ = 322 g/lh (Figure 31, blue diamonds) with the productivity of enantiopure product P_E (Figure 31, green diamonds) being almost the same due to the high enantiomeric excess. The figure shows that the productivity is constant throughout the process showing that a steady state is reached soon after the process start and the process is very stable. Comparing the overall productivity P (blue diamonds, Figure 31) with the theoretical P_{th} = 346 g/lh (yellow line, Figure 31), it is shown that they are very close, as indicated by the yield.

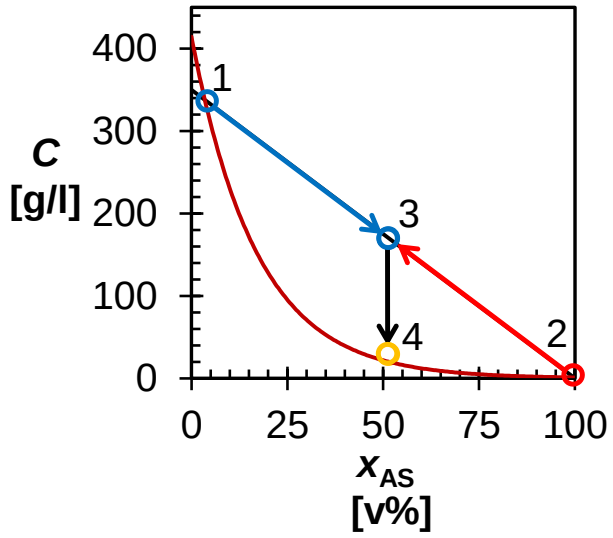

Figure 29: Phase diagram of sodium bromate in water-ethanol mixtures at 20 °C, representing the continuous antisolvent crystallization experiment C1 at x_{AS}=51.4v%; τ = 26 min; Solution feed flow composition (1), pure antisolvent feed flow composition (2), mixing point of both feed streams at x_{AS}=51.4% (3) on operating line , measured solution concentration within the crystallizer solution in steady state (4).

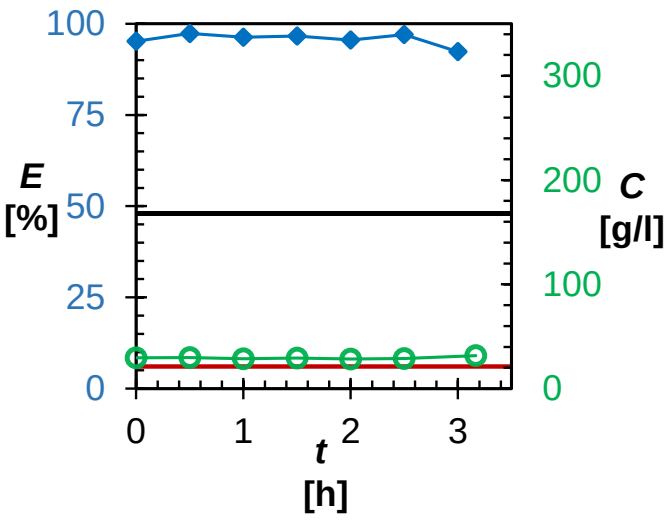

Figure 30: Product purity (blue lozenges) and concentration (green circles) of continuous antisolvent deracemization experiment 1 at 20°C, a residence time of 26 min and constant antisolvent fraction of 51.4 v%. (Experiment C1, Table 2) with the overall concentration (black line) and the solubility (red line).

At the same time the productivity of the pure enantiomer P_E is far away from the red line (Figure 31), which represent the productivity of pure enantiomer if racemate was to be produced. As the antisolvent fractions remains constant throughout the process, the product loss $L = C/\tau$ (green line, Figure 31) of the remaining solids in solution flushed out also remains unchanged. The antisolvent fraction of 51.4% allows for a high productivity at a low loss of L = 49 g/lh.

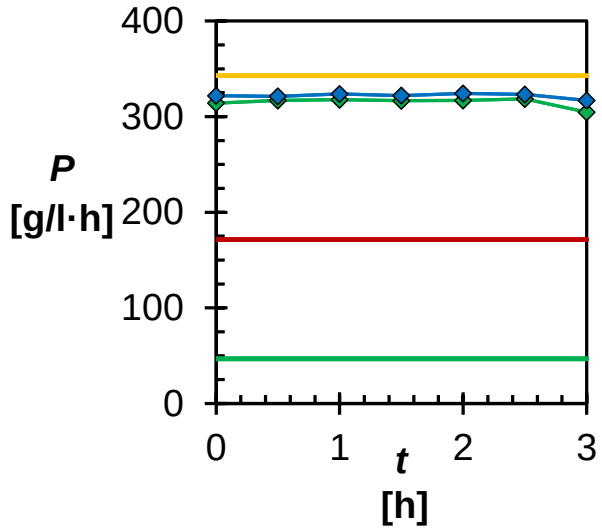

Figure 31: Overall productivity *P* (blue diamonds) over process time *t* for experiment C1 with the theoretical productivity P_{th} possible (yellow line); productivity of the pure enantiomer produced P_E (green diamonds) and the productivity of one enantiomer if all product mass flow would be racemic (red line).

Table 2: Overview of the experimental conditions (antisolvent fraction x_{AS}, residence time τ, enantiomeric excess E_i of seed crystals) and results (enantiomeric excess E_p of product crystals, the productivity *P* and the yield *X*) of the continuous antisolvent crystallization experiments.

No of Experiments	Experimental conditions			Results		
	x_{AS} [v%]	τ [min]	E_i [%]	E_P [%]	P [g/lh]	X [-]
C1	51.4	26	95.2	92.3	321.9	93.9
C2	19.6	24	95.2	91.2	360.2	91.4
C3	80.3	26	95.2	95.4	153.3	99.9
C4	18.4	9	95.2	59.4	837.3	90.3
C5	20.4	5	95.2	45.4	1674.9	90.2

3.3.4 Effect of antisolvent fraction on product Purity and Productivity

Additional continuous antisolvent crystallization experiments were performed to observe the influence of the antisolvent fraction at close to constant residence time of 24-26 min. The results are shown in Figure 32, where the seed crystal purity $E = 95.2\%$ (blue line), the enantiomeric excess measured of C1 (blue rectangles) on average $E = 95.8\%$, C2 (green rectangles) at an average of $E = 91.7\%$ and C3 (orange rectangles) on average $E = 95.7\%$ are plotted over the number of residences. The results show the enantiomeric excess of the crystalline product can be preserved close to that of the seed material at all 3 antisolvent fractions used. While at higher antisolvent fractions the local supersaturation would

seemingly increase as the crystallizer solution also contains a high antisolvent fraction, the addition rate of the saturated solution is also lower in order to keep the overall flow rate. Therefore the mixing effect for the lower addition rate of saturated solution is much stronger preventing primary nucleation.

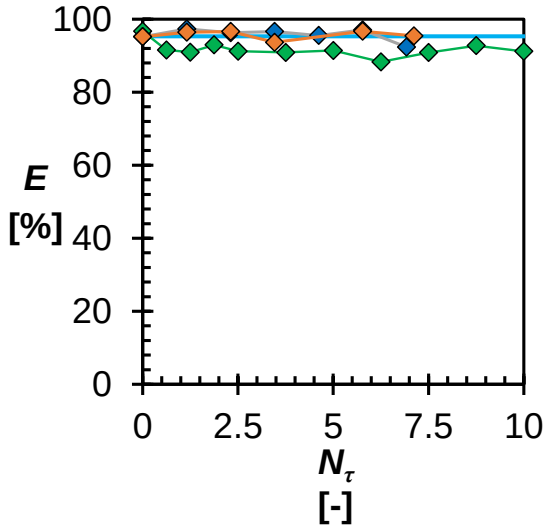

Figure 32: Change in enantiomeric excess *E* of the product crystals over the number of residence times N_T at different antisolvent fractions in continuous antisolvent deracemization experiments C1 (x_{AS} = 51.4 v%), blue rectangles C2 (x_{AS} = 20 v%), green rectangles and C3 (x_{AS} = 80.3 v%), orange rectangles at constant resdience times.

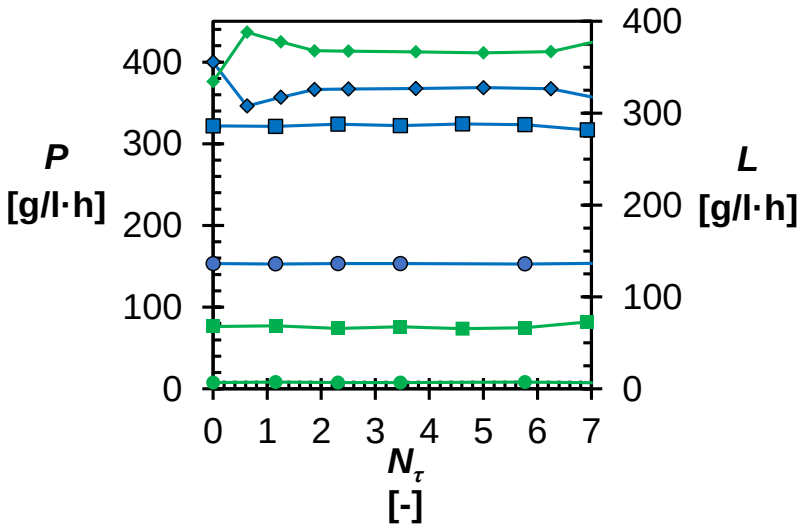

Figure 33: Overall productivty (blue) and product loss *L* (green) against the number of residence times N_T for experiments C1 (squares); C2 (diamond) and C3 (circles).

The overall productivity *P* in a continuous process can be calculated through the concentration difference between operating C_M and line and measured solution concentration *C*, as well as the residence time τ.

$$P = \frac{C_M - C}{\tau} \tag{3}$$

Figure 33 shows the overall Productivities *P* (blue, Figure 33) and product loss *L* (green, Figure 33) over the number of residences for C1 (rectangles), C2 (diamonds) and C3 (circles) . The product loss $L = C/\tau$ can be determined through the measured concentration *C* of the solution in the crystallizer which is flushed out and the residence time τ. In experiments C1 and C3, the overall productivity and losses are constant throughout each experiment, showing that the process remains in steady state and is very stable. At the high antisolvent fractions in C1 and C3 the product loss remains comparably low with it almost being zero at C3. In comparison the product loss in C2 is almost as high as the productivity itself as there is still a large fraction of solid remaining in solution at 19.6 % antisolvent fraction. Experiment C2 shows some initial fluctuations of the productivity, which can be explained by the discrepancy between initial saturation at an antisolvent fraction of 20 v% and 19.6 v% during the experiment, as the solubility curve has a very steep increase at this antisolvent fraction as shown in Figure 29, while the slope is much less steep at higher antisolvent fractions. This could also explain the

slightly lower enantiopurity measured in experiment C2 as shown in Figure 32. As less antisolvent is supplied than initially present in the crystallizer, experiment C2 needs to reach a new steady state for about 2 residences, the after which the productivity and loss remain stable throughout the process.

Thus, a residence time of around 25 minutes allows control over the product handedness in a continuous antisolvent crystallization with an antisolvent fraction between 20 < x_{AS} < 80 v%.

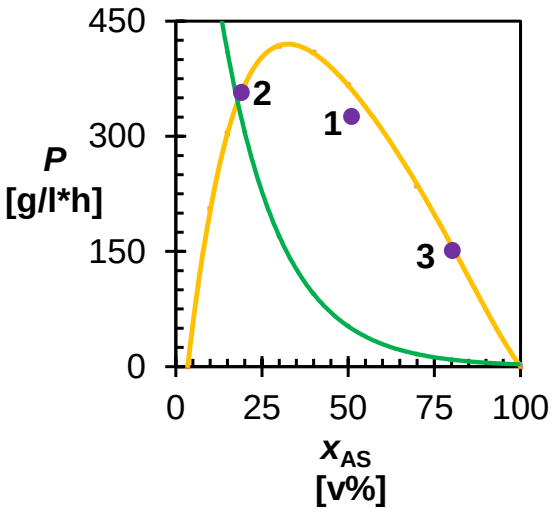

Figure 34: Measured productivities *P* (purple circles) at constant residence time $\tau = 26$ min in the continuous antisolvent crystallization experiments compared to the theoretically maximum productivity *P* (yellow line) and loss of product *L* (green line).

Figure 34 shows the productivities at the respective antisolvent fractions (purple triangles, Figure 34) for experiments C1-C3 (Table 2). The yellow line represents the theoretical productivity based on the maximum possible concentration difference, that between operating and solubility line. The measured productivities from the experiments are very close to the theoretical values.

The antisolvent fraction for the process chosen should not only result in a high productivity and purity but also in a low loss of product. The green line shown in Figure 34 represents the loss of product due to the solubility in the remaining solution mixture. While experiment C2 allows for a high productivity close to the theoretical line (yellow, Figure 34), the solubility at that antisolvent fraction (x_{AS} = 19.6%) is still very high (C^* = 130.5 g/l) resulting in losses of 313 g/lh at a residence time of 24 min. In comparison experiment C1 (x_{AS} = 51.4%) shows a similar productivity but the solubility is significantly lower (C^* = 20.3 g/l) resulting in much lower losses of 48.4 g/lh.

The productivity and product loss versus antisolvent fraction (Figure 34) can be used to determine optimized process conditions. The derived plot showing the theoretical productivity has a maximum referring to the highest productivity which can be achieved in the process, as a function of the antisolvent fraction. From the graph the antisolvent fraction which allows for the highest productivity can be determined at x_{AS} = 33 v%. If the loss however, is taken into consideration this antisolvent fraction might not be very attractive. If

a maximum loss of 10 w% of the initial concentration (35 g/l) is deemed acceptable, the maximum productivity for this process can be achieved under conditions similar to experiment C1.

3.3.5 Influence of the residence time

The effect of the residence time on the enantiomeric excess *E* of the product is investigated through experiments C2, C4 and C5 by keeping the antisolvent fraction constant at x_{AS} = 20 v% but varying the overall flow rate *F* through the crystallizer from 20.8 up to 100 ml/min. The resulting enantiomeric excess *E* as a function of the number of residences $N_\tau = t/\tau$ is then compared with the reference experiment C2 in Figure 35.

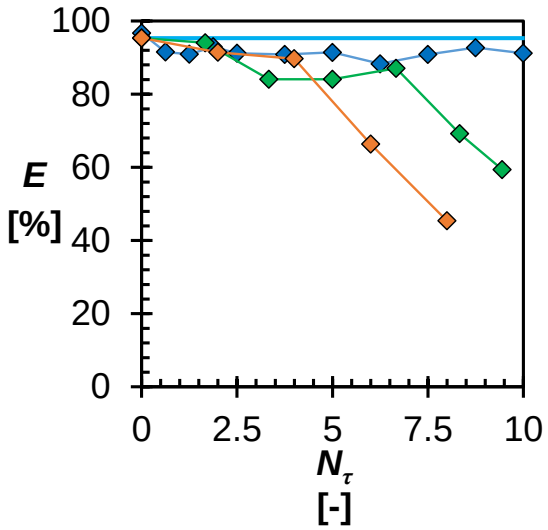

Figure 35: Change in enantiomeric excess *E* of the product crystals over the number of residence times N_τ for experiment C2 (blue rectangles, τ = 24 min); C4 (green rectangles, τ = 9 min) and C5 (orange rectangles, τ = 5 min). The enantiomeric excess in the seed material is indicated by the blue solid line.

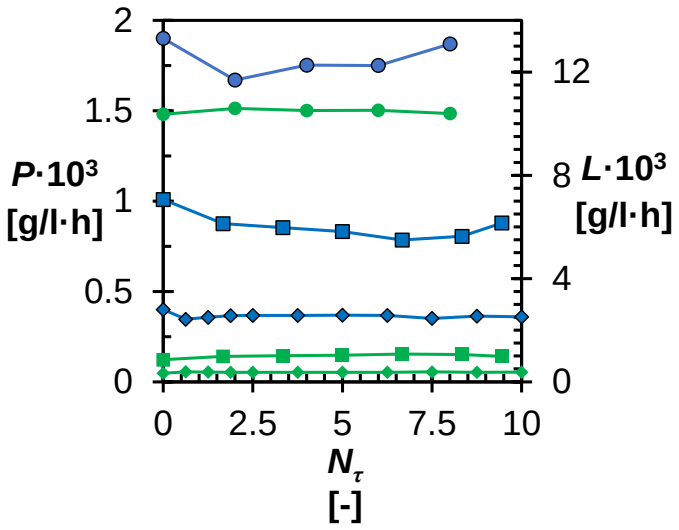

Figure 36: Productivity (blue) and product Loss *L* (green) over number of residence times N_τ for experiments C2 (diamonds); C4 (squares); C5 (circles).

While the enantiomeric excess *E* for experiment C2 remains close to the purity of the seed crystals (blue line, Figure 35), if the residence time is reduced to 9 min the enantiomeric excess *E* of experiment C4 declines rapidly after 7 residences. Decreasing the residence time further to 5 min in experiment C5 (orange, Figure 35) leads to a loss over the handedness after 4.5 residences. It is shown that the enantiomeric excess declines sooner with decreasing residence times. As the flowrate is much higher than in experiments C1-C3, it also possible that, besides the higher local supersaturation, seed material is removed too quickly from the process, in time flushing out the crystals from the crystallizer. This can be explained with the deposition rate of crystalline material being smaller than product flow, which causes the product flow to decreases in time and supersaturation to builds up in process.

With decreasing residence times, the productivity is increased as shown in Figure 36. However at the same time the product loss is increased as the process is not given enough time to crystallize the product. While the loss in experiments C2 (green diamonds, Figure 36) and C4 (green rectangles, Figure 36) is the same as the productivity, the loss increases almost by a tenfold of the productivity in experiment C5 (green cycles, Figure 36).

In order to compare all continuous experiments with regards to productivity and process stability, the productivity of the pure enantiomer $P_E = E(C_M\text{-}C)/\tau$, is plotted against the overall process productivity *P,* in Figure 37. Experiments C1-C3, represented by squares show almost no scattering, following a linear trend along the dashed grey line (Figure 37), indicating a constant productivity of the overall and enantiopure product produced.. At the same time, for the experiments C4 and C5, the scattering is increasing with decreasing residence times. The strong fluctuation between the overall and enantiopure productivity in C5, result in a clear diversion from the grey dotted line as shown in Figure 37 (red cycles).

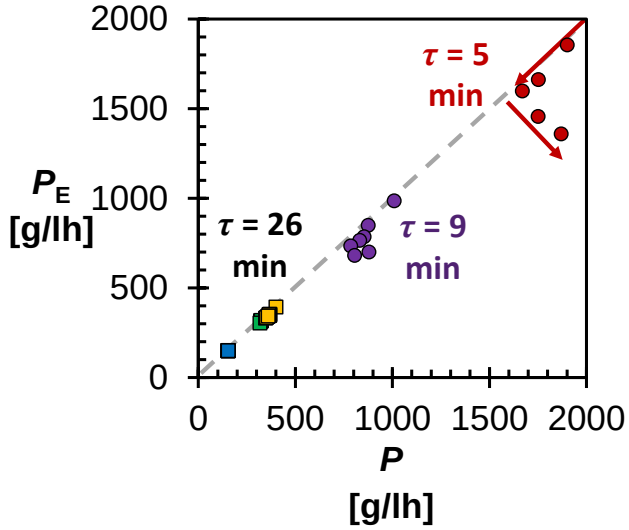

Figure 37: Productivity of the pure enantiomer product P_E over overall product productivity *P* for each continuous experiment conducted with C1 (green squares), C2 (blue squares), C3 (orange squares), C4 (purple cycles) and C5 (red cycles). The grey dashed line represents an ideal process producing only pure enantiomer.

The experiments conducted with sodium bromate are serving as an initial proof of concept where antisolvent is used to achieve an almost enantiopure product. However as sodium bromate is achiral in solution this needs to be adapted for molecules which are chiral in solution as well.

3.4 Discussion

The high enantiomeric excess, which can be retained throughout the process in a very stable manner as shown in Figure 27, is surprising, as antisolvent crystallization usually involves comparably high supersaturations, especially locally around the mixing point of bulk solution and antisolvent inlet, with a high likelihood of primary nucleation of the undesired handedness. The higher the local supersaturation the higher the risk of primary nucleation of the undesired handedness occurring in the crystallizer. At the mixing point of bulk solution and antisolvent the local antisolvent concentration at that point is higher than in the rest of the suspension. This indicates that no significant primary nucleation occurred but rather that enantioselective secondary nucleation is the dominating mechanism for crystal formation from solution. Therefore, the secondary nuclei, generated from the crystals already present in the suspension, retain the handedness of the seed crystals during the fed-batch antisolvent crystallization.

The fed-batch as well as the continuous antisolvent crystallization showed to produce product of high chiral purity. During the fed-batch experiment, the initial feasibility of the antisolvent deracemization process with respect to enantiomeric excess of the product is demonstrated. In addition we are able to show that control over the secondary nucleation mechanism is preserved. For the fed-batch, the antisolvent addition rate controls the process duration and speed of which the supersaturation is provided. Comparing the purity of the seeds with the product achieved (Table 1), it is shown that, despite increasing flowrates, the handedness can be preserved even at high antisolvent addition rates. The measured enantiomeric excess during the experiments and the produced mass of product showed that secondary nucleation was the dominating mechanism during the process.

Looking at the continuous experiments where the stability of the process is investigated with regards to operating antisolvent fraction and residence time, it is proven that a continuous antisolvent deracemization produces high product purities, at high yield and productivities. A consistent product at constant purity and productivity is produced during experiments C1, C2 and C3 where the residence time remains constant, clearly indicating that control over the secondary nucleation mechanism was retained. This shows that if the suspension is given enough time to reduce supersaturation through secondary nucleation and growth rather than primary nucleation at the local mixing points, the supersaturation is apparently not high enough to cause substantial primary nucleation. While the overall average enantiomeric excess for experiment C2 is slightly lower than for C1 and C3, the plotted values in Figure 32 (green diamonds) are remaining close to the average enantiomeric excess throughout the experiment, showing that secondary nucleation to be the dominating mechanism in this experiment as well. Therefore, antisolvent crystallization allows for high yield isothermal crystallization based separation.

Despite the high supersaturations involved in such a process, secondary rather than primary nucleation is predominating throughout the process, opening up new routes for continuous deracemization processes. Moreover, by preserving the control over the secondary nucleation, this process can also be extended to polymorphism control. By starting a process with the desired polymorph instead of relying on primary nucleation or phase transfer, the production of the desired form can be ensured.

As sodium bromate is a salt which mimics infinitely fast racemization behaviour, preliminary experiments are run using the organic compound clopidogrel-imine in acetonitrile with 2w% DBU as deracemization agent and water as antisolvent. Purity measurements of the products of these experiments show that a high enantiomeric excess of 85 % can be reached. Therefore, initial fed-batch experiments suggest that this method is also be applicable to organic compounds racemizing at crystallization conditions.

This suggests that the process obtained with a compound achiral in solution can be adapted to a chiral organic molecule to design a successful separation process. It also proves the concept of using a controlled antisolvent crystallization process for a deracemization process, expanding the range of application for such processes.

3.5 Conclusions

Showing that antisolvent crystallization results in a close to enantiopure product as long as conditions prevent the counter enantiomer crystals to nucleate, antisolvent crystallization can be added to the suite of validated crystallization-enhanced deracemization processes. In addition, the results of the processes show the importance of secondary nucleation, which shows implications for fundamental understanding of industrial crystallization processes.. Since chirality is maintained in these antisolvent crystallization processes despite the high local supersaturations, secondary nucleation rather than primary nucleation is the dominant mechanism for the formation of new crystals. It remains to be shown whether this dominance of secondary nucleation generally is the case. The prevalence of secondary rather than primary nucleation has important implications for the design and operation of industrial crystallization processes in general since their key controlling factors differ.

3.6 Acknowledgements

This research has received funding as part of the CORE project (October 2016 – September 2020) from the European Union's Horizon 2020 research and innovation programme under the Marie Sklodowska-Curie grant agreement No 722456 CORE ITN. We thank the EPSRC Centre for Innovative Manufacturing in Continuous Manufacturing and Crystallisation (http://www.cmac.ac.uk) for support (EPSRC funding under grant reference: EP/I033459/1).

3.7 Literature

[1] W.H. De Camp, Chiral drugs: The FDA perspective on manufacturing and control, Journal of Pharmaceutical and Biomedical Analysis 11(11) (1993) 1167-1172.

[2] L.A. Nguyen, H. He, C. Pham-Huy, Chiral drugs: an overview, Int J Biomed Sci 2(2) (2006) 85-100.

[3] T. Stephens, R. Brynner, Dark Remedy: The Impact Of Thalidomide And Its Revival As A Vital Medicine, 2001.

[4] T. Vetter, C.L. Burcham, M.F. Doherty, Separation of conglomerate forming enantiomers using a novel continuous preferential crystallization process, AIChE Journal 61(9) (2015) 2810-2823.

[5] H. Lorenz, A. Perlberg, D. Sapoundjiev, M.P. Elsner, A. Seidel-Morgenstern, Crystallization of enantiomers, Chemical Engineering and Processing: Process Intensification 45(10) (2006) 863-873.

[6] H. Lorenz, A. Seidel-Morgenstern, Processes to separate enantiomers, Angew Chem Int Ed Engl 53(5) (2014) 1218-50.

[7] C. Rougeot, J.E. Hein, Application of Continuous Preferential Crystallization to Efficiently Access Enantiopure Chemicals, Org. Process Res. Dev. 19(12) (2015) 1809-1819.

[8] C.l. Rougeot, J.E. Hein, Application of continuous preferential crystallization to efficiently access enantiopure chemicals, Organic Process Research & Development 19(12) (2015) 1809-1819.

[9] G. Coquerel, Chiral Discrimination in the Solid State: Applications to Resolution and Deracemization, (2015) 393-420.

[10] R.M. Kellogg, Practical Stereochemistry, Acc Chem Res 50(4) (2017) 905-914.

[11] W.L. Noorduin, W.J.P. van Enckevort, H. Meekes, B. Kaptein, R.M. Kellogg, J.C. Tully, J.M. McBride, E. Vlieg, The Driving Mechanism Behind Attrition-Enhanced Deracemization, Angewandte Chemie International Edition 49(45) (2010) 8435-8438.

[12] R. Oketani, C. Brandel, P. Cardinaël, G. Coquerel, Optimization of SOAT: Example of Naphthamide deracemization, Summer School on Chiral Crystallization, Resolution & Deracemization, Nijmegen, Netherlands, 2017.

[13] C. Xiouras, E. Van Cleemput, A. Kumpen, J.H. Ter Horst, T. Van Gerven, G.D. Stefanidis, Towards Deracemization in the Absence of Grinding through Crystal Transformation, Ripening, and Racemization, Crystal Growth & Design 17(2) (2016) 882-890.

[14] A. Myerson, Handbook of industrial crystallization, Butterworth-Heinemann2002.

[15] R.R.E. Steendam, J.H. ter Horst, Continuous Total Spontaneous Resolution, Crystal Growth & Design 17(8) (2017) 4428-4436.

[16] T. Buhse, D. Durand, D. Kondepudi, J. Laudadio, S. Spilker, Chiral Symmetry Breaking in Crystallization: The Role of Convection, Physical Review Letters 84(19) (2000) 4405-4408.

[17] A.S. Myerson, M. Krumme, M. Nasr, H. Thomas, R.D. Braatz, Control Systems Engineering in Continuous Pharmaceutical Manufacturing May 20–21, 2014 Continuous Manufacturing Symposium, Journal of Pharmaceutical Sciences 104(3) (2015) 832-839.

[18] K. Plumb, Continuous Processing in the Pharmaceutical Industry: Changing the Mind Set, Chemical Engineering Research and Design 83(6) (2005) 730-738.

[19] D.B. Amabilino, R.M. Kellogg, Spontaneous Deracemization, Israel Journal of Chemistry 51(10) (2011) 1034-1040.

[20] F. Breveglieri, G.M. Maggioni, M. Mazzotti, Deracemization of NMPA via Temperature Cycles, Crystal Growth & Design 18(3) (2018) 1873-1881.

[21] A.H.J. Engwerda, R. Maassen, P. Tinnemans, H. Meekes, F.P.J.T. Rutjes, E. Vlieg, Attrition-Enhanced Deracemization of the Antimalaria Drug Mefloquine, Angewandte Chemie International Edition 58(6) (2019) 1670-1673.

[22] A.H.J. Engwerda, H. Meekes, B. Kaptein, F.P.J.T. Rutjes, E. Vlieg, Speeding up Viedma ripening, Chemical Communications 52(81) (2016) 12048-12051.

[23] W.W. Li, L. Spix, S.C.A. de Reus, H. Meekes, H.J.M. Kramer, E. Vlieg, J.H. ter Horst, Deracemization of a Racemic Compound via Its Conglomerate-Forming Salt Using Temperature Cycling, Crystal Growth & Design 16(9) (2016) 5563-5570.

[24] M.L. Maarten W. van der Meijden, Edith Gelens, Wim L. Noorduin, Hugo Meekes, Willem J. P. van Enckevort, Bernard Kaptein, Elias Vlieg and Richard M. Kellogg, Attrition-Enhanced Deracemization in the Synthesis of Clopidogre l - A Practical Application of a New Discovery, Org. Process Res. Dev. 13(6) (2009) 1195-1198.

[25] W.L. Noorduin, B. Kaptein, H. Meekes, W.J.P. van Enckevort, R.M. Kellogg, E. Vlieg, Fast Attrition-Enhanced Deracemization of Naproxen by a Gradual In Situ Feed, Angewandte Chemie International Edition 48(25) (2009) 4581-4583.

[26] L. Spix, H. Meekes, R.H. Blaauw, W.J.P. van Enckevort, E. Vlieg, Complete Deracemization of Proteinogenic Glutamic Acid Using Viedma Ripening on a Metastable Conglomerate, Crystal Growth & Design 12(11) (2012) 5796-5799.

[27] R.R. Steendam, M.C. Brouwer, E.M. Huijs, M.W. Kulka, H. Meekes, W.J. van Enckevort, J. Raap, F.P. Rutjes, E. Vlieg, Enantiopure isoindolinones through Viedma ripening, Chemistry 20(42) (2014) 13527-30.

[28] K. Suwannasang, A.E. Flood, G. Coquerel, A Novel Design Approach To Scale Up the Temperature Cycle Enhanced Deracemization Process: Coupled Mixed-Suspension Vessels, Crystal Growth & Design 16(11) (2016) 6461-6467.

[29] P. Wilmink, C. Rougeot, K. Wurst, M. Sanselme, M. van der Meijden, W. Saletra, G. Coquerel, R.M. Kellogg, Attrition Induced Deracemisation of 2-Fluorophenylglycine, Org. Process Res. Dev. 19(1) (2015) 302-308.

[30] C. Xiouras, A.A. Fytopoulos, J.H. Ter Horst, A.G. Boudouvis, T. Van Gerven, G.D. Stefanidis, Particle Breakage Kinetics and Mechanisms in Attrition-Enhanced Deracemization, Crystal Growth & Design 18(5) (2018) 3051-3061.

[31] C. Xiouras, J.H. Ter Horst, T. Van Gerven, G.D. Stefanidis, Coupling Viedma Ripening with Racemic Crystal Transformations: Mechanism of Deracemization, Crystal Growth & Design 17(9) (2017) 4965-4976.

[32] A.J. Alvarez, A.S. Myerson, Continuous Plug Flow Crystallization of Pharmaceutical Compounds, Crystal Growth & Design 10(5) (2010) 2219-2228.

[33] Q. Su, Z.K. Nagy, C.D. Rielly, Pharmaceutical crystallisation processes from batch to continuous operation using MSMPR stages: Modelling, design, and control, Chemical Engineering and Processing: Process Intensification 89 (2015) 41-53.

[34] Y. Yang, Z.K. Nagy, Combined Cooling and Antisolvent Crystallization in Continuous Mixed Suspension, Mixed Product Removal Cascade Crystallizers: Steady-State and Startup Optimization, Industrial & Engineering Chemistry Research 54(21) (2015) 5673-5682.

[35] M. Qin, J. Bartus, O. Vogl, Stereospecific polymerization and chiral initiation, chiral crystallization and chiral nucleation, Macromolecular Symposia 98(1) (1995) 387-402.

[36] C. Viedma, Selective Chiral Symmetry Breaking during Crystallization: Parity Violation or Cryptochiral Environment in Control?, Crystal Growth & Design 7(3) (2007) 553-556.

[37] R.M. Pagni, R.N. Compton, Asymmetric Synthesis of Optically Active Sodium Chlorate and Bromate Crystals, Crystal Growth & Design 2(4) (2002) 249-253.

4 Chiral Separation at the Eutectic Point: A Case Study of Mandelic Acid

4.1 Abstract

A large number of active pharmaceutical ingredients is chiral. Only one enantiomer usually has the desired pharmaceutical action and as the counter enantiomer can be harmful there are strict regulations on the enantiopurity of chiral drugs or nontoxicity of the counter enantiomer. As the direct production of the desired handedness by asymmetric synthesis is not always possible, separation methods are needed. Crystallization-based chiral separation has shown to be a selective and efficient method to separate conglomerate systems. However, most drugs are racemic compound forming systems. These systems require initial enrichment prior to the preferential crystallization process in a hybrid process coupled with another separation method, such as chromatography. Such processes allow to produce enantiopure product from racemic compounds with high productivity and yield. Therefore developing new, efficient and robust crystallization-based separation processes is of high importance to the pharmaceutical industry. Here we present a new strategy to separate one of the enantiomers of racemic compound forming systems, achieving high purities and yield. The process shows robustness against temperature fluctuations and over time. Applying this process as part of a hybrid process in the pharmaceutical industry will allow for cost reduction and increased overall process yield while producing high enantiopurities of chiral drugs. The proposed process has the potential to be applied to any system forming a eutectic.

4.2 Introduction

The majority of pharmaceutical substances are chiral molecules [1, 2], where only one enantiomer has the desired effect in the body. Asymmetric synthesis [3] during the formulation of the molecule allows for the production of only the desired handedness, however, this route is not always available. In cases where asymmetric syntheses cannot be performed and the racemic mixture or solution is produced instead, a chiral separation has to be performed, which can be done through techniques like chromatography [4] or crystallization [5]. Pharmaceutical industry seeks access to a broad range of chiral resolution methods to separate enantiomers of chiral compounds as chiral compounds have varying physical properties such as solubility or density as well different crystal shapes which each can require different approaches to the separation process.

There are two major types of chiral solid systems: conglomerate forming systems (Figure 38, left) and racemic compound forming systems (Figure 38, right). Conglomerate systems form enantiomerically pure crystals of both handedness that are physically mixed with one another at an equal ratio at the racemic composition [6, 7]. The enantiomers of conglomerates form one eutectic in the solution, which is indicated by the compositional point C^*_{eu} the ternary phase diagram in Figure 38, in which the solvent is saturated with respect to both enantiopure

solids. In the case of racemic compound forming systems, the molecules of both enantiomers form a single crystal phase with both enantiomers being incorporated in the crystal lattice at racemic composition. As shown in the ternary phase diagram (Figure 38, left), racemic compound forming systems possess mirror symmetry with a reflection in the line of racemic composition and form two eutectics. At these eutectic compositions, the solution is saturated with regards to one of the enantiopure solid (either D or L) and the racemic compound solid DL. As shown in the ternary phase diagrams in Figure 38, both systems have single phasic domains, where only the solution without a solid phase exists, biphasic domains where the one solid phase and a liquid phase are in equilibrium and triphasic domains with two solid phases and the solution in equilibrium.

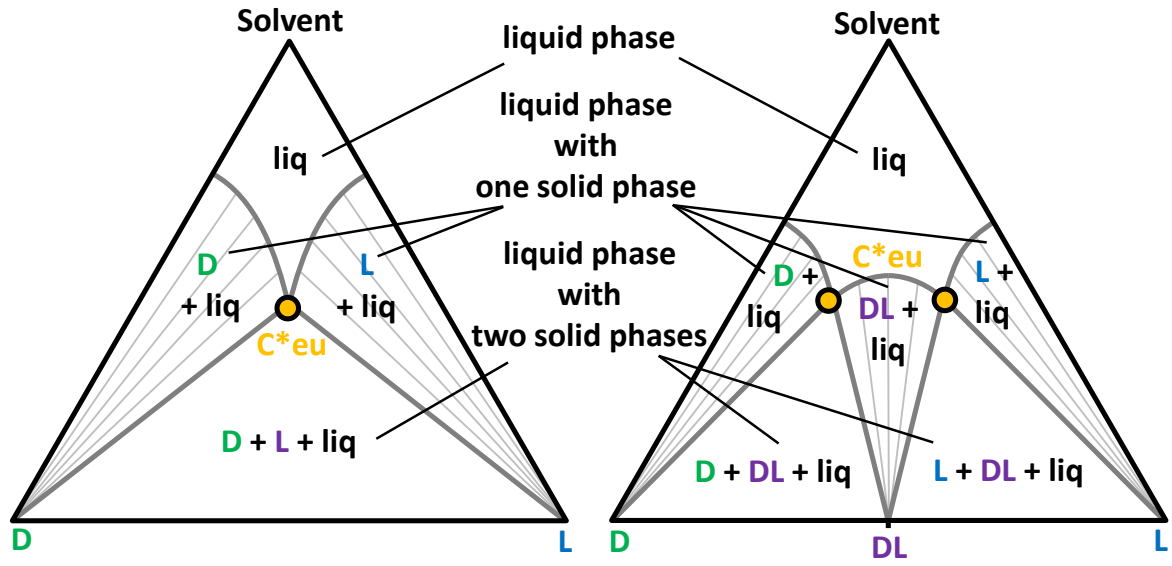

Figure 38: Ternary phase diagram schematic of a conglomerate forming system (left) and a racemic compound forming system (right) at constant temperature and pressure, with the number of phases being indicated.

A solution with a composition within the triphasic domain is supersaturated with respect to both solids. If the conditions are within the metastable zone width of both solid phases, the solution is metastable and providing seeds of only one of the phases will allow the crystallization of this phase while the other phase does not form. It is, therefore, possible to crystallize only one of the two solid phases with the help of pure seeds. For conglomerate forming systems this is often referred to as preferential crystallization, for which several preferential crystallization processes are available in literature [8-11]. For racemic compound forming systems in solutions with a composition in the triphasic domain, such a seeded process in principle can also be applied. To this end, first, a separation method such as chromatography [4, 12] or membrane separation [13] can be used to enrich the solution with overall composition in the triphasic domain so that only one of the solids, for instance, the enantiopure compound rather than the racemic compound, can be preferentially crystallized. Hybrid processes have been shown to work for the separation of the racemic compound forming systems [13-17], where specially designed coupled crystallizers were used to

separate the pure enantiomer from the racemic compound, starting from a supersaturated solution at eutectic composition.

Here, our objective is to design and validate a generally applicable process to separate two mixed solids in a triphasic domain suspension using a process configuration of two preferential crystallizers, either in series or parallel. Mandelic Acid (MA) is used as a model compound as it is well investigated [18-21] and commercially available in large quantities. Mandelic acid in water is a racemic compound forming system and therefore needs an enrichment step in one of the enantiomers to access the triphasic domain. However, compared to a conglomerate system that does not need such an enrichment step, the chosen model system is relatively easy to monitor in situ through for instance Raman spectra differences between the racemic and enantiopure crystals. A parallel and serial process design of 2 crystallizers is investigated for their suitability to separate the racemic compound Mandelic Acid (MA) at its eutectic composition.

4.3 Experiments

4.3.1 Material and Chemicals

In the experiments deionized water (Milli-q) was used as a solvent for DL- and D-MA (purity >99%), acquired from Tokyo Chemical Industry. For controlling the temperature Pt 100 temperature probes in combination with thermostats from Lauda proline were used.

4.3.2 Experiment preparation

The parallel and serial set up consists of a feed vessel and two crystallizers, one for the crystallization of the racemic compound, the DL-crystallizer, and the other for the pure enantiomer, the D-crystallizer (Figure 39). The difference between the parallel and serial configuration is the way the vessels are connected.

First, a saturated solution at the eutectic composition of 25°C was prepared in the feed vessel by dissolving 51.7 g D-MA and 84.3 g DL-MA in 500 ml water. The eutectic saturation concentration $C^*_{F,eu} = C^*_D + C^*_{DL}$ =272.0 mg/ml at 25°C in the feed vessel is composed of the saturation concentrations C^*_D = 103.4 mg/ml of the D-MA and C^*_{DL} = 168.6 mg/ml of the DL-MA. Then, 57 g D-MA and 93 g DL-MA were added to the saturated solution in the feed vessel to create a mixed suspension with an overall composition in the triphasic domain of the MA/water phase diagram at 25°C.

Similar to the feed vessel, a saturated starting solution at eutectic composition $C^*_{eu} = C^*_{D,C} + C^*_{DL,C}$, consisting of a mix of solubilities of D-MA and DL-MA, was prepared at the crystallization temperature for each experiment (Table 3) in 200 ml water for each crystallizer. Afterwards, 3 g seed crystals of respectively DL-MA and D-MA were added to the DL- and D-crystallizer. The solubility data and information of the ternary phase diagram have been previously investigated by Lorenz [22]. The enantiomeric excess of the eutectic composition is E_{eu} = 0.38 %, representing the the fraction of D-MA which can be crystallized.

Table 3: Amounts of D-MA and DL-MA used to create eutectic starting solution in the crystallizers and feed vessel at different crystallization temperatures.

Temperature [°C]	Mass of D-MA [g]	Mass of DL-MA [g]	C^*_{eu} [mg/ml]	$C^*_{D,C}$ [mg/ml]	$C^*_{DL,C}$ [mg/ml]
20	14.1	23	185.5	70.5	115
23	17	28	225	85	140
24	19.8	32.3	260.5	99	161.5
25	51.7	84.3	$C^*_{F,eu}$ = 272	C^*_{D} = 104	C^*_{DL} = 169

The feed vessel suspension has a temperature T_{high} = 25°C for each experiment, while the temperature $T_{low} < T_{high}$ is chosen equally for both crystallizers (Table 3). The values for the saturation concentrations and masses of added D-MA and DL-MA for each experiment can be found in Table 3 and Table 4. After preparing the starting conditions in each vessel, the solid excess is added in the feed and the seeds of D-MA and DL-MA are added to each D- and DL-crystallizer, respectively. During the experiments, all vessels were stirred at 400 rpm with exception of the D-MA crystallizers which was stirred at 800 rpm to avoid floating of the crystallized product. To ensure that only clear solution is transferred from one vessel to another, sintered glass filters (Robu, Por. 3) are used for the outflow in each vessel.

4.3.3 Process Monitoring

As the racemic compound DL-MA and the enantiopure D-MA have different physical properties and crystal structures, they can be distinguished using optical process analytical tools such as Raman spectroscopy [23]. Differences in the spectra and the dependence of the spectra intensity on the suspension density of the solid crystals in the crystallizer can be used to monitor the suspension density of the crystallized solids in-situ during the process. An immersive type Raman probe (RXN2, Kaiser Instruments) was used in the D-MA crystallizer to monitor the suspension density of the D- and DL-MA crystallized during the process. The power of the laser bean was 355 mW and the laser wavelength was 785 nm to reduce fluorescence. To quantify the solid composition, the Raman probe was calibrated against varying compositions of DL-MA and D-MA at different suspension densities, particle sizes, and temperatures. A partial least squares regression (PLS) model was built using the calibrated data for quantification of the solid phase enantiomeric excess as shown in a soon to be published paper by Venkatramanan. As the D-MA and DL-MA suspension densities can be determined separately in the same suspension, also the solid enantiomeric excess *E* is known. To monitor the suspension density of the racemic compound and pure enantiomer, the intensity of the Raman spectra was calibrated against suspension density, solid composition and particle size. Afterwards suspensions of known composition were measured with Raman and chiral HPLC to verify the method and determine the error. The Raman method showed an accuracy of at ± 7.5 g/l for the total measured suspension density. Details of the method can be found in a soon to be published paper by Venkatramanan. Additionally, to monitor the overall concentration of the solution in the crystallizers during the process, an immersive ATR UV-Spectroscopy (Hellma ATR Probe, Carl Zeiss spectrometer) [23] was used during the process. The UV was calibrated against different concentrations and temperatures for quantification of overall solute concentration. A PLS model was built using solute calibration.

Besides in-situ monitoring, the resulting solid product from both crystallizers was analyzed for its purity using HPLC. For the method, a lux 3 µm i-Cellulose LC column 150*3 mm (Phenomenex) was used with an 80/20 mix of hexane (0.1 % formic Acid) and IPA (0.1 % formic acid) as eluent at a flow rate of 0.6 ml/min and an injection volume of 1 µm. For the solid samples, 1 w% was dissolved in 100 ml water, of which 1 ml was taken for analysis in an HPLC vial.

4.3.4 Parallel Configuration of Crystallizers

A schematic of the parallel crystallization configuration is shown in Figure 39, in which both crystallizers are directly connected to the feed vessel with an in and outflow. The experiment began by starting all the pumps (Watson Marlow 520u) simultaneously to transfer the filtered solution between the feed vessel and the crystallizers. The pumps were calibrated to ensure the flow rate F is the same for all pumps in the system and crystallizer and feed vessel volume and solution residence times are constant during the process. The feed flow at temperature T_{high} going to the crystallizers at temperature T_{low} provided the supersaturated solution to grow the seed crystals. The depleted solution recycled from the crystallizers back to the feed vessel is concentrated by crystal dissolution in the feed vessel at T_{high}.

Experiments were conducted at two different crystallization temperatures T_{low}, changing the supersaturation ratios with respect to the pure enantiomer and racemic compound crystallized. Two supersaturation ratios, one for the D-MA, $S_D = C_{D,F}/C^*_{D,eu}$, and the other for DL-MA, $S_{DL} = C_{DL,F}/C^*_{DL,eu}$, can be defined that characterize the supersaturation ratios in a feed solution at the crystallizer temperature T_{low} for those compounds. The enantiomeric excess in the solution at eutectic composition does not vary too much within the low temperature T_{low} region of the performed experiments and we have set this enantiomeric excess to E_{eu} = 0.38 based on literature values [24]. Also the overall solution concentration ($C_{eu} = C_{D,eu}+C_{LD,eu}$) at the eutectic is known from literature [ref] and given in table 1 for the different T_{low}. This overall solution concentration is prepared by dissolving the right amounts of D-MA ($C_{D,eu} = E_{eu}C_{eu}$) and DL-MA ($C_{DL,eu} = C_{eu} - C_{D,eu}$). The solution residence time in the crystallizers were chosen to be 60 and 90 min (Table 4), depending on the experiment, to give the D-MA and DL-MA crystals time to grow. Each experiment was run between 10-18 residences, allowing the solid excess to be fully consumed.

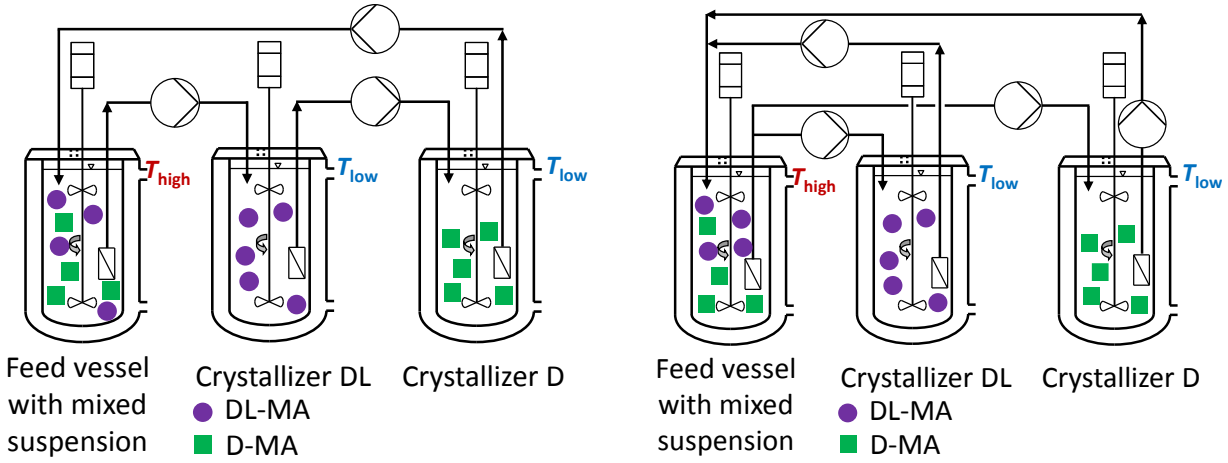

Figure 39: Schematic of the serial (left) and parallel (right) set up with feed vessel, DL-crystallizer and D-crystallizer. The feed vessel contains a mixed suspension at high temperature T_{high} and in the DL- and D-crystallizer at low temperature $T_{low}<T_{high}$ respectively DL-Mandelic Acid and D-Mandelic Acid are crystallized.

During the process, the suspension densities of D-MA and DL-MA in the D-crystallizer were determined using the Raman probe and the overall MA concentration in the D-crystallizer was measured by the ATR-UV.

Table 4: Process parameters used for the parallel experiments P1, P2 and P3.

Parallel experiment		P1	P2	P3
Flow rate	F [ml/min]	3.3	2.2	3.3
Residence Time	τ [min]	60	90	60
Feed Temperature	T_{high} [˚C]	25		
Feed Concentration	C_F [mg/ml]	272		
Crystallization Temperature	T_{low} [˚C]	23		24
Eutectic Concentration	C^*_{eu} [mg/ml]	225		260.5
Supersaturation Ratio D	S_D	1.21		1.04
Supersaturation Ratio DL	S_{DL} [-]	1.21		1.04

4.3.5 Serial Configuration of Crystallizers

Figure 39 shows a schematic of the serial crystallization configuration. In the serial configuration, the DL-MA crystallizer receives solution from the feed vessel and feeds solution in the D-MA crystallizer which, in turn, feeds depleted solution back into the feed vessel.

The experiment was initiated by starting the pumps simultaneously at a defined flow rate F (Table 5). The preparation and procedure for serial experiments are otherwise identical to that of the parallel experiments. The supersaturation ratios in the serial systems can be calculated the same way as in the parallel process but only in the DL-crystallizer S_D and S_{DL} are present, while only the DL-MA is crystallized. In the D-crystallizer the DL-MA has already been widely removed from the solution so only S_D is present. In serial experiment S3 the crystallizer temperature was reduced from experiment S1 so the supersaturation varies. In the second

serial experiment S2 a decrease in residence time was investigated. All process conditions for each serial experiment can be found in Table 5. Each experiment was run for 12 to 18 residences to allow for the solid excess to be fully consumed during the process.

Table 5: Process parameters used for the serial experiments S1, S2 and S3.

Serial Experiment		S1	S2	S3
Flowrate	F [ml/min]	3.3	6.6	3.3
Residence Time	τ [min]	60	30	60
Feed Temperature	T_{high} [˚C]	25		
Feed Concentration	C_F [mg/ml]	272		
Crystallization Temperature	T_{low} [˚C]	23		20
Crystallizer Concentration	C^*_{eu} [mg/ml]	225		185.5
Supersaturation Ratio D	S_D [-]	1.21		1.04
Supersaturation Ratio DL	S_{DL} [-]	1.21		1.04

4.4 Separation in the Eutectic: Parallel Crystallizers

4.4.1 Parallel experiment P1: Feasibility investigation

For the parallel experiment P1 at ΔT = 2°C and τ = 60 minutes, the suspension density of D-MA and DL-MA is plotted in Figure 40 as a function of the process time. Shortly after adding the seeds, the pumps are started to initiate the processes (point 1, Figure 40). Following the start of the process, the D-MA suspension density remains constant until reaching 1 h process time (point 2, Figure 40), after which it increases roughly linearly until a process time of 3 h (point 3, Figure 40). During these two hours between points 2 and 3 highlighted in Figure 40, thus a roughly linear deposition rate is observed. This period is referred to in the following as the stable growth phase. The linear deposition rate G_D = 11.3 g/l.h. During the stable growth phase, the suspension density of D-MA increases from an initial average value of 19 g/l at 1 h to 42 g/l at 3 h process time with a linear deposition rate G_D. During the stable growth phase, only D-MA is produced, therefore the deposition rate is equal to the productivity P of the D-MA during this time frame.

At a process time of 3 h, primary nucleation of the DL-MA in the D-crystallizer occurs, indicated by a slow increase of the DL-MA suspension density (purple dots, Figure 40). At this point, the suspension in the D-crystallizer is a mixture of D-MA and D-MA crystals and the product will not be enantiopure. After its primary nucleation the DL-MA is growing with a linear deposition rate of $G_{,DL}$ = 24.5 g/lh. Using the measured suspension densities of D-MA and DL-MA, the solid enantiomeric excess $E = \rho_D/(\rho_D + \rho_{DL})$ is determined and plotted in Figure 3 (right). As in the first 3 hours, only D-MA is present, the enantiomeric excess E>99% is very high. After 3 h the racemic compound appears and substantially decreases the initial product E to below 50 % within 3 hours.

The yield $X = G_D/G_{th,D} = 63.9\%$ at which D-MA could be produced is calculated using the theoretical linear deposition rate $G_{th,D} = (C^*_D - C^*_{D,C})/\tau = (\Delta C\, E_{eu})/t = 17.8$ g/lh of D-MA. While the yield is not very high, the uncrystallized D-MA is recycled back to the feed vessel and reintroduced into the system. However, considering the short duration of the stable growth phase in combination with the yield, the parallel process only allows for a small amount of D-MA to be separated from the racemic compound under this process conditions.

Figure 41 shows the solution composition in the D-crystallizer during the stable growth phase in the ternary phase diagram. The solution composition can be determined from the overall concentration measured in the D-crystallizer, during the stable growth phase, the equations described in the experimental section are used.

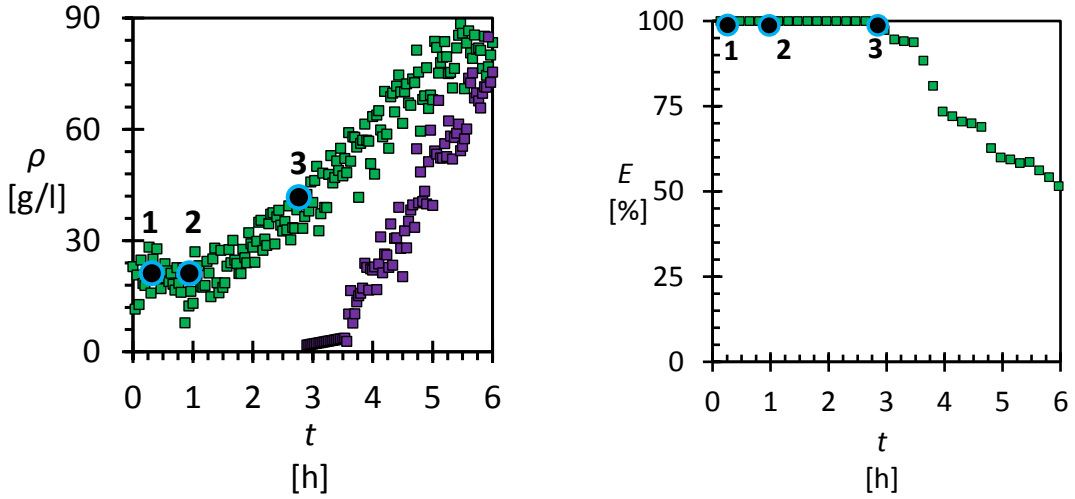

Figure 40: Suspension density of D-MA (green) and DL-MA (purple) in the D-crystallizer during parallel experiment P1 (left) with $\Delta T = 2$ °C, $\tau = 60$ min and seed addition at $t = 0$. 1) Start of pumps; 2) Beginning of stable growth phase; 3) Primary nucleation of DL MA in D-crystallizer, as well as the corresponding solid product enantiomeric excess E over time (right) for the parallel experiment P1.

Assuming ideal mixing and neglecting the growth kinetics and using linear deposition rates instead, the D-MA and L-MA solution concentrations during the stable growth phase can be determined. The overall concentration in the D-crystallizer changes because the feed concentrations of D-MA and L-MA are higher than those in the initial solution in the crystallizer. The overall concentrations of D-MA C_D and L-MA C_L in the crystallizer and thus also the solution concentrations leaving the crystallizer, therefore, increase over time. The overall L-MA concentration is equal to the L-MA solution concentration as no DL-MA is crystallizing in the stable growth region and this concentration can be determined as a function of time by assuming ideal mixing.

$$V dC = F\left(C_{L,F} - C_L\right)dt \tag{4}$$

With the residence time $\tau = F/V$ the change of concentration in the crystallizer can be defined as:

$$\frac{dC}{C_{L,F} - C_L} = \frac{dt}{\tau} \tag{5}$$

Therefore the change of concentration can be written as:

$$\frac{C_{L,F} - C_L(t)}{C_{L,F} - C_{L,0}} = \exp\left(-\frac{t}{\tau}\right) \tag{6}$$

With the initial concentration of L-MA $C_{L,0} = 0.5C^*_{DL,C}$ in the crystallizer being the L-MA fraction of the eutectic ($x_{L,eu} = 0.31$), which is known, the L-MA concentration accumulating in the crystallizer over time can be defined as:

$$C_L(t) = \frac{\left(C_{L,F} - 0.5C^*_{DL,C}\right)}{C_{L,F}} \exp\left(-\frac{t}{\tau}\right) \tag{7}$$

As DL-MA is accumulating in the crystallizer, which consists of equal amounts of D-and L-MA, the D-MA fraction of the DL-MA is the same concentration as the L-MA and therefore known. However as there is a fraction of the D-MA in equilibrium with the L-MA, another fraction of the D-MA from the feed can be crystallized. When determining the overall D-MA concentration the crystallized D-MA has to be accounted for. This can be done through the deposition rate $G_D = d\rho/dt$ = constant measured by the Raman, which is constant during the stable growth phase.

$$\frac{VdC}{dt} = F\left(C_{D,F} - C_D\right) - \frac{Vd\rho}{dt} \tag{8}$$

As the deposition rate G_D is constant, we assume the concentration C_D in crystallizer to be constant ($dC/dt = 0$). The actual change, in case of dC/dt not being zero, can be determined from the UV signal, as the linear deposition rate is known, as well as the DL-MA concentration coming from the feed crystallizer.

$$F\left(C_{D,F} - C_D\right) = VG_D \tag{9}$$

With the deposition rate, suspension density change, flowrate and feed concentration is known, the concentration of D-MA in the crystallizer during the stable growth phase can be determined.

$$C_D = C_{D,F} - \tau G_D \tag{10}$$

The uncrystallized D-MA concentration $C_{D,R}$ during of the crystallizable D-MA fraction can be determined using the measured overall concentration form ATR-UV in the crystallizer C_C, and the concentration of the DL-MA remaining in the crystallizer which is $2C_L(t)$.

$$C_{D,R} = C_C - 2C_L(t) \tag{11}$$

At some point in time, a sufficient amount of DL-MA enriches in the solution of the D-crystallizer, which triggers primary nucleation of the racemic compound rendering the product impure.

While the D-MA is crystallized in the D-crystallizer, the DL-MA enriches in the solution, increasing the overall concentration. This is observed in Figure 41 (right), where the concentration (green dots, Figure 41) of D-MA and L-MA increases along a trajectory until a certain enrichment of the DL-MA is reached and the concentration remains at this composition. This accumulating concentration of DL-MA in the crystallizer is presenting a supersaturation of the DL-MA concentration with regards to the eutectic concentration (yellow dot, Figure 41) in the crystallizer, which leads to primary nucleation of the DL-MA in

the D-crystallizer at some point during the process. For the parallel experiment P1 the stable growth phase lasts for two residences until the primary nucleation occurs as shown in Figure 40. The green line shown in Figure 41, starting at the eutectic represents the overall composition of the suspension during the stable growth phase, which consists of the solution concentration, plus the suspension density of the crystallized D-MA. As the DL-crystallizer is not monitored during the parallel experiments, it is assumed that DL-MA is crystallized with a yield of X = 85%, estimated through the linear deposition rate of the DL-MA from Figure 40 and the theoretical linear deposition rate calculated using the DL-MA fraction x_{DL}.

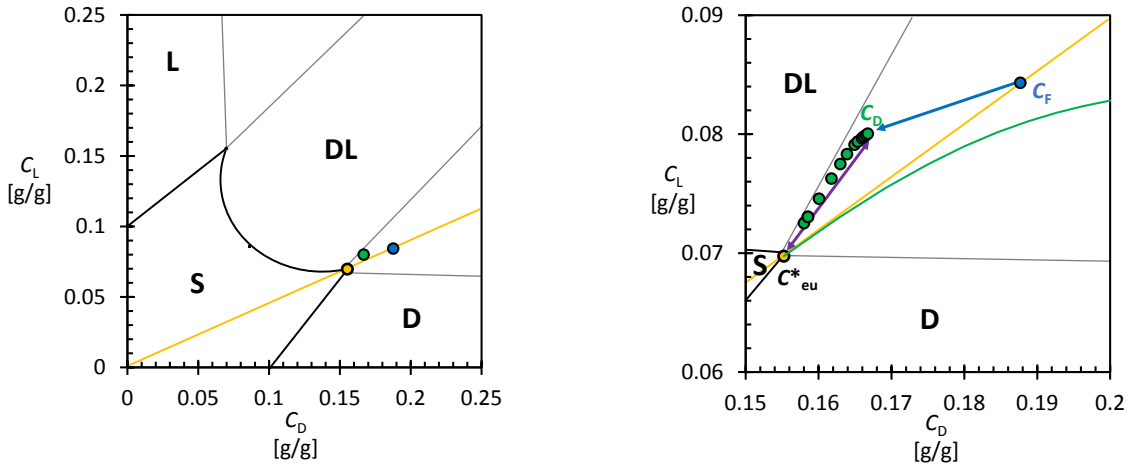

Figure 41: Left: Ternary phase diagram of MA in water and the compositions in parallel experiment P1 at crystallization temperature of 23 ˚C and its zoom (right) on the process concentrations, with the feed concentration C_F (blue) and the solution concentration C_D in the D-crystallizer (green) during the stable growth phase. The accumulation of DL-MA in solution in the D crystallizer (purple arrow), is indicated. The green line starting from the eutectic concentration in the crystallizer represents the overall composition including the crystallized D-MA during the stable growth phase.

4.4.2 Effect of increasing the residence time in Parallel experiment P2

As the stable growth phase for this experiment lasts only 2 h, it was investigated in experiments P2 and P3 if a higher residence time can prolong the duration of the stable growth phase and allow for more product to be produced.

Due to the short duration of the stable growth phase, the flow rate is reduced to F = 2.2 ml/min in a second parallel experiment P2, which increases the residence time to 90 min in comparison to 60 min P1. Figure 42 shows the measured suspension densities of D- and DL-MA for P2. Like in the first experiment, the pumps are started 15 min after seeding (1, Figure 42), but no visible increase in the suspension density of D-MA can be observed until point 2 (Figure 42) at 1 h processes time. After 1 h, the D-MA suspension density starts to increase at a linear deposition rate of 5.7 g/lh for 4 hours until point 3 (Figure 42) is reached after 5 h process time. At this point, the DL-MA primary nucleates in the D-crystallizer rendering the produced product chirally impure as shown in Figure 5 (right), with the enantiomeric excess going down rapidly after the primary nucleation event. The DL-MA suspension density increases with a linear deposition rate of 12.7 g/lh after the primary nucleation.

During the stable growth phase, the suspension density of the D-MA increases from 12.2 g/l at point 2 (Figure 42) to 37.5 g/l at point 3 (Figure 42). The yield X = 48.4% at which the product can be produced is lower than in P1, leaving more D-MA uncrystallized in the solution.

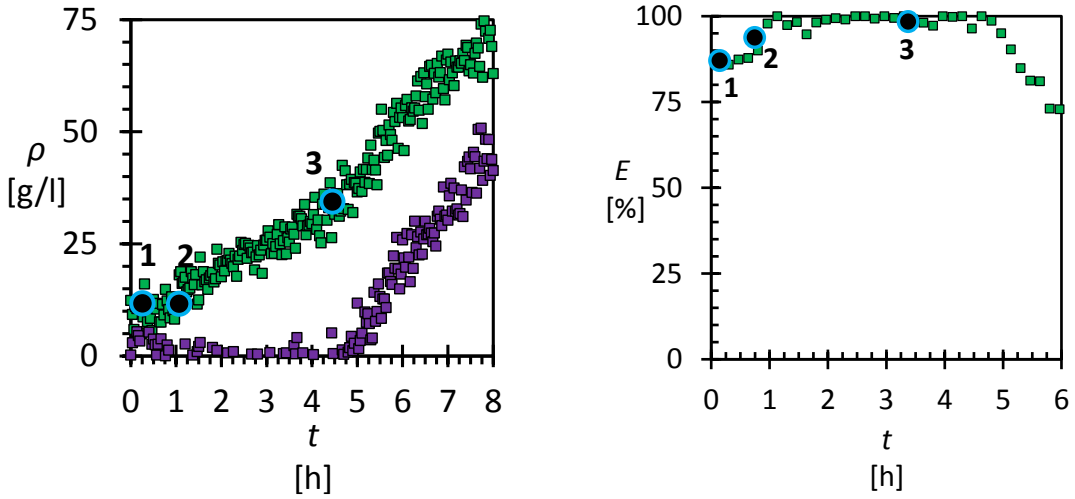

Figure 42: Suspension density of D-MA (green) and DL-MA (purple) in the D-crystallizer during parallel experiment P2 (left) with ΔT=2 ˚C, τ=90 min and seed addition at t=0. 1) Start of pumps; 2) Beginning of stable growth phase; 3) Primary nucleation of DL MA in D-crystallizer,, as well as the corresponding solid product enantiomeric excess E over time (right) for the parallel experiment P2.

Comparing the results of P2 with P1, increasing the residence time does increase the duration of the stable growth phase but decreased productivity by half and lowers the yield. Therefore increasing the residence time by lowering the flowrate is not beneficial for this process.

4.4.3 Parallel experiment 3 with decreased temperature difference

As increasing the residence time is not allowing for the production of more pure D-MA, in a third parallel experiment P3 it is investigated if lowering the overall concentration difference between feed and crystallizer ΔC, by increasing the crystallizer temperature to 24°C, leads to a prolonged stable growth phase and to a higher mass of product which can be produced. Figure 43 shows the measured suspension densities for this experiment. The pumps are started shortly after seeding as indicated by 1 (Figure 43), while the suspension density of D-MA starts to increase with a linear deposition rate after 1 h process time at point 2 (Figure 43). The stable growth phase in P3 lasts for 14 h until point 3 (Figure 43) is reached and the DL-MA nucleates. During the stable growth phase, the suspension density increases from 18.3 g/lh at point 2 (Figure 43) to 62.6 g/lh at point 3 (Figure 43), with a linear deposition rate of 2.7 g/lh which is equal to the productivity achieved during this experiment. The yield X = 24.7% is lower than in P1 and P2, while the stable growth phase is substantially prolonged. Despite the low productivity, the mass of pure product which can be produced during this experiment is much higher than in P1 and P2. This can also be observed in Figure 43 (right), showing the enantiomeric excess of the experiment. It remains high during the stable growth phase for 15 h until the primary nucleation occurs (point 3, Figure 6).

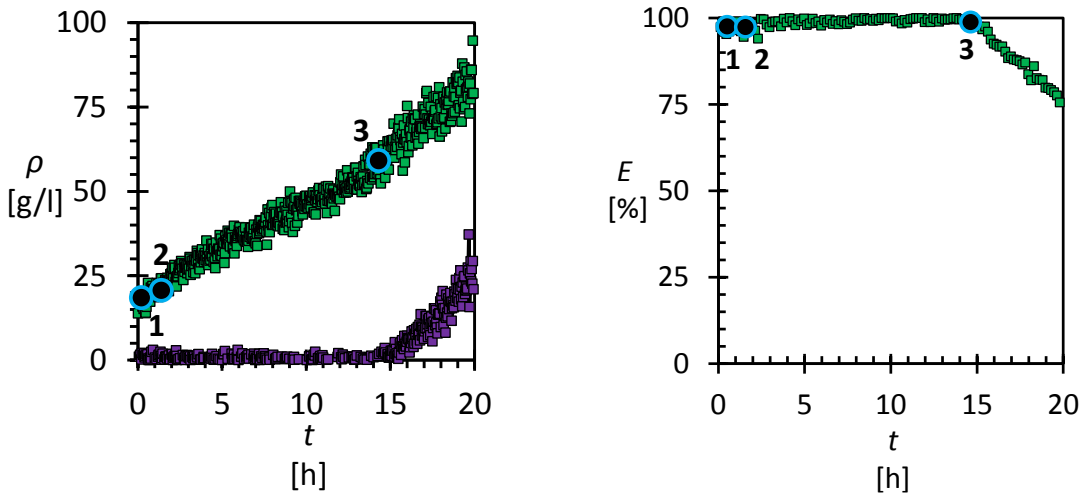

Figure 43: Suspension density of D-MA (green) and DL-MA (purple) in the D-crystallizer during parallel experiment P3 (left) with ΔT=1˚C, τ=60 min and seed addition at t=0. 1) Start of pumps; 2) Beginning of stable growth phase; 3) Primary nucleation of DL MA in D-crystallizer, as well as the corresponding solid product enantiomeric excess E over time (right) for the parallel experiment P3.

This experiment shows that lowering the overall concentration difference between feed and crystallizers prolongs the duration of the stable growth phase, as the concentration difference with regards to the accumulated DL-MA in the D-crystallizer and the eutectic point is also decreased. However, this experiment requires a very low temperature difference to achieve the small ΔC, which makes the processes very susceptible to temperature fluctuations, which can cause local supersaturation, resulting in primary nucleation of the counter enantiomer. Moreover, if the processes were to be scaled up, the temperature fluctuations would increase as the efficiency of the heat transfer decreases with increasing volume to heat transfer area.

In order to compare all parallel processes, the overall produced product mass over time in the D-crystallizer and the mass of the pure D-MA enantiomer are plotted as a function over the number of residences N_τ in Figure 44. For each experiment, the mass of pure enantiomer and overall mass produced are identical until the primary nucleation. Comparing the produced masses of P1 (squares) and P2 (triangles), it is observed that in both experiments the primary nucleation of the counter enantiomer occurs after the same number of residences as indicated by I (Figure 44) and II (Figure 44), which reflects the primary nucleation of DL-MA in the D-crystallizer observed in Figure 40 and Figure 42 On the other hand, for the third experiment P3, the primary nucleation starts only after 15 residences.

As the duration of the stable growth phases for P1 and P2 are short and therefore only yield low product masses, the parallel processes under this conditions is not feasible to separate the D-and DL-MA at the eutectic point robustly and economically, considering that 3 g of seeds yield only a maximum 4.6 g of pure product.

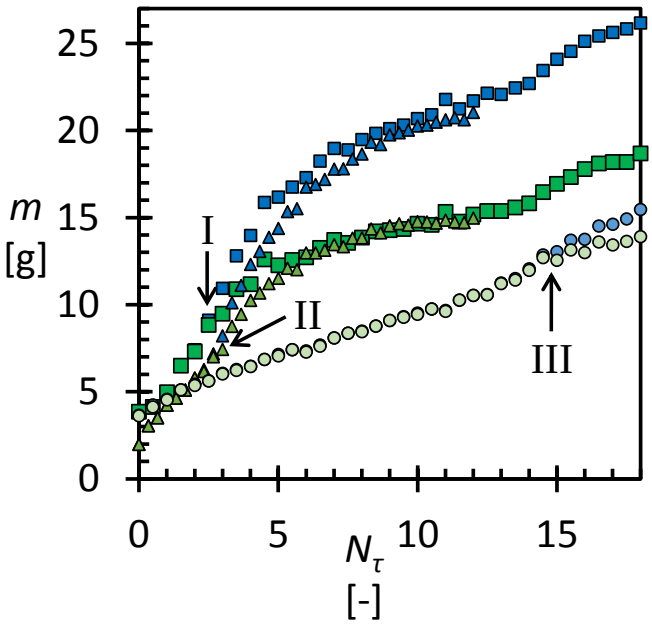

Figure 44: Overall mass of product (blue) and pure enantiomer (green) produced during the parallel crystallization experiments P1 (Squares); P2 (Triangles) and P3 (Circles) with the occurrence of DL-MA primary nucleation in the D-crystallizer indicated by the numbers I, II and III for each process respectively.

The third parallel experiment P3 allows for a much higher amount of product to be produced. However, the small temperature difference between the feed and crystallizers causes issues regarding the scalability of the process as conserving the temperature will be increasingly difficult at larger vessel sizes. As the root cause for the primary nucleation of the DL-MA in the D-crystallizer is the accumulation of DL-MA in the solution during the process, a serial crystallizer configuration is investigated with regards to its applicability.

4.5 Separation in the Eutectic: Crystallizers in Series

4.5.1 Serial Experiment 1: Feasibility Investigation

To prevent the primary nucleation of the DL-MA in the D-crystallizer, it is necessary to remove the DL-MA from the solution before it enters the D-crystallizer. To that end, a serial crystallizer configuration is used, where first the DL- and then the D-MA are crystallized sequentially in different crystallizers. The feasibility of the serial process configuration is investigated in the first serial experiment S1, using the same process conditions as P1. Like in the parallel experiments, the suspension density of the D-and DL-MA crystallized in the D crystallizer is monitored and plotted in Figure 45. The process was started 1 h after the seeding, indicated by 1 (Figure 45), to establish a clear baseline suspension density for the D-MA seeds. After starting the pumps, the suspension density of D-MA does not significantly increase until point 2 (Figure 45) is reached after 2 h processes time, or in this case, 1 residence time after the pumps are started. After this point, the suspension density of D-MA increases with a linear deposition rate of 13.3 g/lh, indicating the stable growth phase is reached at 8 h process time and lasts for 6 residences after point 3 (Figure 45). No primary nucleation of the DL-MA can be observed, as the suspension density of the DL-MA shown in Figure 45 remains below the error margin (± 7.5 g/l) of the monitoring method. At this point 3, the suspension density

stops increasing at a linear rate, indicating that less D-MA is supplied from the DL-crystallizer. This is likely due to primary nucleation of D-MA in the DL-crystallizer, as the solid excess in the feed vessel is not depleted at this time. This is confirmed by HPLC measurements of the product extracted from the DL-crystallizer, where an excess of D-MA with respect to the L-MA is identified (s. SI). Like in parallel experiments, the suspension density and overall concentration of the solution in the D-crystallizer is used to determine the composition of the concentrations in the crystallizers during the stable growth phase using the equations in the experimental section and plot them in a ternary phase diagram as shown in Figure 46.

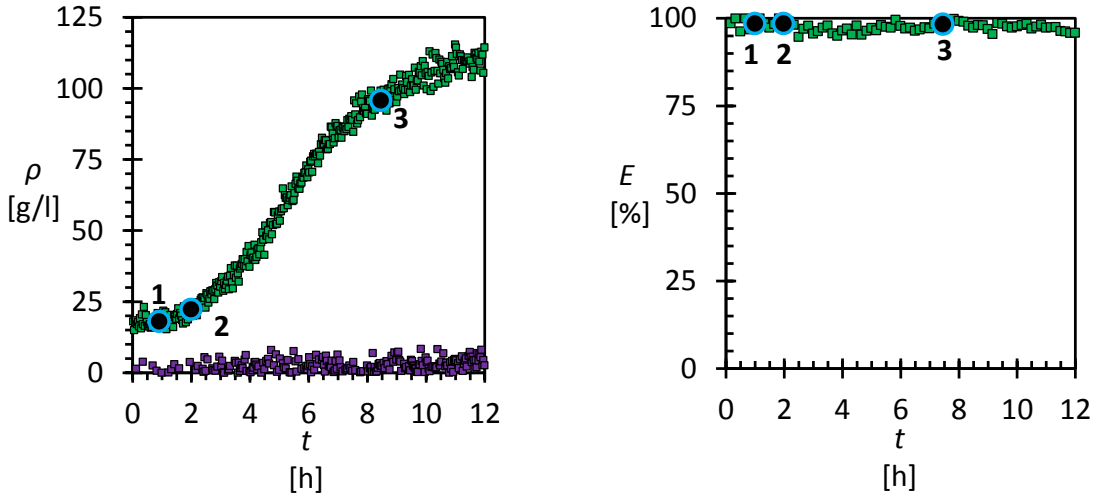

Figure 45: Suspension density of D-MA (green) and DL-MA (purple) in the D-crystallizer during serial experiment S1 (left) with ΔT=2˚C, τ=60 min and seed addition at t=0. 1) Start of pumps; 2) Beginning of stable growth phase; 3) End of stable growth phase, as well as the corresponding solid product enantiomeric excess E over time (right) for the serial experiment S1.

For the serial process, the calculation is more complex as two crystallizers have to be considered, but only the concentration of the D-crystallizer is available as the ATR-UV probe from the DL-crystallizer showed unusable results likely due to a bend in the probe. In the serial process, the DL-MA is crystallized first while the crystallizable D-MA fraction remains in solution. For this set of equations, only the stable growth phase is considered. It is assumed that during the stable growth phase the concentration of crystallizable D-MA coming from the feed vessel remains constant and passes through the DL-crystallizer.

$$VdC = F\left(C_{F,D} - C_{D,1}\right)dt \tag{12}$$

As no crystallizable D-MA is removed from the solution, no change in the D-MA concentration coming from the feed is assumed. Therefore the concentration of D-MA in the DL-crystallizer $C_{D,1}$ is the same as crystallizable D-MA in the feed $C_F E_{eu}$.

$$C_{D,1} = C_F E_{eu} \tag{13}$$

The concentration of D-MA in the DL-crystallizer serves as a feed for the D-crystallizer. At the same time, L-MA is removed in the DL-crystallizer, as the racemic compound is crystallized from the solution.

$$\frac{VdC}{dt} = F\left(C_{L,F} - C_L\right) - \frac{Vd\rho}{dt} \tag{14}$$

It is assumed that during the stable growth phase the concentration in the DL-crystallizer remains constant, as only the uncrystallized D-MA remains in the solution.

$$C_L = C_{L,F} - \tau G_L \tag{15}$$

The D-MA which passes through the DL-crystallizer is crystallized in the D-crystallizer with $C_{D,2}$ being the overall D-MA concentration in the D-crystallizer.

$$\frac{VdC}{dt} = F\left(C_{D,1} - C_{D,2}\right) - \frac{Vd\rho}{dt} \tag{16}$$

As the deposition rate G_D is constant during the stable growth phase, we assume the concentration $C_{D,2}$ in crystallizer to be constant (dC/dt = 0).

$$F\left(C_{D,1} - C_{D,2}\right) = VG_D \tag{17}$$

With the deposition rate, residence time and D-MA concentration form the DL-crystallizer known, the concentration of D-MA in the D-crystallizer during the stable growth phase can be determined.

$$C_{D,2} = C_{D,1} - \tau G_D \tag{18}$$

The uncrystallized DL-MA concentration $2C_{L,R}$ in the D-crystallizer for the serial process can be determined from the measured overall concentration with ATR-UV C_2:

$$2C_{L,R} = C_2 - C_{D,2} \tag{19}$$

As no DL-MA nucleated in the D-crystallizer, the concentration of L-MA in solution remains constant in the D-crystallizer. Therefore is the concentration of the remaining DL-MA in the DL-crystallizer $2C_{L,R.}$ The concentration in the DL-crystallizer during the stable growth phase can, therefore, be described using the measured concentration in the D-crystallizer plus the crystallized D-MA $C_{DL} = C_2 + \tau G_D$.

The saturated feed solution C_F (blue circle, Figure 46) is constantly pumped into the DL-crystallizer where it is subsequently cooled, supersaturating the feed solution. The DL-MA is crystallized while the D-MA remains in solution, as shown in Figure 46 by the increased D-MA fraction in the DL-crystallizer (purple dots, Figure 46) in comparison to the concentration values of the D-crystallizer (green dots, Figure 46), which are reduced by the amount of crystallized D-MA τG_D, during the stable growth phase. Also, uncrystallized DL-MA accumulates in the DL-MA crystallizer ($2C_L$), leading to an increase in the C_L concentration until reaching a maximum enrichment, which is shown by the trajectory of concentration values in the DL-crystallizer C_{DL} (purple dots, Figure 46). As the residual DL-MA along with the D-MA fraction from the feed $C_{D,1}$ is transferred to the D-crystallizer, where only D-MA is crystallized, the uncrystallized DL-MA $2C_{L,R}$ remains inert in the solution, leading to a similar trajectory for the concentration values of C_L in the D-crystallizer C_D, which also contains uncrystallized D-MA. From the D-crystallizer, the solution is recycled back to the feed vessel. By using the serial crystallizer configuration, the undesired product must be crystallized in the first crystallizer, in this case, the DL-crystallizer, as the desired enantiomer enriches in the liquid phase of the DL-crystallizer as shown in Figure 46 by the difference in D-MA fraction between D- and DL- crystallizer concentrations. As the D-MA from the feed remains in the solution of the DL-crystallizer a supersaturation of the D-MA with regards to the eutectic point

is created, which will eventually lead to primary nucleation of the D-MA in the DL-crystallizer. Once this occurs the D-MA concentration excess will be consumed in the DL-crystallizer, causing the stable growth phase to end as shown in Figure 45 (point 3).

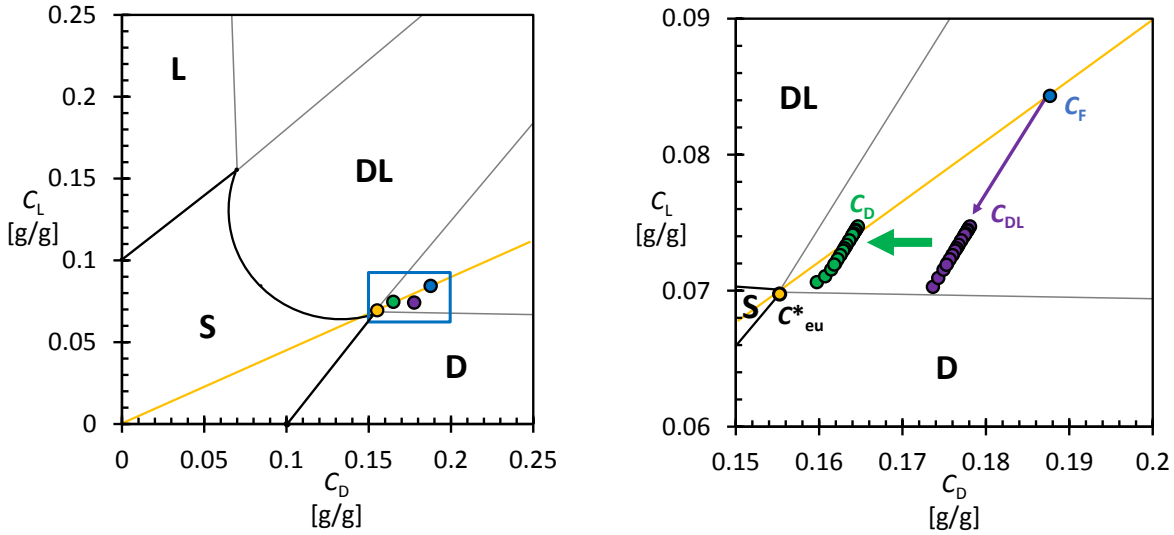

Figure 46: Left: Ternary phase diagram of serial experiment S1 at a crystallization temperature of 23 ˚C and its zoom (right) on the process concentrations, with the yellow line representing the eutectic composition; the feed concentration C_F (blue), the solution concentrations C_D in the D-crystallizer (green); C_{DL} in the DL-crystallizer (purple) during the stable growth phase and a purple arrow indicating the crystallization of the DL-MA, as well as the green arrow indicating the crystallization of the D-MA from the solution coming from the DL- to the D-crystallizer.

During the stable growth phase, a linear deposition rate G_D = 13.3 g/lh is measured, increasing the suspension density from 22.1 g/l at point 2 (Figure 45) to 94.8 g/l at point 3 (Figure 45). The yield achieved during the stable growth phase for this experiment is X = 75 %, where both the yield and the productivity during the stable growth phase are higher than in P1. Using the suspension densities, the solid enantiomeric excess can be monitored during the process, which is shown in Figure 45. Unlike any of the parallel experiments, the purity of the produced product remains high throughout the process. The duration of the stable growth phase is 6 h, which is three times longer than in P1, at higher productivity, at the same process conditions, showing that the serial process allows for a much better separation process of D-and DL-MA than the parallel configuration.

As no primary nucleation of the DL-MA in the product crystallizer occurred during this process, the robustness of the process with regards to residence time fluctuations is investigated.

4.5.2 Serial experiment 2: Effect of decreasing the residence time

In a second serial experiment S2 the effect of reducing the residence time from 60 min to 30 min by increasing the flow rate to 6.6 ml/min on product purity, productivity, yield and duration of the stable growth phase is investigated.

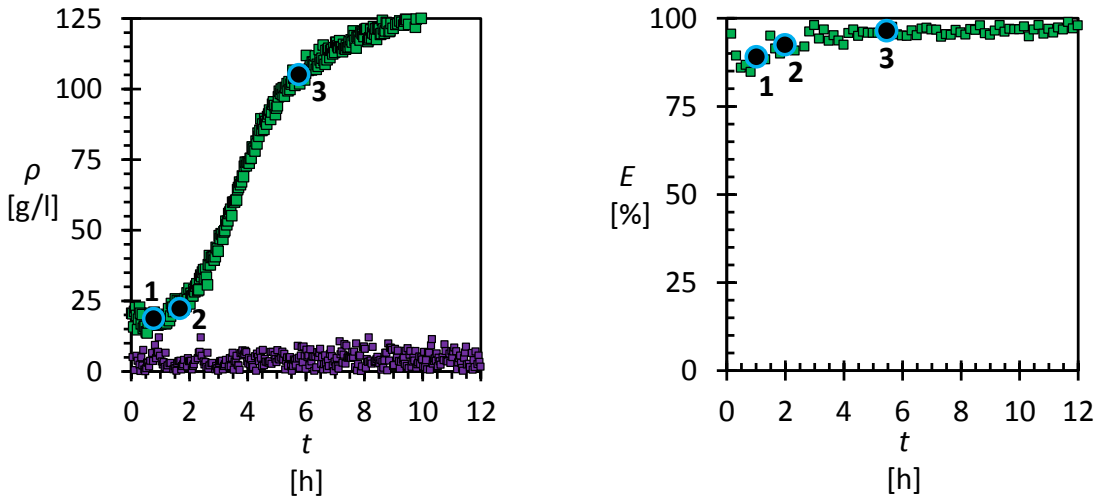

Figure 47: Suspension density of D-MA (green) and DL-MA (purple) in the D-crystallizer during serial experiment S2 (left) with ΔT=2˚C, τ=30 min and seed addition at t=0. 1) Start of pumps; 2) Beginning of stable growth phase; 3) End of the stable growth phase, as well as the corresponding solid product enantiomeric excess E over time (right) for the serial experiment S2.

Figure 47 shows the measured suspension density of the D-and DL-MA during the experiment. The figure shows no increase of the DL-MA suspension density, as observed in the parallel experiments, indicating that no primary nucleation of DL-MA occurred during the experiment. Like in S1, the process was started 1 h after seeding (1, Figure 47). After two residences, indicated by point 2 (Figure 47), the suspension density started to increase from 26.6 g/l at point 2 (Figure 47) to 107.7 g/l in point 3 (Figure 47), with a linear deposition rate of G_D = 22.4 g/lh, which is equal to the productivity. The stable growth phase lasts for 4 h or 8 residences, indicated by point 3 (Figure 47), after which the growth rate begins to dissipate. Looking at the linear deposition rate in absolute time in comparison to S1, more D-MA is provided to the system to be crystallized, allowing for a higher deposition rate at the same overall supersaturation. The yield X = 63.2 % achieved in S2 is lower than in S1 indicating that more D-MA is provided than can be crystallized during one residence time. Looking at the solid enantiomeric excess in Figure 10, up until 3 hours of process time fluctuation can be observed, but the overall purity remains high after that time. The fluctuations are likely due to the initial floating of the solid D-MA in the crystallizer, which can occur during the process. The ternary phase diagram for this experiment can found in the supporting material, as well as the concentration measured in the D-crystallizer.

In this experiment, it is shown that the serial crystallization configuration is robust against flowrate fluctuations as no primary nucleation of the DL-MA is observed in the D-crystallizer. Furthermore, it is demonstrated that a shorter residence time leads to higher linear deposition rates during the stable growth phase, allowing to produce more D pure product in a shorter process time in comparison to S1. In the next experiment, the robustness of the process with regards to temperature fluctuations is investigated, as this is a bottleneck for the parallel configuration in P2 and P3.

4.5.3 Serial experiment 3: increasing the temperature difference

In a third serial experiment S3, the crystallization temperature of the crystallizers is reduced from 23°C (S1 and S2) to 20°C, leading to a supersaturation of 1.41, to investigate the

limitations and range of applicability of the process with regards to temperature difference between feed and crystallizers, represented by the supersaturation. The experiment is started at 1 h after seeding as shown at point 1 in Figure 48. After starting the process, a slight increase in the suspension density of D-MA can be observed for one residence or 1 h process time, until point 2 (Figure 48) is reached, where the suspension density begins to increase at a linear deposition rate of G_D = 24.4 g/lh, which is equal to the productivity per residence in this experiment. The stable growth phase lasts for 2 h hours, increasing the suspension density from 32.9 g/l in point 2 (Figure 48) to 75.9 g/l in point 3 (Figure 48). After 4 h process time, the growth dissipates as in the previous experiments, which is caused by D-MA nucleating in the DL crystallizer. Even though the stable growth phase is the shortest from all serial experiments in terms of overall and residence time, no primary nucleation of the DL-MA occurs in the product crystallizer, allowing for pure D-MA to be extracted at the end of the process. The ternary phase diagram for this experiment can found in the supporting material, as well as the concentration measured in the D-crystallizer.

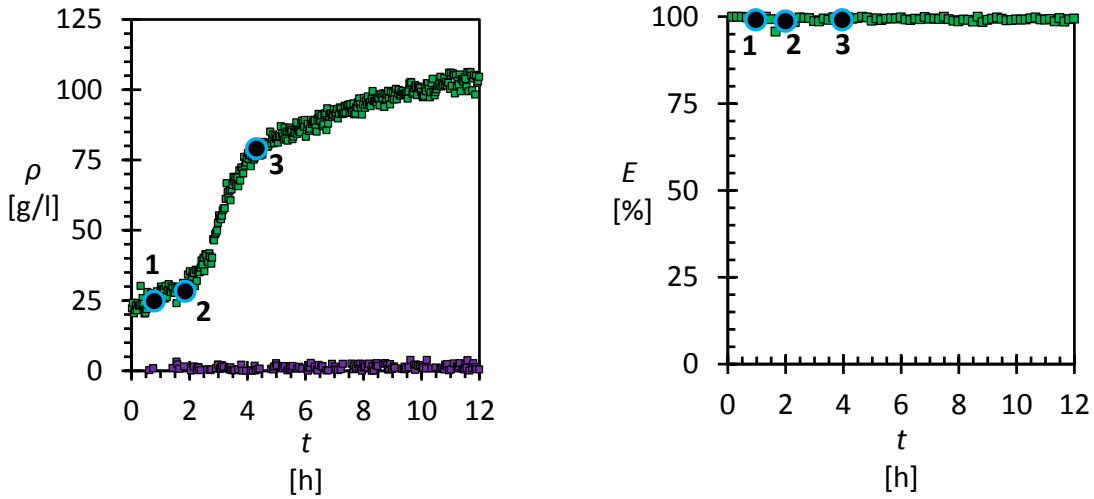

Figure 48: Suspension density of D-MA (green) and DL-MA (purple) in the D-crystallizer during serial experiment S3 (left) with ΔT=5˚C, τ=60 min and seed addition at t=0. 1) Start of pumps; 2) Beginning of stable growth phase; 3) End of the stable growth phase, as well as the corresponding solid product enantiomeric excess E over time (right) for the serial experiment S3.

The product purity is also represented in Figure 11 (right), which shows no drop in purity during this experiment. The yield during the stable growth phase of this experiment is X = 75.4 % similar to the yield in S1. This experiment shows that the serial crystallizer configuration is not just robust against flowrate but also temperature fluctuations, allowing for the crystallization of pure D-MA product.

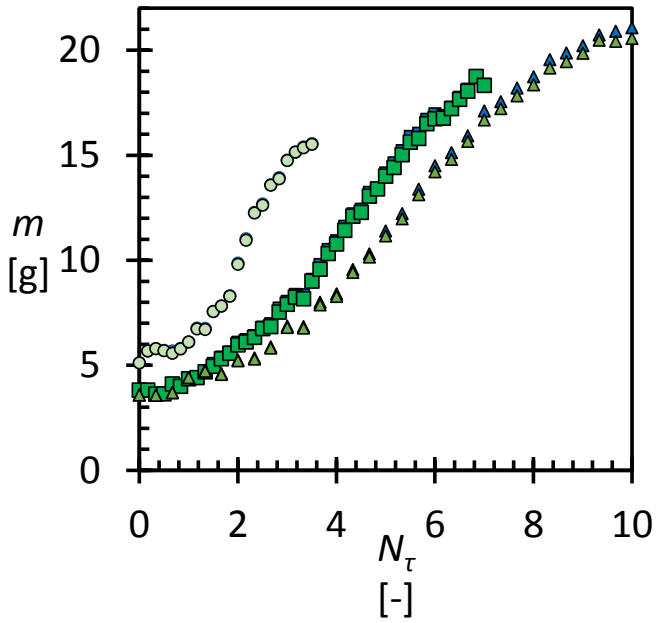

Figure 49: Overall amount of total product (blue) and pure enantiomer (green) produced during the serial crystallization experiments S1 (Squares); S2 (Triangles) and S3 (Circles).

The findings of all serial experiments can be highlighted in Figure 50, where the overall mass produced for each serial experiment (blue) and the mass of the enantiomerically pure product (green) is plotted over the number of residences for each experiment. It is shown in the figure that the produced overall and enantiopure product mass either overlap (S1, S3) or are very close (S2) to one another. These results confirm that the product was produced with very high purity and no primary nucleation occurred, whereas in Figure 44 (for the parallel configuration) the pure and overall mass started to deviate at some point. Figure 51 also shows that S2 (triangles) is the experiment with the highest number of residences, while S3 had the highest linear deposition rate per residence. In addition to the Raman in-situ measurement, the purity of the produced D-MA product was confirmed by analyzing the solids with HPLC to confirm that no primary nucleation occurred. The chiral HPLC for all serial experiments show an enantiomeric excess of more than 99 % for all produced D-MA. In previous work conducted by Gou [13] and Polenske [17], where a hybrid process is used to enrich MA to the eutectic composition followed by a preferential crystallization, with purities of more than 98 % but at lower productivities than in the serial process.

Comparing the results of the parallel and serial crystallizer configurations under the same process conditions in P1 and S1, the serial experiment S1 yields more than 3 times the pure D-MA product of P1. While the primary nucleation of DL-MA occurred in the D-crystallizer in each parallel experiment, this was not observed in any serial experiment. It is also shown that the serial process is more robust against temperature or higher supersaturation and residence time changes, while the parallel process requires a very narrow temperature difference between feed and crystallizer. The here presented serial process can be used in a hybrid process, for instance with chiral chromatography [4] to enrich the starting solution to the eutectic composition. The racemic compound which is produced as a side product can be recycled back to the chromatography for enrichment, allowing for an overall higher yield and higher efficiency of the chiral separation.

4.6 Discussion

The investigation of the parallel and serial crystallization process revealed that both processes can in principle be used to separate enriched the racemic compound forming system mandelic acid in the triphasic domain. During all parallel experiments, the primary nucleation of the racemic compound is observed in the D-crystallizer after a short time in the parallel experiment P1, resulting in a short stable growth phase and little product to be obtained. In a serial experiment conducted under the same process conditions, the stable growth phase is prolonged by a factor of three, at higher productivity and yield than the once reached in P1. Also, no primary nucleation occurred in the D-crystallizer during this experiment showing that crystallizing the DL-MA before the D-MA allows for a more stable process. In second and third parallel experiments, it is investigated if increasing the residence time and decreasing the temperature difference allows for a prolonged stable growth phase. It is shown that while a longer residence time does not affect the system, a decrease of the temperature does allow for a prolonged separation and more product to be produced. However considering that realizing a very low temperature difference is difficult to achieve in larger crystallizers, the parallel process can be deemed not feasible to separate MA at the eutectic composition, as robust processes are desired in industry. The serial process, on the other hand, showed no sign of the racemic compound primary nucleating in the D-crystallizer, even after the residence time was reduced by half and the temperature difference between feed and crystallizer was increased from two to five degrees Celsius. This shows that the serial process is robust against changes in temperature and residence time.

Comparing the productivities, which are the same as the linear deposition rates during the stable growth phase, the parallel and serial processes can be compared. Productivities of P = 11.3 g/lh for P1, P = 5.7 g/lh for P2 and P = 2.7 g/lh for P3 are reached. In comparison the productivities reached during the serial experiments are P = 13.3 g/lh for S1, P = 22.4 g/lh for S2 and P = 24.4 g/lh for S3. While the productivity in P1 is the highest the duration of the stable growth phase is the shortest with only 2 h, resulting in a low mass of enantiopure product being produced.. While increasing the residence time from 60 to 90 min doubled the duration of the stable growth phase, the productivity is almost halved, resulting in no gain of pure product. The third experiment P3 had the lowest productivity but the longest stable growth phase, resulting in the purest product produced in any of the parallel experiment. During the serial process S1 at the same process conditions as P1, higher productivity is reached, for a longer stable growth phase. In S2 the residence time was reduced by half, resulting in more residences being achieved at the same process time as S1, significantly increasing the productivity and produced overall product mass. The third serial experiment S3 showed high robustness against temperature difference as a high productivity and enantiopure product was obtained, showing the serial process to be very robust and reliable.

While it was shown that serial crystallization is a viable method for the separation of chiral compounds, it has its limitations. The intention of the serial process is to support a primary separation method which enables the separation of a racemic compound forming system, like chromatography, which can recycle the produced racemic compound and re-enrich it to be reused as feed. Using the serial configuration in such a hybrid process would increase the

overall yield and lower the costs of chromatographic separation. Indeed, chromatography allows for large enrichments starting with a racemic compound, while more solvent and initial material are required to separate enantiomers from an already enriched feed[4, 15]. On the other hand, crystallization is efficient when an already enriched starting solution is used. Therefore, hybrid processes combine the benefits of both methods. The limitation of this process is towards racemic compounds which have an eutectic point that requires a very high enrichment of one enantiomer (>85 % of D in L). However, regarding the common appearance of racemic compound forming systems, the serial configuration in combination with a primary separation method represents a highly flexible and robust method to efficiently and selectively separate racemic compound forming systems at eutectic composition, yielding enantiopure product at purities over 99 %. While so far reported hybrid processes only allow for a batch-wise separation of the enriched compound, this process allows for a semi-batch separation with a solution recycle, enabling higher productivities and overall yield in comparison to other processes. Since all vessels and flowrates are constant during the process, it can be monitored and controlled easily, allowing for reproducible product quality.

4.7 Conclusions

The results show that both the parallel and the serial configurations can be used for the separation of mandelic acid at eutectic composition. However, the serial configuration is shown to be a very robust, stable and controllable separation process. With the Raman spectroscopy, we show a reliable process analytical tool, which allows monitoring the suspension density and solid product purity produced in situ during the process, and apply direct process control if needed. Given the robustness of the serial process configuration with the high yields and chiral product purity, this process provides an efficient tool to separate racemic compound forming systems at the eutectic composition in a hybrid process. While prior enrichment is needed for the process to work, it is shown to be highly selective and efficient in enriched solutions, while primary separation techniques such as chromatography are more efficient and much cheaper to apply starting at racemic compositions. Not all chiral racemic compound forming systems have a favorable eutectic rather close to the racemic composition, which is needed for this process to produce an ample amount of pure product. But given the common appearance of racemic compound forming systems, those with a favorable eutectic are more common than conglomerate forming systems for which a large number of crystallization based chiral separation processes are designed. By combining this semi-batch serial process configuration, with a primary separation method like chromatography, the strength of both processes can be used to their full potential to reduce production costs and increase the overall efficiency.

4.8 Acknowledgments

This research has received funding as part of the CORE project (October 2016 – September 2020) from the European Union's Horizon 2020 research and innovation program under the Marie Sklodowska-Curie grant agreement No 722456 CORE ITN. We thank the EPSRC Centre

for Innovative Manufacturing in Continuous Manufacturing and Crystallisation (http://www.cmac.ac.uk) for support (EPSRC funding under grant reference: EP/I033459/1).

4.9 References

[1] J. Chen, B. Sarma, J.M.B. Evans, A.S. Myerson, Pharmaceutical Crystallization, Crystal Growth & Design 11(4) (2011) 887-895.

[2] H. Lorenz, A. Seidel-Morgenstern, Processes to separate enantiomers, Angew Chem Int Ed Engl 53(5) (2014) 1218-50.

[3] I.R. Baxendale, R.D. Braatz, B.K. Hodnett, K.F. Jensen, M.D. Johnson, P. Sharratt, J.-P. Sherlock, A.J. Florence, Achieving Continuous Manufacturing: Technologies and Approaches for Synthesis, Workup, and Isolation of Drug Substance May 20–21, 2014 Continuous Manufacturing Symposium, Journal of Pharmaceutical Sciences 104(3) (2015) 781-791.

[4] K.G. Feitsma, B.F.H. Drenth, Chromatographic separation of enantiomers, Pharmaceutisch Weekblad 10(1) (1988) 1-11.

[5] J.W. Mullin, Crystallization, in: J.W. Mullin (Ed.), Crystallization (Fourth Edition), Butterworth-Heinemann, Oxford, 2001, pp. 536-575.

[6] H. Lorenz, A. Perlberg, D. Sapoundjiev, M.P. Elsner, A. Seidel-Morgenstern, Crystallization of enantiomers, Chemical Engineering and Processing: Process Intensification 45(10) (2006) 863-873.

[7] A.C. J. Jacques, S. H. Wile, Enantiomers, Racemates and Resolutions, Krieger, Malabar1994.

[8] D. Binev, A. Seidel-Morgenstern, H. Lorenz, Continuous Separation of Isomers in Fluidized Bed Crystallizers, Crystal Growth & Design 16(3) (2016) 1409-1419.

[9] J.H. Chaaban, K. Dam-Johansen, T. Skovby, S. Kiil, Separation of Enantiomers by Continuous Preferential Crystallization: Experimental Realization Using a Coupled Crystallizer Configuration, Org. Process Res. Dev. 17(8) (2013) 1010-1020.

[10] M.P. Elsner, G. Ziomek, A. Seidel-Morgenstern, Simultaneous preferential crystallization in a coupled batch operation mode. Part II: Experimental study and model refinement, Chemical Engineering Science 66(6) (2011) 1269-1284.

[11] C. Rougeot, J.E. Hein, Application of Continuous Preferential Crystallization to Efficiently Access Enantiopure Chemicals, Org. Process Res. Dev. 19(12) (2015) 1809-1819.

[12] S. Swernath, M. Kaspereit, A. Kienle, Coupled Continuous Chromatography and Racemization Processes for the Production of Pure Enantiomers, Chemical Engineering & Technology 37(4) (2014) 643-651.

[13] L. Gou, S. Robl, K. Leonhard, H. Lorenz, M. Sordo, A. Butka, S. Kesselheim, M. Wolff, A. Seidel-Morgenstern, K. Schaber, A hybrid process for chiral separation of compound-forming systems, Chirality 23(2) (2011) 118-27.

[14] M.D.D. Heike Lorenz, E.D.L.K. Polenske, M.D. Andreas, M.D. Seidel-Morgenstern, METHOD FOR SEPARATION OF RACEMIC COMPOUND-FORMING CHIRAL SUBSTANCES BYA CYCLIC CRYSTALLIZATION PROCESS AND A CRYSTALLIZATION DEVICE, in: U.P. Office (Ed.) United States, 2012.

[15] H. Kaemmerer, Z. Horvath, J.W. Lee, M. Kaspereit, R. Arnell, M. Hedberg, B. Herschend, M.J. Jones, K. Larson, H. Lorenz, A. Seidel-Morgensten, Separation of Racemic Bicalutamide

by an Optimized Combination of Continuous Chromatography and Selective Crystallization, Org. Process Res. Dev. 16(2) (2012) 331-342.

[16] H. Lorenz, D. Polenske, A. Seidel-Morgenstern, Application of preferential crystallization to resolve racemic compounds in a hybrid process, Chirality 18(10) (2006) 828-40.

[17] D. Polenske, H. Lorenz, A. Seidel-Morgenstern, Potential of different techniques of preferential crystallization for enantioseparation of racemic compound forming systems, Chirality 21(8) (2009) 728-737.

[18] W.R. Angus, R.P. Owen, The Stability of Racemates. Mandelic Acid and Some of its Derivatives, J. Chem. Soc. (1943) 227.

[19] C.F. Curitiba Marcellos, H. Durand, J.S.-I. Kwon, A. Gomes Barreto Jr., P. Laranjeira da Cunha Lage, M. Bezerra de Souza Jr., A.R. Secchi, P.D. Christofides, Optimal operation of batch enantiomer crystallization: From ternary diagrams to predictive control, AIChE Journal 64(5) (2018) 1618-1637.

[20] H. Lorenz, A. Seidel-Morgenstern, Binary and ternary phase diagrams of two enantiomers in solvent systems, Thermochimica Acta 382(1) (2002) 129-142.

[21] A. Perlberg, H. Lorenz, A. Seidel-Morgenstern, Crystal Growth Kinetics via Isothermal Seeded Batch Crystallization: Evaluation of Measurement Techniques and Application to Mandelic Acid in Water, Industrial & Engineering Chemistry Research 44(4) (2005) 1012-1020.

[22] H. Lorenz, D. Sapoundjiev, A. Seidel-Morgenstern, Enantiomeric Mandelic Acid SystemMelting Point Phase Diagram and Solubility in Water, J. Chem. Eng. Data 47 (2002) 1280.

[23] K. Bakeev, Process Analytical Technology: Spectroscopic Tools and Implementation Strategies for the Chemical and Pharmaceutical Industries, 2nd Edition, 2010.

[24] H. Lorenz, D. Sapoundjiev, A. Seidel-Morgenstern, Enantiomeric Mandelic Acid SystemMelting Point Phase Diagram and Solubility in Water, Journal of Chemical & Engineering Data 47(5) (2002) 1280-1284.

4.10 Appendix 1: Raman Spectra of solid D and DL Mandelic Acid Crystals

As the racemic compound DL MA and the enantiopure D MA have different physical properties and crystal structures, they can be distinguished using Raman spectroscopy [1]. The Raman spectra of the solid D and DL mandelic acid are shown in Figure 52, with the wavelength of the Raman shift used in this work highlighted. Overlaying both spectra clearly shows a number of peaks which are specific for the racemic compound and pure enantiomer respectively. Using the Raman, pure solid enantiomer and racemic compound can be distinguished, however, both the D and L enantiomer in solute phase have the same spectra which allows this method only for the analysis in solid state.

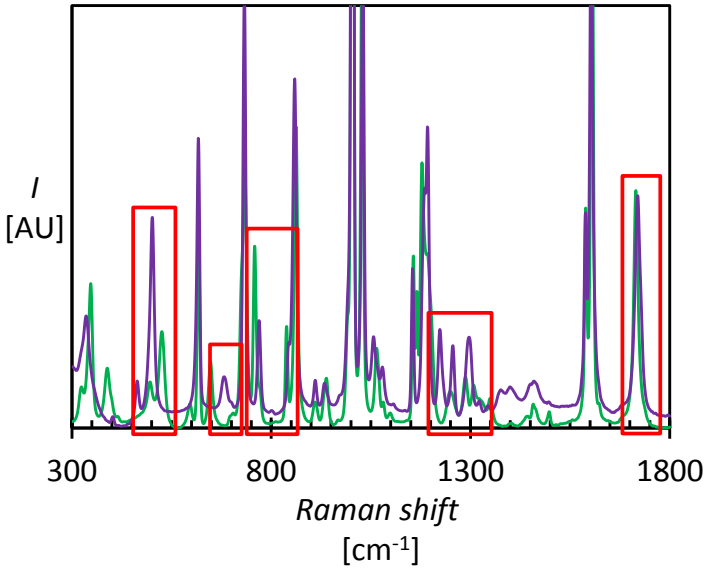

Figure 52: Raman Spectra of D (green) and DL (purple) mandelic acid with the used wavelength indicated.

4.11 Appendix 2: Measured Concentrations in the D Crystallizer during the Parallel and Serial experiments using an ATR-UV Probe

For the determination of the overall concentrations in the D crystallizer, the solution concentration is measured using an ATR-UV probe. The probe is calibrated against different eutectic concentrations at changing temperatures. For all calibrations, a starting concentration at 25°C at eutectic composition was created and subsequently cooled to the temperature at which the calibration is to be obtained. Then defined amounts of solvent (water) are added periodically until a concentration of 150 g/l is reached. This procedure is repeated for 25, 23 and 20°C to cover the whole range of temperatures used during all conducted experiments.

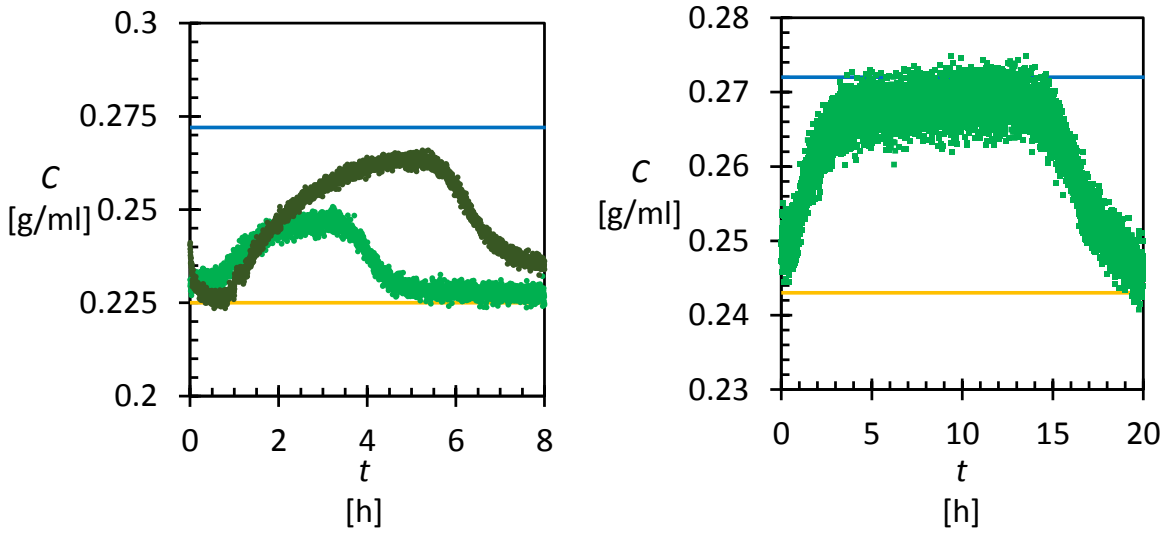

Figure 53: Overall Concentrations measured during the parallel experiments P1 (light green, left), P2 (dark green, left) and P3 (light green, right), with the eutectic feed (blue) and crystallizer (orange) concentrations indicated.

Figure 53 shows the overall concentrations measured in the D-crystallizer during the parallel experiments. The light green plot in Figure 53 (left) shows the concentration measured during the first parallel experiment P1. After starting the pumps at 1 h process time, the accumulation of the DL-MA in the D-crystallizer can be observed by an increasing concentration. Initially, the concentration increases sharply, but with increasing enrichment of DL-MA in solution, the increase slowly decreases until it suddenly decreases, which is due to the primary nucleation of the DL-MA in the D-crystallizer as shown by the suspension density. Similar behaviour is observed for the concentration measured during the second parallel experiment P2 (Figure 53, left dark green). During this experiment, a higher residence time is used, which results in higher process time and more DL-MA accumulating in the crystallizer solution. Once a certain enrichment of DL-MA is reached, primary nucleation occurs, resulting in a drop of concentration. The concentration measured for the parallel experiment P3 (Figure 53, right) shows a long period of stable concentration (0.268 g/ml) between 3 to 14 h after which the concentration drops due to the primary nucleation of the DL MA.

The measured overall concentrations in the D crystallizer during the serial experiments are shown in Figure 54. The concentration initially increases and then begins to slowly decrease. This can be explained by the surface area present in the crystallizer increasing during the process, where at some point the supplied supersaturation of D MA can be fully crystallized with the given surface area. Also a primary nucleation event of D MA occurring in the DL crystallizer, leading to less D-MA being supplied to the D crystallizer, resulting in a decrease of the concentration after the stable growth phase ends. The occurrence of the primary nucleation of D-MA in the DL-crystallizer is shown in the HPLC measurements conducted from the extracted product from the DL crystallizer can be found in Appendix 4. Similar behaviour of the concentration profile like in experiment S1 is observed in serial experiments S2 and S3 (Figure 54, right). As the stable growth phase in serial experiment S3 only lasts for two hours the decrease in concentration is due to the primary nucleation of the D-MA in the DL-crystallizer.

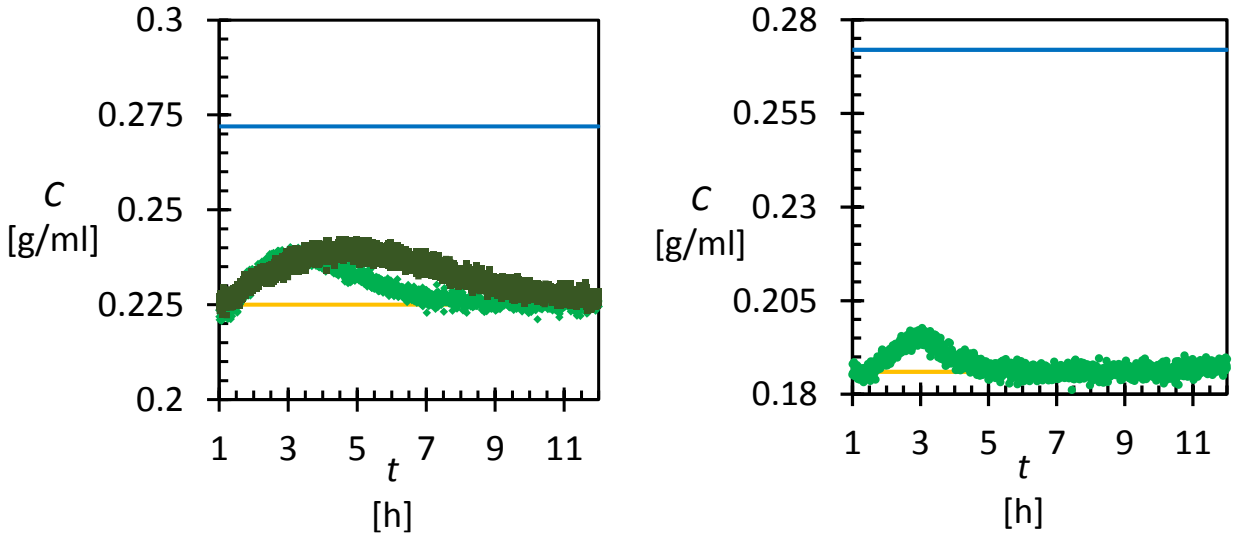

Figure 54: Overall Concentrations measured during the serial experiments S1 (light green, left), S2 (dark green, left) and S3 (light green, right), with the eutectic feed (blue) and crystallizer (orange) concentrations indicated.

4.12 Appendix 3: Ternary Phase diagrams as plots of concentration of D and L Mandelic Acid

While the ternary phase diagrams represented by the concentrations of D and L MA of the first parallel and serial process are discussed in the publication, the phase diagrams for the remaining serial and parallel experiments are shown in the following section.

4.12.1 Parallel Experiments P2 and P3

The ternary phase diagram for the concentrations measured in the D-crystallizer during the second parallel experiment P2, conducted at a higher residence time of 90 min is shown in Figure 41. As the process lasts longer and a higher concentration of DL-MA is reached in the solution than in P1, the concentration C_D in the D-crystallizer follows a trajectory until reaching a value which is close to the theoretical value, which is shown in Figure 41 (right) as the blue arrow coming from the feed to the D-crystallizer concentration C_D only changes in the D-MA concentration but not in the L-MA concentration, indicating that the amount of L-MA accumulated in the crystallizer is equal to the L-MA in the feed solution and no more enrichment is possible.

In the second parallel experiment, the temperature difference used is 1°C between feed and crystallizer. The driving force for this experiment is, therefore, lower than the other parallel processes. Figure 56 shows the ternary phase diagram of this experiment. Similar to the second parallel experiment P2, the concentration in the D-Crystallizer C_D reaches an enrichment of DL-MA which very close to the theoretical value as the L-MA fraction is similar to the L-MA fraction in the feed, as shown in Figure 56.

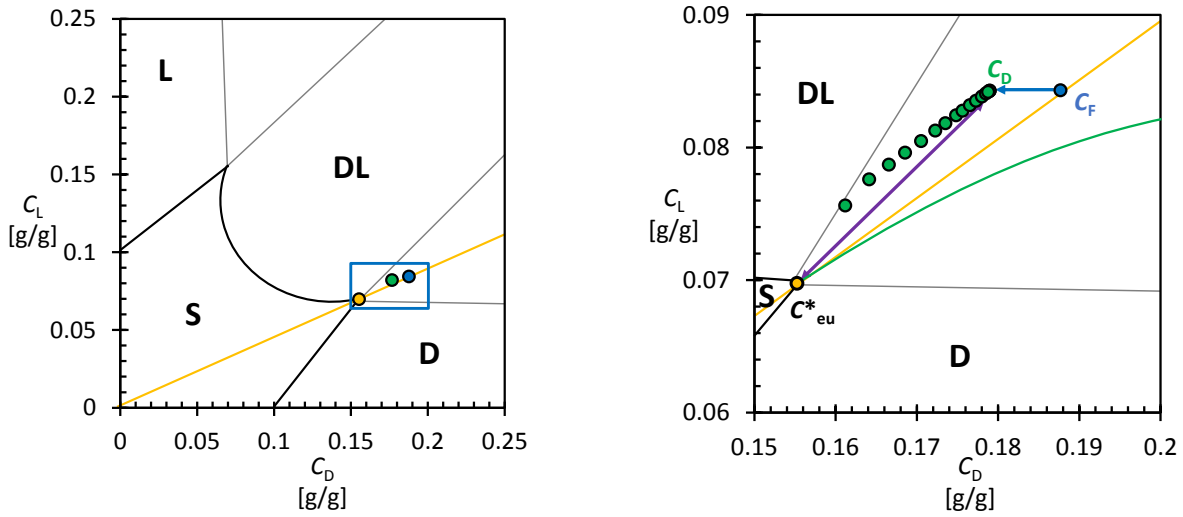

Figure 55: Left: Ternary phase diagram of MA in water and the compositions in parallel experiment P2 at crystallization temperature of 23 ˚C and residence time 90 min, as well as its zoom (right) on the process concentrations, with the feed concentration C_F (blue) and the solution concentration C_D in the D-crystallizer (green) during the stable growth phase. The accumulation of DL-MA in solution in the D crystallizer (purple arrow), is indicated. The green line starting from the eutectic concentration in the crystallizer represents the overall composition including the crystallized D-MA during the stable growth phase.

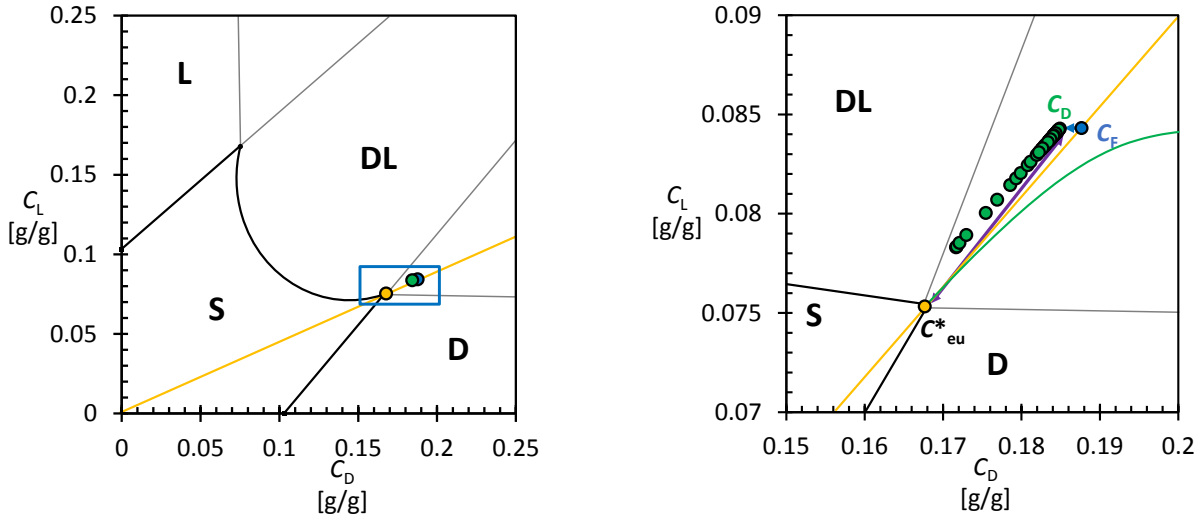

Figure 56: Left: Ternary phase diagram of MA in water and the compositions in parallel experiment P3 at crystallization temperature of 24 ˚C and its zoom (right) on the process concentrations, with the feed concentration C_F (blue) and the solution concentration C_D in the D-crystallizer (green) during the stable growth phase. The accumulation of DL-MA in solution in the D crystallizer (purple arrow), is indicated. The green line starting from the eutectic concentration in the crystallizer represents the overall composition including the crystallized D-MA during the stable growth phase.

4.12.2 Serial Experiments S2 and S3

The ternary phase diagram of serial experiment S2 during the stable growth phase, where the residence time is decreased to 30 min, is shown in Figure 46. Figure 58 shows the ternary phase diagram of serial experiment S3 during the stable growth phase, where a larger temperature difference between feed and crystallizer is used.

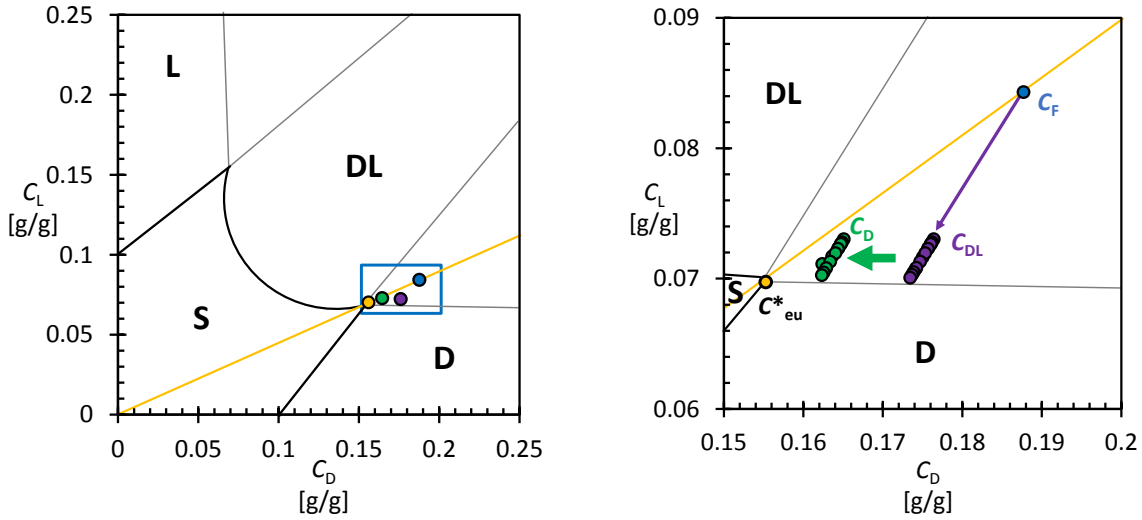

Figure 57: Left: Ternary phase diagram of serial experiment S2 at a crystallization temperature of 23 ˚C and its zoom (right) on the process concentrations, with the yellow line representing the eutectic composition; the feed concentration C_F (blue), the solution concentrations C_D in the D-crystallizer (green); C_{DL} in the DL-crystallizer (purple) during the stable growth phase and a purple arrow indicating the crystallization of the DL-MA, as well as the green arrow indicating the crystallization of the D-MA from the solution coming from the DL- to the D-crystallizer.

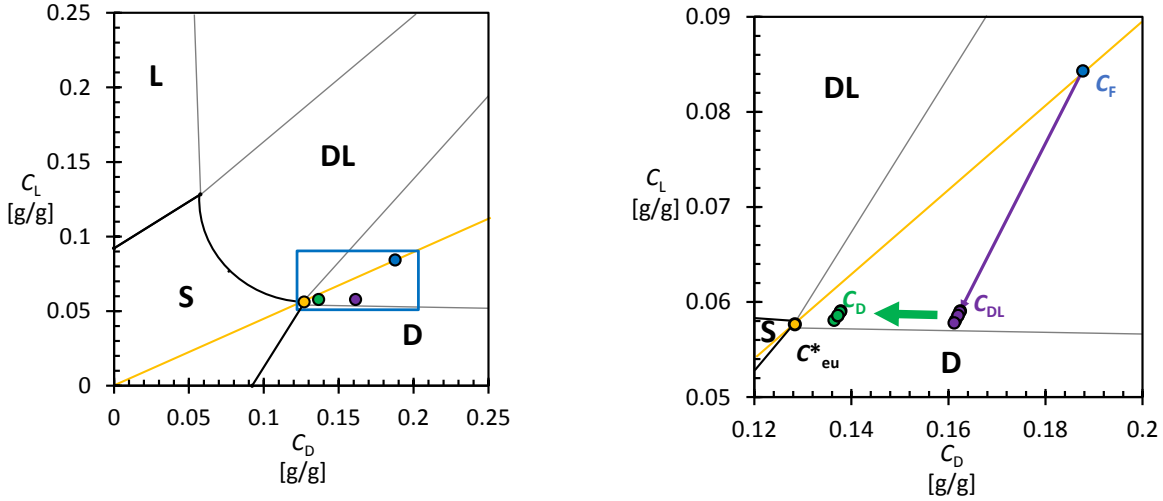

Figure 58: Left: Ternary phase diagram of serial experiment S3 at a crystallization temperature of 20 ˚C and its zoom (right) on the process concentrations, with the yellow line representing the eutectic composition; the feed concentration C_F (blue), the solution concentrations C_D in the D-crystallizer (green); C_{DL} in the DL-crystallizer (purple) during the stable growth phase and a purple arrow indicating the crystallization of the DL-MA, as well as the green arrow indicating the crystallization of the D-MA from the solution coming from the DL- to the D-crystallizer.

4.13 Appendix 4: Chiral HPLC Method and Results

Chiral chromatography is performed on samples of all compounds used in this work to measure the enantiomeric excess. The surface is under the peaks of the chromatogram are used for the determination of the enantiomeric excess $E = (A_1\text{-}A_2)/(A_1+A_2)$.

4.13.1 Mandelic Acid Product D-Crystallizer

For measuring the mandelic acid enantiomeric excess a lux 3 µm Amylose-1 LC column 150x3 mm (Phenomenex) was used with a 80/20 mix of hexane (0.1 % formic Acid) and IPA (0.1 %

formic acid) as eluent at a flow rate of 0.6 ml/min and an injection volume of 1 µm. The method was given on request by Phenomenex and can also be found in their databank.

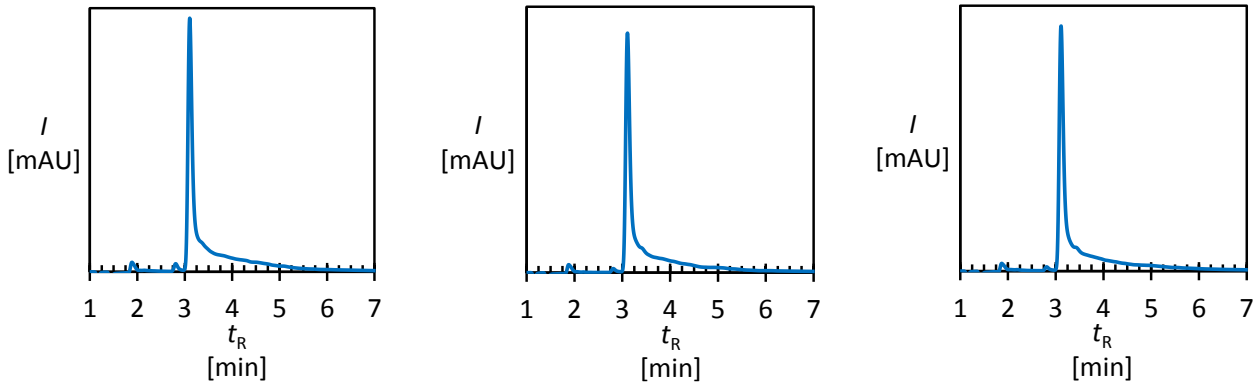

Figure 59: Intensity versus retention time chromatogram of the final product in D crystallizer measured with chiral HPLC for Serial experiments S1 (left), S2 (middle), S3 (right).

Figure 59 shows the chromatograms of the product extracted from the D-crystallizer at the end of every serial experiment, with the ratios of D- and L-MA shown in Table 6. As shown from the ratios, as well as the chromatograms, the extracted product from the D-crystallizer is nearly enantiopure. In all a samples irrespective of D- or DL-MA an unidentified impurity is detected at 1.9 min retention time, which could be due to a solvent impurity or a residue in the chromatography column.

Table 6: Measured areas under the chromatographic peaks with retention times of the peaks for each species identified in the chromatogram.

Species	Ratio of *A* [%]	Retention Time [min]
L MA (S1)	1.73	2.808
D MA (S1)	98.27	3.104
L MA (S2)	0.94	2.811
D MA (S2)	99.06	3.111
L MA (S3)	0.87	2.813
D MA (S3)	99.13	3.114

4.13.2 Mandelic Acid Product DL-Crystallizer

To show that primary nucleation of D-MA occurred in the DL-crystallizer, the extracted product from the DL-crystallizer is analysed with HPLC, with the resulting chromatograms being shown in Figure 60. The chromatograms clearly show the D-MA peak at a retention time of 2.8 min, followed by a D-MA peak with a larger peak height and area under the peak. The higher area under the peak and peak height of the D-MA with respect to L-MA show that primary nucleation of D-MA occurred during the experiments.

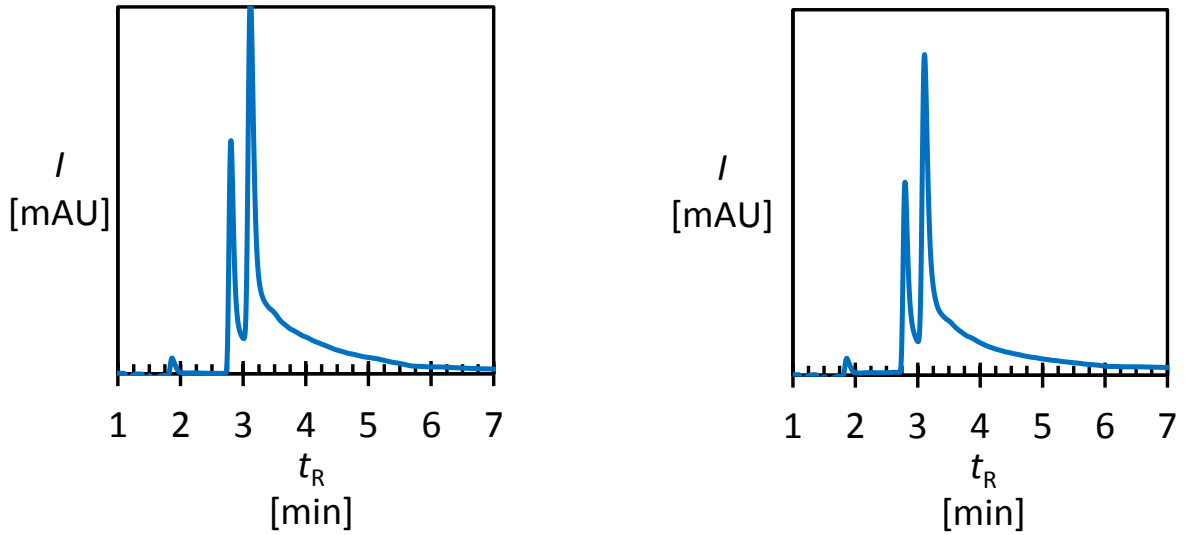

Figure 60: Intensity versus retention time chromatogram of the final product in DL crystallizer measured with chiral HPLC for Serial experiments S1 (left) and S2 (right).

The measured ratios of the peak areas and retention times are shown in Table 7. The exact ratio, in this case, is hard to quantify due to the imperfect separation of both peaks, which results in an increased area under the peak for D MA in this case. As the product for the third serial experiment S3 could not be extracted from the DL crystallizer due to the severe agglomeration and very high suspension density (~1 g/ml), it is assumed that primary nucleation of D MA also occurred in the DL crystallizer during S3.

Table 7: Measured areas under the chromatographic peaks with retention times of the peaks for each species identified in the chromatogram for product extracted from crystallizer 1 and product crystallizer 2 after the serial ASN experiment.

Species	Ratio of *A* [%]	Retention Time [min]
L MA	18.90	2.801
D MA	81.10	3.112
L MA	18.70	2.799
D MA	81.30	3.110

4.14 References

1. De Beer, T., et al., *Near-infrared and Raman spectroscopy for the in-process monitoring of pharmaceutical production processes.* International Journal of Pharmaceutics, 2011. **417**(1): p. 32-47.

5 Separation, Resolution and Deracemization in Chiral Eutectic Solutions

In the pharmaceutical industry, the reproducible production of enantiopure compounds is of high importance as often only one enantiomer has the desired effect in the human body, while the other can be harmful. Crystallization-based separation, resolution, and deracemization are highly selective and potentially efficient processes to produce enantiopure crystalline materials. In this work, we aim to develop and validate a general process design that allows for the crystallization-based separation, resolution, and deracemization of chiral compounds at the eutectic composition through a set of crystallizers in series. Mandelic acid, Asparagine, and Clopidogrel-imine are used as model compounds to exemplify and validate respectively the separation, resolution and deracemization process in the proposed process configuration. By using the proposed semi-batch process configuration a large range of chiral compounds can be separated at consistently reproducible quality, presenting an alternative for the existing processes.

5.1 Introduction

The majority of modern APIs (Active Pharmaceutical Ingredients) are chiral molecules, where usually only one enantiomer has the desired effect in the body, while the counter enantiomer can be harmful or have no effect at all [1]. An example of this is Naproxen, an anti-inflammatory medicine, where the counter enantiomer can cause liver damage [2, 3]. Therefore it is necessary to produce the right enantiomer or ensure the other handedness does not cause any undesired side effects in the human body. If the pure enantiomer cannot be produced, chiral separation can be necessary, where crystallization based techniques have proven to be a selective and reliable technique [4]. In this work crystallization based chiral separation, resolution, and deracemization were used on three different model compounds, two conglomerate, and one racemic compound forming system, in one process configuration.

There are two major types of chiral solid systems for mixtures of enantiomers, the less common conglomerate and frequently occurring racemic compound forming systems [4-6]. In the case of a conglomerate system, the enantiomers form enantiomerically pure crystals which are physically mixed at an equal molar ratio at racemic composition [7]. Racemic compound systems form crystals with both enantiomers being incorporated into the crystal lattice at racemic composition [5] In a ternary solution the eutectic point represents a composition at which the solution is saturated in equilibrium with respect to both solid phases, at a certain temperature. For conglomerate forming systems, the eutectic composition can be reached if a racemic mixture of crystals is equilibrated in a solvent at a constant temperature. Racemic conglomerate mixtures can be separated directly through preferential crystallization as both enantiomers form only pure crystals and have the same physical properties such as solubilities, growth kinetics, and melting points. Racemic compound forming systems form two eutectic compositions. This liquid composition is specific for the racemic compound forming system and its solvent at a certain temperature.

In the case of racemic compound forming systems, the pure enantiomer and racemic compound solid phases are in equilibrium with each other in the triphasic domain at eutectic composition. Therefore preferential crystallization [4, 6] can be used to separate the pure enantiomer and racemic compound. During a preferential crystallization process, one enantiomer is crystallized, by adding seed crystals of that enantiomer to a supersaturated solution, while the undesired handedness remains in solution. The addition of seed crystals of the preferred handedness leads to the chirally selective secondary nucleation [8], of crystals of the same handedness. Primary nucleation on the other hand is a stochastic event, chirally unselective and therefore not suited for chiral separation. However for preferential crystallization to be applied to racemic compound forming systems, prior enrichment to the eutectic composition is needed using a primary separation technique such as chromatography [9]. For conglomerate forming systems, where the eutectic composition is equal to the racemic composition in equilibrium at a certain temperature, preferential crystallization can be used to resolve the system directly into its respective enantiomers from racemic composition. To achieve chiral resolution from racemic composition, the enantiomers of a conglomerate are each preferentially crystallized consecutively in a different crystallizer. Once the undesired handedness reaches a certain enrichment it will primary nucleate, rendering the product chirally impure. There are several ways to prevent the enrichment of the counter enantiomer by using certain process configurations [4, 10, 11] or the addition of additives [12]. One way to prevent primary nucleation is by initializing a racemization reaction in the solution which transforms the enantiomer in excess to the one being crystallized, ensuring a racemic composition is preserved in the solution throughout the process. If a racemization reaction is combined with preferential crystallization, the process is called deracemization.

In this work, we aim to develop and validate a general process design that allows for the crystallization-based separation of chiral compounds at the eutectic composition through a crystallization process configuration with crystallizers in series. During the serial crystallization, the byproduct is (optionally) crystallized in the first crystallizer while the target product is crystallized in the second crystallizer. As a feasibility study and validation of the process design and setup, three chiral model compounds (Mandelic acid, Asparagine, and clopidogrel-imine) are used in respectively a separation, resolution and deracemization. Unlike enantiomers of conglomerates, the racemic compound DL-Mandelic acid and its pure enantiomer crystals have different physical properties such as solubilities, growth kinetics, densities, and melting points. In addition, they are also distinguishable with optical methods such as Raman spectroscopy [13], showing different spectra, which allows them to be measured in-situ, as they do not require recognition of the left and right-handed solids.

5.2 Experimental

We performed a separation, resolution, and deracemization in the same setup. Enantiopure D-Mandelic acid (D-MA, TCI, 99% pure) and racemic compound DL-Mandelic acid (DL-MA, TCI, 99% pure) with the solvent deionized water are used as separation example. For the resolution example, we used racemic DL-Asparagine monohydrate (DL-ASN, Sigma-Aldritch, 99% pure), enantiopure L-Asparagine monohydrate (L-ASN, Sigma, 99% pure) and D-

Asparagine monohydrate (D-ASN, Sigma, 99% pure) in deionized water. The model compound RS-Clopidogrel-imine (Syncom B.V., the Netherlands, 99%) and its enantiopure S-Clopidogrel-imine (S-CPG) enantiomer, were used to exemplify a deracemization process, in acetonitrile in the presence of the racemization catalyst 1,8-Diazabicyclo[5.4.0]undec-7-ene (DBU, Sigma, 98% pure).

As no pure S-CPG was commercially available, a racemic solution containing 300 g of Acetonitrile with 10 g of RS-CPG and 2 ml of DBU, was saturated at 40°C in a 500 ml batch reactor and crash cooled to 25°C, held for three hours and then cooled further to 15°C for 5 h, followed by a further reduction of temperature to 5°C, at which the suspension was held overnight. The suspension was then vacuum filtrated, washed with methyl-tert-butyl ether to remove all DBU and measured for purity with chiral HPLC. The resulting solids with a purity of 83 %, were then suspended again in acetonitrile and stirred for 24 h, so that half of the produced solids dissolved and with it the counter enantiomer. The resulting solids were again analyzed with chiral HPLC and showed a purity of 99.6 %. The temperature-dependent solubilities were determined using the Crystal16 setup (Technobis, the Netherlands) and can be found in the supporting material, as well as the experimental details.

The productivity $P = \Delta\rho_P/\Delta t$ was used to compare the experiments in regard to the amount of produced product suspension density $\Delta\rho_P$ which can be produced in a crystallizer over a period of time Δt. The product suspension density which was produced over time can be determined using the initial suspension density ρ_S, were only seeds are presents and a suspension density at a certain point in time $\rho_P(t)$ during the process $\Delta\rho_P = \rho_P(t)-\rho_S$. In addition, the yield $X = m_P/m_{th}$ was determined to show the amount of product produced with regards to the theoretical product m_{th} which could have been produced if the process were to be ideal. This theoretical value is determined by the phase diagram of the compound, and can usually not be achieved.

5.2.1 Crystallization Process Configuration

The setup (Figure 61) consists of a feed vessel and two crystallizers connected in series and a remaining solution recycle from the second crystallizer back to the feed vessel. Only solution is exchanged between vessels as all outflows are equipped with filters (Robu, Por. 3).

In the feed vessel at temperature T_F, a saturated eutectic solution of a composition $C_F = (C_D,C_L)_F$ is equilibrated with a mixed suspension of crystals m_E (Figure 61, green rectangles and purple circles), at a slightly elevated temperature T_1. If not bypassed, Crystallizer 1 at temperature T_1 initially contains a suspension of saturated solution at concentration $C_1=(C_D,C_L)_{E1}$ with an eutectic composition at a slightly reduced temperature $T_1 < T_F$ and seed crystals (purple circles) of the byproduct 1 (P1). Crystallizer 2 at temperature T_2 initially contains a suspension at concentration $C_2=(C_D,C_L)_{E2}$ of saturated solution at the eutectic composition and seed crystals (green rectangles) of the desired enantiomer product P2. We chose to work with equal temperatures $T_1=T_2<T_F$ in the crystallizers 1 and 2.

At the start of the process, all flows between vessels of equal rate F are switched on. Thus, continuously a flow rate F of filtered solution flows from the feed vessel into crystallizer 1 (Figure 61, middle). Here the first product P1 is crystallized, while the target product P2 remained in the solution. From crystallizer-1, the filtered solution is continuously pumped

into the second crystallizer, where the target product is crystallized from the solution and recycled back to the feed for enrichment. At the end of the process, the products of both crystallizers are extracted, and the undesired product P1 can be used to recycle if applicable.

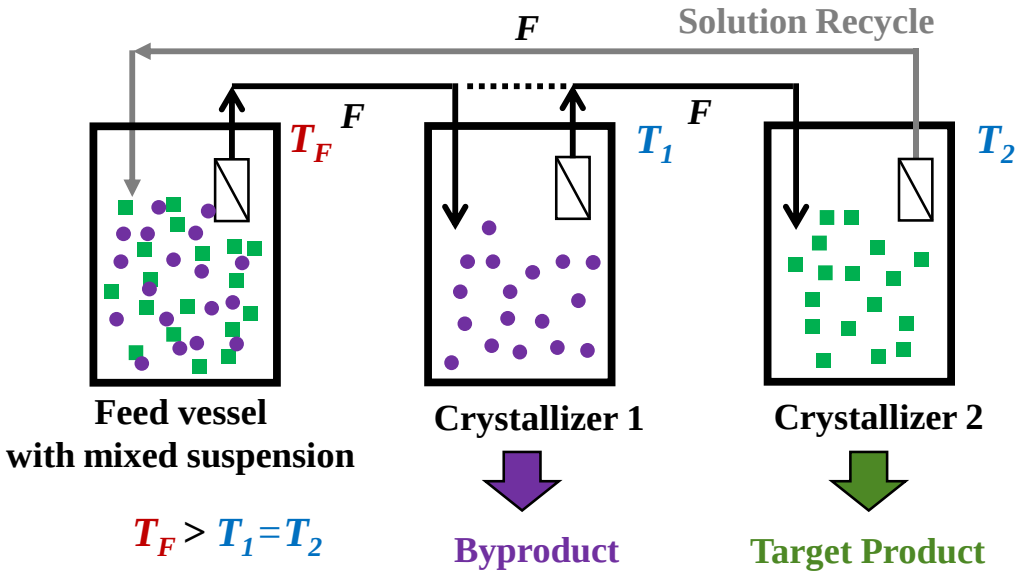

Figure 61: The schematic of the serial crystallization setup used for the separation of the racemic compound forming mandelic acid, the conglomerate forming asparagine monohydrate and the conglomerate forming clopidogrel-imine, racemizing in solution, with feed vessel (left), crystallizer 1 for the less valuable byproduct (middle) and crystallizer 2 for the Target Product (right) and recycle of the depleted solution back to the feed vessel (grey line) with a bypass for crystallizer 1 (dotted line) in case of a deracemization process. Temperature T_F of the feed vessel is higher than the temperature $T_1 = T_2$ of the crystallizers. Solution flow through all vessels is indicated.

In the case where deracemization processes are performed (i.e. for racemic forming compounds), only the feed and one crystallizer are needed so crystallizer 1 is bypassed as shown in Figure 61 through the dotted line. The preparation of the feed and crystallizer 2, as well as the process procedure, remain the same only that a racemization catalyst, in this case, DBU is added to both the feed and crystallizer solution. While P2 is crystallized in crystallizer 2 the enantiomer of the undesired handedness remains in solution and is transformed to the desired handedness being crystallized. This ensures the equimolar ratio between both enantiomers is kept in solution preventing the enrichment of one and thus primary nucleation of the undesired handedness in the crystallizer 2.

The flow rate F between all vessels is constant during the process to ensure a constant suspension volume in the feed vessel (V_F) and crystallizers (V_1 and V_1), as well as a stable residence time $\tau = V/F$ for each experiment.

The used process conditions such as flow rate F, vessel temperatures T_1 and T_2 and volumes as well as the initial mass of seeds m_S and concentrations vary for each model compound used and are shown in table 1.

Table 8: Model compound dependent process conditions used for the serial experiments.

Description	Process Conditions	Asparagine Monohydrate	Clopidogrel - imine	Mandelic Acid
Flow rate	F (ml/min)	6.4	5.7	3.3
Crystallizer Residence Time	τ (min)	31.3	67	60
Volume Feed vessel	V_F (ml)	500	380	500
Feed Temperature	T_F (°C)	25	34	25
Overall initial Crystallizer Concentration	C_1 $(C_D,C_L)_{E1}$ = $C_2(C_D,C_L)_{E2}$ (g/l)	47.1 (23.55, 23.55)	16.1 (8.05, 8.05)	225 (155, 70)
Initial Feed Suspension Density (Solid Excess)	ρ_E (ρ_D,ρ_L) (g/l)	15.20 (7.1, 7.1)	7 (3.5, 3.5)	150 (104, 46)
Volume Crystallizers	V_1 =V_2 (ml)	200	380	200
Crystallizer Temperature	T_1 = T_2 (°C)	20	20	23
Overall Feed Concentration	$C_F(C_D,C_L)_F$ (g/l)	61.2 (30.6, 30,6)	19.8 (9.9, 9.9)	272 (188, 85)
Seed suspension density	ρ_{S1} = ρ_{S2} (g/l)	2	0.5	3
Crystallizable mass fraction of one enantiomer in eutectic <<unclear what is meant.>>	$x_{E1,eu}$	0.5	0.5	0.38

In order to pump the solution, peristaltic pumps (Watson Marlow, 520u) and flowmeters (Bronkhorst) were used to ensure high accuracy of the flow resulting in a constant suspension volume in all vessels. The temperature was controlled with heater-chillers (Lauda, Proline) attached to Pt100 temperature sensors in the vessels.

5.2.2 Separation of D- and DL-Mandelic-Acid

In crystallizer 2, a higher stirring rate of 600 rpm compared to 350 in crystallizer 1 was used as the D-MA was observed to float at lower rpm during preliminary experiments. Once all solid excess was depleted from the feed vessel, the process was stopped and the by-product and main product were obtained by filtration of the suspension remaining in the crystallizers. Chiral HPLC (high-performance liquid chromatography) was performed on the obtained byproduct and main product from the crystallizers 1 and 2, respectively. Details of the HPLC method can be found in the supporting material. Further details regarding the used process conditions can be found in Table 8.

In order to monitor this process, Raman spectroscopy was used as D-MA and DL-MA solids show different Raman due to their different crystal structures. A submergible Raman probe (RXN 2, Kaiser Instruments)was used to monitor the fraction of D-MA in the solid phase in the suspension of crystallizer 2 where the main product D-MA is crystallized. In addition, as the intensity of the spectra increases with suspension density ρ_D and ρ_{DL} of D-MA and DL-MA, respectively, these can be monitored as well, using a calibration [Raghus Paper]. Using this calibration, the enantiomeric excess $E = I_D/(I_D + I_{DL})$ can be monitored using the intensities of

the Raman spectra, where the peaks of the D- and DL-MA overlap. If no DL-MA is crystallized the intensity remains unchanged, while the intensity of the D-MA increases with increasing suspension density over time. The suspension densities ρ_D and ρ_{DL} of the solid bulk in crystallizer 2 could be monitored in-situ with an accuracy of ± 7.5 g/l for the total suspension density $\rho_D + \rho_{DL}$.

5.2.3 Resolution of Asparagine

The process conditions used for the resolution experiment of DL-ASN can be found in Table 8. For this experiment, the D-ASN was crystallized in crystallizer one as the by-product, while the L-ASN was the target product, produced in crystallizer 2. For this experiment stirring rates of 400 rpm where used in both crystallizers to ensure a well-mixed suspension.

The process is initiated by starting the flow *F* which is monitored through flowmeters during the experiment as filter fouling can occur using ASN [14]. In the case of filter fouling, the filter is switched to a backup filter to ensure the volume is conserved. During the process, suspension samples of 2.5 ml were taken from each crystallizer at regular intervals, using a syringe with an attached tube, subsequently filtered, washed and dried. The dried solids were then analyzed using HPLC [14] to determine the chiral purity. Using the area under the curves A_i of the enantiomers *i,* provided by the resulting chromatogram, the enantiomeric excess can be calculated $E = (A_1-A_2)/(A_1+A_2)$. The subscript 1 indicates the target product while 2 the undesired product. The corresponding method can be found in the supporting material.

5.2.4 Deracemization of Clopidogrel-imine

The second conglomerate system RS-CPG was deracemized using DBU (5 mg/g solvent) in the solvent as racemization catalyst. As the racemization reaction in solution ensures a racemic solution composition during the process, only the target enantiomer was crystallized. Therefore crystallizer 1 was bypassed and the solution was cycled between the feed and crystallizer 2. After the solid excess in feed was depleted, the pure S-CPG was extracted and washed vigorously using methyl-tert-butyl ether (MTBE), to ensure all DBU is removed from the solid product.

To measure the enantiomeric excess of the produced CPG crystals, the same method as during the ASN experiment was used to take samples from the slurry and analyze them using chiral HPLC [15, 16] (Method can be found at supporting material).

5.3 Results

5.3.1 Separation of racemic compound Mandelic-Acid

As a racemic compound forming system, preferential crystallization for chiral separation of D- and DL-MA can only be applied at the eutectic composition, as the enantiopure D-MA and racemic compound DL-MA crystals can co-exist in the solution. Therefore, an enriched starting solution, corresponding to the eutectic composition is required in feed. Additionally, the solid excess added also needs to reflect the eutectic composition in solid state for the separation to be possible. In this work we only focus on the separation process, however, such enrichment can be achieved through a second purification method like chromatography [9, 17-20] or membrane separation [21] in a hybrid process. The system has been well

investigated and the solubilities, as well as the ternary phase diagram in water (MilliQ) at several temperatures and the eutectic composition, are known [22]. The solid eutectic composition as measured by melting point phase diagram [23] is 62 % DL- and 38 % D- or L-MA, wherein this case we used D-MA due to its commercial availability.

During the serial crystallization process, the eutectic saturated solution from the feed (0, Figure 62, right) is cooled upon reaching crystallizer 1, leading to a crystallization of DL-MA, through which the solution is enriched in D-MA (1,Figure 62, right) indicated by the arrow moving towards the D-MA in the ternary phase diagram in Figure 62 (right). Using the enriched solution as feed for the second product crystallizer, the D-MA is crystallized, moving the solution composition towards the DL-MA domain (2, Figure 62, right). As indicated in Figure 62 (right), point 2 does not reach the eutectic equilibrium composition as some D-MA remains in the solution, and cannot be crystallized under the process conditions given. At the same time, some DL-MA which could not be crystallized in the first crystallization step remains inert in the solution going to crystallizer 2. Figure 62 (left) shows a very high enantiomeric excess of more than 98 % over the process time.

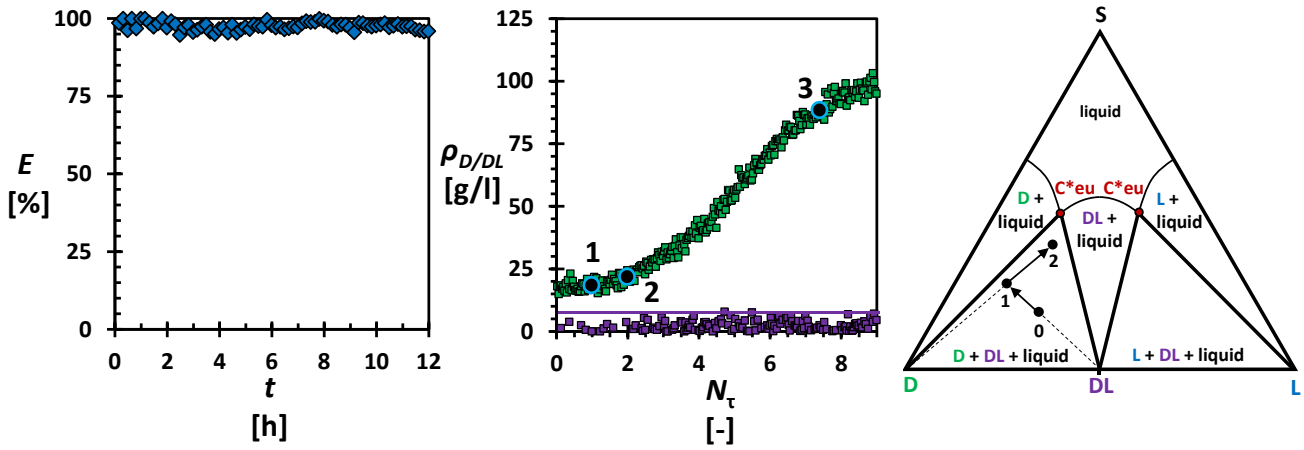

Figure 62: Left: Enantiomeric excess *E* of D-MA in product crystallizer 2 of D-MA and DL-MA measured by Raman during the process. Middle: Suspension densities ρ_D and ρ_{DL} of D-MA (green) and DL-MA (purple) as a function of process time. with error bar (purple line) measured for the serial separation process in crystallizer 2 with 1: start of pumps at t=0; 2: beginning of stable growth phase with linear deposition rate and 3: End of stable growth phase; over the number of residences N_T. Right: Schematic of a ternary phase diagram showing D, DL, and L MA, the eutectic compositions (red dots) at the eutectic equilibrium concentration C^*_{eu} depicting the serial process with the feed concentration 0; the concentration in crystallizer 1 and 2.

The enantiomeric excess, shown in Figure 62 (left) reflects the suspension densities shown in Figure 62 (middle), as no DL-MA nucleated. As the measured suspension density of DL-MA remains below the margin of error during the process it can be assumed that no primary nucleation of the undesired DL-MA product occurred in the product crystallizer. The measured suspension densities for the D-MA product can be subdivided in 3 parts during the experiment. After starting the flow (1, Figure 62, middle) a slow growth can be observed for one residence until the suspension density begins to increase with an almost linear deposition rate (2, Figure 62, middle) until the indicated point 3 in Figure 62 (middle). This period is referred to as stable growth showing an almost linear deposition rate of the D-MA product. During the stable state, D-MA is produced with a productivity P = 13.3 g/hl, which can be considered a high value in comparison to the other tested model compounds in this work. A yield of X = 75.5 % is reached during the stable state, which represents the amount of D-MA

which could be produced from the overall amount of D-MA available for crystallization during the stable growth phase. As the solution is continuously recycled during this process, continuous production of the target enantiomer is achieved during this period and the product which did not crystallize is recycled, preventing the loss of product. After the 7.5 residences, the stable growth phase is ending indicated by a decrease in the growth rate. In this case, this was caused by primary nucleation of D-MA in the DL-MA crystallizer. As D-MA is enriched in the solution in crystallizer one, after a period of time it will primary nucleate, reducing the amount of D-MA which is available for crystallization in crystallizer 2. The same behavior can be observed when the feed is depleted of solid excess.

In order for this process to be effectively applied to racemic forming compounds at eutectic composition, it requires a decent induction time [24, 25] of the target enantiomer so a long stable state can be reached. Furthermore, this process configuration requires an eutectic composition that does not exceed a solid composition of 85 % pure enantiomer. If higher enrichment is needed, the resulting yields might be too low, as a large quantity of the pure enantiomer must already be provided to reach the eutectic point. However, the biggest drawback of this process is that it needs a second purification method to achieve an eutectic starting solution. At the same time, using this process in a hybrid mode can increase the overall process productiveness as purification methods such as chiral chromatography achieve lower enrichment with respect to one enantiomer with increasing overall purity[9]. On the other hand, the serial processes configuration allows for very high purities to be produced. In order to verify that no nucleation of the undesired DL-MA occurs in crystallizer 2 during the experiment, samples of the final product are analyzed using HPLC, confirming no chiral impurities are present in the product (details can be found in the supporting material).

5.3.2 Resolution of the conglomerate system Asparagine Monohydrate

It is an amino acid and crystallizes as a monohydrate in the stable form. This model compound has been very well investigated [12, 26-31] and was used in many works regarding the chiral separation of conglomerate forming systems. The solubilities, growth kinetics and ternary phase diagram of asparagine monohydrate (ASN) in water are well known and published [29, 30].

Following the results of the MA experiments, the separation of the conglomerate forming compound ASN in the serial process configuration is investigated. Figure 63 (left) shows the enantiomeric excess of the solid samples taken from both crystallizers, analyzed with chiral HPLC. The graph shows that both enantiomers are separated with a very high purity of >99 % throughout the experiment. No respective counter enantiomer formation was observed in either crystallizer as shown through the suspension densities of each respective counter enantiomer in Figure 63 (middle, purple markers), which are remaining close to zero as indicated in the graph.

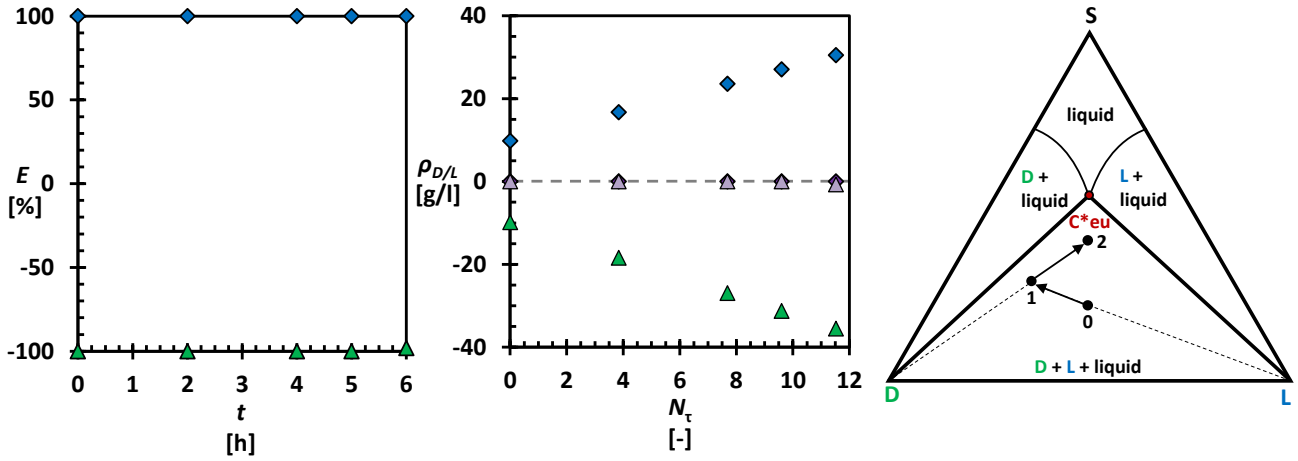

Figure 63: Left: Enantiomeric excess of main product L-ASN (blue) and byproduct D-ASN (green) in crystallizer 2 and crystallizer 1, respectively, during the resolution process. Middle: Suspension densities ρ_{L2} and ρ_{D2} of main product L-ASN (blue diamonds) and D-ASN (purple diamonds) in product crystallizer 2 and suspension densities ρ_{L1} and ρ_{D1} of byproduct D-ASN (green triangles) and L-ASN (purple triangles) in crystallizer 1. Right: Schematic of the resolution process for ASN in a ternary phase diagram with the concentrations of the feed (0); in crystallizer 1 (1) and in crystallizer 2 (2).

During the separation process, saturated feed solution (0, Figure 63, right) is continuously transferred into crystallizer 1, where it is subsequently cooled and the D-ASN is crystallized, enriching the solution in crystallizer 1, with respect to L-ASN as indicated by the arrow in Figure 63 (right) going from point 0 to point 1. The L-ASN rich solution is then used as feed for the second crystallizer, where L-ASN is crystallized indicated by the black arrow going from point 1 to point 2 in Figure 63 (right).

After the solid excess in the feed tank is visibly depleted, the process is stopped and the product extracted, washed and analyzed. For the L-ASN a yield of 54.6 % and a productivity of $P = 3.5$ g/l*h is achieved. While for the D-ASN, which was the undesired product, a productivity $P = 4.3$ g/l*h at a yield of 67 % is achieved. The difference in the values for both crystallizers can be explained by the different supersaturations as the feed solution for the second crystallizer is already depleted with regards to D-ASN. This leads to a different driving force and can result in fewer product being crystallized in the second crystallizer at the same process time. For the crystallization process of L ASN, a supersaturation $S = C_F/C_2 = 1.29$ can be calculated based on the solubilities used for this experiment [29]. Comparing this value with work by A. Dunn [14] where productivities between 0.96-3.91 g/l*h are reached at supersaturations of 1.2-1.45, the achieved productivity in the serial process is comparable. Similar values are achieved in a work by Carneiro and Bhandari [27], where productivities in the range of 0.5-4 g/lh at supersaturations ranging from 1.2-1.5 are reached. Using these two processes as a comparison, the results of the serial process configuration are well within the expected range of a preferential cooling crystallization for this compound.

The productivity and yield for this process can be improved through optimizing process parameters such as supersaturation, or design changes like the sizes of the vessels to use a higher flowrate by keeping the residence times the same. Both enantiomers are successfully separated with an enantiomeric excess of almost 100 % which underlines the applicability of the process especially for the pharmaceutical industry where very high purities are required

due to GMP (Good Manufacturing Practice) standards and FDA (Food and Drug Administration) regulations [32-34].

5.3.3 Deracemization of the conglomerate system Clopidogrel-imine

Clopidogrel-imine is a drug precursor for Plavix, an anticlotting medicine. The compound is not very well investigated even though it has been used in Viedma ripening [15, 16, 35] and temperature cycling studies [36].

While clopidogrel-imine is a conglomerate forming system, the separation process was different in comparison to ASN. Figure 64 (left) shows the enantiomeric excess of the solid samples measured during the experiment, showing that the product was produced with a very high purity of more than 98 % like the products in the previous processes. This is supported by the suspension densities shown in Figure 64(middle), where the counter enantiomer remains close to zero. The process procedure is shown in Figure 64 (right), where feed solution from point 0 (Figure 64, right) is entering the crystallizer at the composition in point 2. As the feed is cooled the supersaturation is induced leading to the crystallization of the target enantiomer, which is indicated by the blue arrow in Figure 64 (right). Unlike the ASN process, no enrichment in either direction of the liquid phase is occurring, but the racemic composition is preserved until the end concentration in crystallizer 2 (2, Figure 64, right) is reached. The yield and productivity can be determined from the suspension densities shown in Figure 64 (middle). Under the process conditions used, 60.3 % of the crystallizable product could be produced with a productivity P = 2.4 g/l*h. This process can be compared to other deracemization processes like temperature cycling or Viedma ripening. If the productivity is compared to a temperature cycling process using a similar compound (N-(2-methylbenzylidene)-phenylglycine amide) [37], where a maximum productivity of 1.97 g/lh is achieved. Here the reached productivity in the serial process is slightly higher. However the scale the experiments are performed on [37] is only up to 8 ml. While Viedma ripening experiment with the same compound has been performed by Maarten [16], no productivities are given for the process.

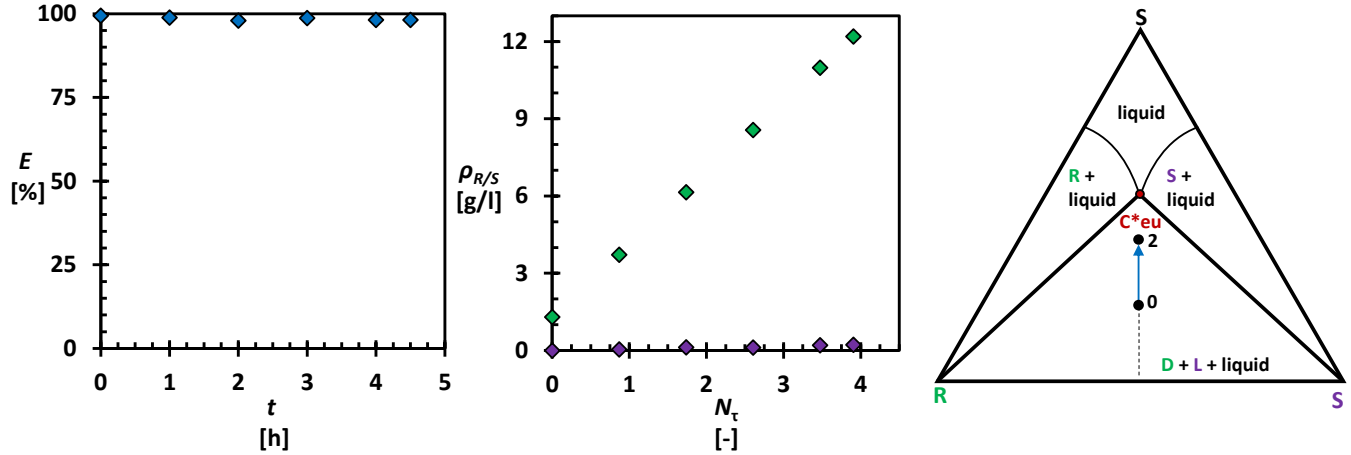

Figure 64: Left: Enantiomeric excess E of CPG (blue) during deracemization in crystallizer 2. Middle: Suspension densities ρ_S (green diamonds) and ρ_R (purple diamonds) of pure S-CPG and its counter enantiomer in product crystallizer 2. Right: Schematic of the serial separation process for CPG in a ternary phase diagram with the concentrations of: the feed (0) and crystallizer 2 (0).

In order to increase the productivity for the serial process configuration with regards to CPG, optimal process parameters for the compound would have to be investigated. However, the serial separation process allows for continuous separation as long as solid racemic excess is added to the feed vessel, while batch wise configurations such as temperature cycling and Viedma ripening does not. The serial process also allows for consistent product purity during the process as shown in this experiment, as well as constant process conditions.

Figure 65 shows the optimization potential of this process in regards of productivity. The graph shows the productivities measured for serial process experiments for each compound investigated. For MA, a second experiment with a higher temperature difference of 5°C (green square, Figure 65) and with that a higher supersaturation, was conducted. If compared to the experiment discussed here (blue square, Figure 65), the productivity is almost doubled, while the pure compound is produced (chromatogram in supporting information). As higher supersaturations still allow for the production of pure product, a further increase of the supersaturation is possible to increase productivity, as long as no primary nucleation occurs. The same can be concluded for the conglomerate compounds ASN and CPG [14, 27, 37]

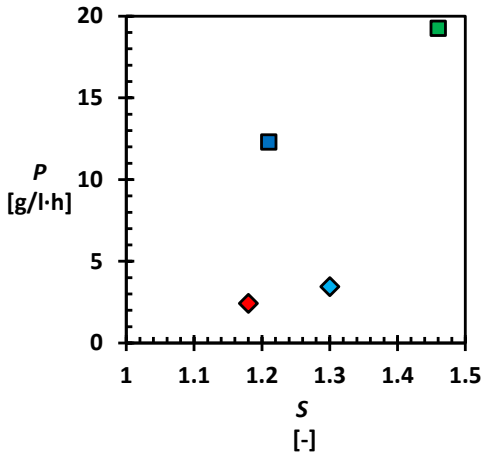

Figure 65: Productivity versus supersaturation for: mandelic acid separation experiments (squares) using a temperature difference between the feed and the crystallizers of 2°C (blue) and 5°C (green); separation of conglomerates (diamonds) ASN (turquoise) and CPG (red).

While there are various processes to preferentially crystallize especially conglomerate forming systems, the process developed here is able to separate racemic compound forming systems as well, allowing for a general application. This serial process can be applied in the pharmaceutical industry, where a high degree of flexibility with regards to the process design and very high product purities are needed. In addition, for the racemic compound forming systems, the cost for purification is reduced as a second purification technology is only needed to provide enrichment up to the eutectic composition and the racemic compound can be recycled. Therefore, it was demonstrated that the serial process configuration can effectively separate different model compounds at the eutectic composition with a high purity level of at least 98 % E.

5.4 Discussion

By using the serial process configuration, we are able to separate all three model compounds investigated in this work with a very high chiral purity of more than 98 % *E*. As the three model

compounds vastly differ with regards to their physical properties and crystallization behavior, given that one is a racemic compound, while the others are conglomerates, designing a generalized process configuration is challenging. Many works can be found in literature where preferential crystallization process approaches are investigated depending on the properties of chiral compounds [4, 6, 10, 11, 14, 17, 26-29, 31, 38-42]. While for some cases the same process configuration can be used for several conglomerate forming systems [4, 10, 11, 28, 38, 41], this process allows for a separation of a chiral compound at the eutectic composition also for racemic compound forming systems, and can furthermore be used in deracemization configuration as well.

The productivities and product purities achieved in the serial process can be compared to existing processes separating the same model compounds. In the case of mandelic acid, a separation process in hybrid mode has been conducted [21, 43] where productivities up to 13 g/lh could be reached, with product purities up to 96.1 % purity in [21] and 96.1-97.4 % in [44], in comparison to more than 99 % in the serial configuration (HPLC result). However, one drawback of the serial crystallization system for the separation in racemic compound forming systems is that an initial enrichment step is required using another separation technology in order to reach the eutectic composition as a starting point in the serial configuration, allowing for this process only to be applied effectively in a hybrid configuration. In principle the serial set up can also be applied for classical resolution [4] in the case for racemic compound forming system combined with a chiral resolving agent, resulting in two diastereomeric salts with differing solubilities. As the process conditions such as temperature and residence time can be varied for each crystallizer, the diastereomer of the byproduct can be crystallized first, by adding the co-former in the first crystallizer. In the second crystallizer, the process conditions can be varied, to allow for the crystallization of the target product for the second crystallizer. As a recycle could not be used in this case as the co-former is added to the solution, to further crystallize the remaining product a cascade with a second set of crystallizers would need to be used. This process can be conducted in semi-batch operation for initial investigation and later made into a continuous process. The applicability of the serial configuration for classical resolution needs to be investigated but could expand the range of application for the serial configuration even further.

For ASN the achieved productivities with the versatile serial configurations are comparable to other specifically designed preferential crystallization processes using the same compound and supersaturation. However, the process in the serial configuration also results in pure D-ASN as a side product. As the counter enantiomer is present in the solution of the first crystallizer the likelihood of primary nucleation of L-ASN is higher. In such a case, only the first crystallizer would be affected, leaving a pure target product in the second product crystallizer, allowing for several control mechanisms to be sued. For example, a back-up vessel for the first crystallizer could be used, where the feed flow can be switched to in case of a primary nucleation event in the first crystallizer, allowing for the production of the target enantiomer to continue. Alternatively, the first crystallizer could also be regenerated as stopping the flow would not lead to primary nucleation of the undesired handedness in the second crystallizer.

In this work, a different approach towards deracemization was taken by directly preferentially crystallizing CPG while ensuring a racemization reaction in solution. In this process, no glass

beads and grinding like in Viedma ripening or changes of temperature, like in temperature cycling are needed. Since the solution is cycled between two vessels at a constant temperature the pure enantiomer can be obtained directly in a short time. Viedma ripening processes suing CPG have been conducted [16, 35] however at a longer process time. Temperature cycling experiments with CPG have been conducted by Maggioni [36] but no productivities are given. In a study by Breveglieri [37] a similar compound to CPG was used in temperature cycling experiments. There the highest productivity achieved was 1.97 g/lh, which lower than what has been reached during this work. If the process where to be applied on a compound with a nucleation kinetic exceeding that of the racemization reaction in solution, primary nucleation could occur. To apply the process to such a compound the residence time would have to be increased, in order to match the racemization kinetics of the compound.

In summary, the achieved productivities for all the model compounds exceed those for other process configurations found in literature. At the same time, purities of more than 98 % enantiomeric excess are reached for every compound, making it a very flexible and efficient process. This process could be further developed to a true continuous process as shown in Figure 66 to allow for higher productivity and process efficiency. The schematic of the process shown in Figure 66 adds a continuous solid removal of the products, as well as a purge and feed stream to the existing serial process. Instead of solution, a suspension would be removed from each crystallizer and subsequently filtered to remove the solid product, while the solution from the first crystallizer would be transferred to the second one. From the product crystallizer, a fraction of the filtered solution would be purged and the rest recycled. To keep the processes running, an eutectic suspension needs to be added to the feed vessel continuously, to conserve the volume of the system.

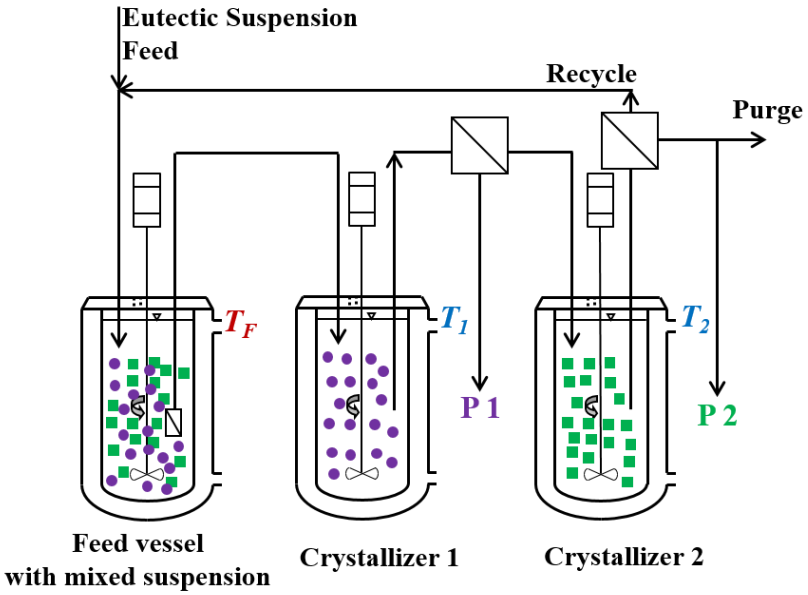

Figure 66: Schematic of a continuous serial crystallization process, with mixed suspension removal, recycle, as well as feed addition.

5.5 Conclusions

Using the serial crystallizer process configuration, we successfully demonstrated a separation, resolution, and deracemization on a racemic, as well as conglomerate forming compounds with and without racemization, at the eutectic composition with a single process configuration. The racemic compound MA was separate at eutectic composition, where the pure enantiomer and racemic compound could be separated at high productivities and yields. Following the in-situ measured separation process, the process configuration was successfully used for a resolution of the racemic conglomerate DL-ASN into its pure D-ASN and L-ASN enantiomers. Furthermore, deracemization was performed on RS-CPG, resulting in pure enantiomer without the use of grinding or temperature cycling. The serial crystallization process configuration showed to be a flexible and robust process for chiral separation, resolution, and deracemization, which can easily be adopted into a continuous process.

5.6 Acknowledgment

This research has received funding as part of the CORE project (October 2016 – September 2020) from the European Union's Horizon 2020 research and innovation program under the Marie Sklodowska-Curie grant agreement No 722456 CORE ITN. We thank the EPSRC Centre for Innovative Manufacturing in Continuous Manufacturing and Crystallisation (http://www.cmac.ac.uk) for support (EPSRC funding under grant reference: EP/I033459/1). We furthermore like to thank Giulio Valenti (Syncom, CORE) for his help with the analysis of Clopidogrel-imine and for providing the details for the chiral HPLC analysis of Clopidogrel-imine, as well as and Maxime Charpentier (University of Strathclyde, CORE) for useful discussions.

5.7 References

[1] L.A. Nguyen, H. He, C. Pham-Huy, Chiral drugs: an overview, Int J Biomed Sci 2(2) (2006) 85-100.

[2] P.G. Cox, W.M. Moons, F.G. Russel, C.A. van Ginneken, Renal disposition and effects of naproxen and its l-enantiomer in the isolated perfused rat kidney, Journal of Pharmacology and Experimental Therapeutics 255(2) (1990) 491-496.

[3] W.F. Kean, C.J.L. Lock, J. Rischke, R. Butt, W. Watson Buchanan, H. Howard-Lock, Effect of R and S Enantiomers of Naproxen on Aggregation and Thromboxane Production in Human Platelets, Journal of Pharmaceutical Sciences 78(4) (1989) 324-327.

[4] H. Lorenz, A. Seidel-Morgenstern, Processes to separate enantiomers, Angew Chem Int Ed Engl 53(5) (2014) 1218-50.

[5] A.C. J. Jacques, S. H. Wile, Enantiomers, Racemates and Resolutions, Krieger, Malabar1994.

[6] H. Lorenz, A. Perlberg, D. Sapoundjiev, M.P. Elsner, A. Seidel-Morgenstern, Crystallization of enantiomers, Chemical Engineering and Processing: Process Intensification 45(10) (2006) 863-873.

[7] G. Coquerel, Chiral Discrimination in the Solid State: Applications to Resolution and Deracemization, (2015) 393-420.

[8] S.G. Agrawal, A.H.J. Paterson, Secondary Nucleation: Mechanisms and Models, Chemical Engineering Communications 202(5) (2015) 698-706.

[9] K.G. Feitsma, B.F.H. Drenth, Chromatographic separation of enantiomers, Pharmaceutisch Weekblad 10(1) (1988) 1-11.

[10] K. Galan, M.J. Eicke, M.P. Elsner, H. Lorenz, A. Seidel-Morgenstern, Continuous Preferential Crystallization of Chiral Molecules in Single and Coupled Mixed-Suspension Mixed-Product-Removal Crystallizers, Crystal Growth & Design 15(4) (2015) 1808-1818.

[11] C. Rougeot, J.E. Hein, Application of Continuous Preferential Crystallization to Efficiently Access Enantiopure Chemicals, Org. Process Res. Dev. 19(12) (2015) 1809-1819.

[12] P. Kongsamai, A. Maneedaeng, C. Flood, J.H. ter Horst, A.E. Flood, Effect of additives on the preferential crystallization of L-asparagine monohydrate, The European Physical Journal Special Topics 226(5) (2017) 823-835.

[13] T. De Beer, A. Burggraeve, M. Fonteyne, L. Saerens, J.P. Remon, C. Vervaet, Near infrared and Raman spectroscopy for the in-process monitoring of pharmaceutical production processes, International Journal of Pharmaceutics 417(1) (2011) 32-47.

[14] A.S. Dunn, V. Svoboda, J. Sefcik, J.H. ter Horst, Resolution Control in a Continuous Preferential Crystallization Process, Org. Process Res. Dev. 23(9) (2019) 2031-2041.

[15] R.M. Kellogg, Practical Stereochemistry, Acc Chem Res 50(4) (2017) 905-914.

[16] M.L. Maarten W. van der Meijden, Edith Gelens, Wim L. Noorduin, Hugo Meekes, Willem J. P. van Enckevort, Bernard Kaptein, Elias Vlieg and Richard M. Kellogg, Attrition-Enhanced Deracemization in the Synthesis of Clopidogre l - A Practical Application of a New Discovery, Org. Process Res. Dev. 13(6) (2009) 1195-1198.

[17] K. Petruševska-Seebach, K. Würges, A. Seidel-Morgenstern, S. Lütz, M.P. Elsner, Enzyme-assisted physicochemical enantioseparation processes—Part II: Solid–liquid equilibria, preferential crystallization, chromatography and racemization reaction, Chemical Engineering Science 64(10) (2009) 2473-2482.

[18] H. Kaemmerer, Z. Horvath, J.W. Lee, M. Kaspereit, R. Arnell, M. Hedberg, B. Herschend, M.J. Jones, K. Larson, H. Lorenz, A. Seidel-Morgensten, Separation of Racemic Bicalutamide by an Optimized Combination of Continuous Chromatography and Selective Crystallization, Org. Process Res. Dev. 16(2) (2012) 331-342.

[19] H. Lorenz, D. Polenske, A. Seidel-Morgenstern, Application of preferential crystallization to resolve racemic compounds in a hybrid process, Chirality 18(10) (2006) 828-840.

[20] S. Swernath, M. Kaspereit, A. Kienle, Coupled Continuous Chromatography and Racemization Processes for the Production of Pure Enantiomers, Chemical Engineering & Technology 37(4) (2014) 643-651.

[21] L. Gou, S. Robl, K. Leonhard, H. Lorenz, M. Sordo, A. Butka, S. Kesselheim, M. Wolff, A. Seidel-Morgenstern, K. Schaber, A hybrid process for chiral separation of compound-forming systems, Chirality 23(2) (2011) 118-27.

[22] H. Lorenz, D. Sapoundjiev, A. Seidel-Morgenstern, Enantiomeric Mandelic Acid SystemMelting Point Phase Diagram and Solubility in Water, J. Chem. Eng. Data 47 (2002) 1280.

[23] H. Lorenz, D. Sapoundjiev, A. Seidel-Morgenstern, Enantiomeric Mandelic Acid SystemMelting Point Phase Diagram and Solubility in Water, Journal of Chemical & Engineering Data 47(5) (2002) 1280-1284.

[24] C. Brandel, J.H. ter Horst, Measuring induction times and crystal nucleation rates, Faraday Discussions 179(0) (2015) 199-214.

[25] S. Jiang, J.H. ter Horst, Crystal Nucleation Rates from Probability Distributions of Induction Times, Crystal Growth & Design 11(1) (2011) 256-261.

[26] D. Binev, A. Seidel-Morgenstern, H. Lorenz, Continuous Separation of Isomers in Fluidized Bed Crystallizers, Crystal Growth & Design 16(3) (2016) 1409-1419.

[27] T. Carneiro, S. Bhandari, E. Temmel, H. Lorenz, A. Seidel-Morgenstern, Shortcut Model for Describing Isothermal Batch Preferential Crystallization of Conglomerates and Estimating the Productivity, Crystal Growth & Design 19(9) (2019) 5189-5203.

[28] J.H. Chaaban, K. Dam-Johansen, T. Skovby, S. Kiil, Separation of Enantiomers by Continuous Preferential Crystallization: Experimental Realization Using a Coupled Crystallizer Configuration, Org. Process Res. Dev. 17(8) (2013) 1010-1020.

[29] K. Petruševska-Seebach, A. Seidel-Morgenstern, M.P. Elsner, Preferential Crystallization of l-Asparagine in Water, Crystal Growth & Design 11(6) (2011) 2149-2163.

[30] E. Temmel, J. Gänsch, H. Lorenz, A. Seidel-Morgenstern, Measurement and Evaluation of the Crystallization Kinetics of l-Asparagine Monohydrate in the Ternary l-/d-Asparagine/Water System, Crystal Growth & Design 18(12) (2018) 7504-7517.

[31] K. Wurges, K. Petrusevska-Seebach, M.P. Elsner, S. Lutz, Enzyme-assisted physicochemical enantioseparation processes-Part III: Overcoming yield limitations by dynamic kinetic resolution of asparagine via preferential crystallization and enzymatic racemization, Biotechnol Bioeng 104(6) (2009) 1235-9.

[32] W.H. De Camp, The FDA perspective on the development of stereoisomers, Chirality 1(1) (1989) 2-6.

[33] W.H. De Camp, Chiral drugs: The FDA perspective on manufacturing and control, Journal of Pharmaceutical and Biomedical Analysis 11(11) (1993) 1167-1172.

[34] B.Y. Shekunov, P. York, Crystallization processes in pharmaceutical technology and drug delivery design, Journal of Crystal Growth 211(1) (2000) 122-136.

[35] W.L. Noorduin, P. van der Asdonk, A.A.C. Bode, H. Meekes, W.J.P. van Enckevort, E. Vlieg, B. Kaptein, M.W. van der Meijden, R.M. Kellogg, G. Deroover, Scaling Up Attrition-Enhanced Deracemization by Use of an Industrial Bead Mill in a Route to Clopidogrel (Plavix), Org. Process Res. Dev. 14(4) (2010) 908-911.

[36] G.M. Maggioni, M.P. Fernández-Ronco, M.W. van der Meijden, R.M. Kellogg, M. Mazzotti, Solid state deracemisation of two imine-derivatives of phenylglycine derivatives via high-pressure homogenisation and temperature cycles, CrystEngComm 20(27) (2018) 3828-3838.

[37] F. Breveglieri, G.M. Maggioni, M. Mazzotti, Deracemization of NMPA via Temperature Cycles, Crystal Growth & Design 18(3) (2018) 1873-1881.

[38] M.P. Elsner, G. Ziomek, A. Seidel-Morgenstern, Efficient separation of enantiomers by preferential crystallization in two coupled vessels, AIChE Journal 55(3) (2009) 640-649.

[39] M.P. Elsner, G. Ziomek, A. Seidel-Morgenstern, Simultaneous preferential crystallization in a coupled batch operation mode. Part II: Experimental study and model refinement, Chemical Engineering Science 66(6) (2011) 1269-1284.

[40] M.P. Elsner, G. Ziomek, A. Seidel-Morgenstern, Simultaneous preferential crystallization in a coupled, batch operation mode—Part I: Theoretical analysis and optimization, Chemical Engineering Science 62(17) (2007) 4760-4769.

[41] G. Levilain, M.J. Eicke, A. Seidel-Morgenstern, Efficient Resolution of Enantiomers by Coupling Preferential Crystallization and Dissolution. Part 1: Experimental Proof of Principle, Crystal Growth & Design 12(11) (2012) 5396-5401.

[42] J. Mahieux, S. Gonella, M. Sanselme, G. Coquerel, Crystal structure of a hybrid salt–cocrystal and its resolution by preferential crystallization: ((±)trans-N,N′-dibenzyldiaminocyclohexane)(2,3-dichlorophenylacetic acid)4, CrystEngComm 14(1) (2012) 103-111.

[43] D. Polenske, H. Lorenz, A. Seidel-Morgenstern, Potential of different techniques of preferential crystallization for enantioseparation of racemic compound forming systems, Chirality 21(8) (2009) 728-737.

[44] H. Lorenz, D. Polenske, A. Seidel-Morgenstern, Application of preferential crystallization to resolve racemic compounds in a hybrid process, Chirality 18(10) (2006) 828-40.

5.8 Appendix 1: Chiral HPLC Methods and Results

Chiral chromatography is performed on samples of all compounds used in this work to measure the enantiomeric excess. The surface are under the peaks of the chromatogram are used for the determination of the enantiomeric excess $E = (A_1\text{-}A_2)/(A_1+A_2)$.

5.8.1 Mandelic Acid

For measuring the mandelic acid enantiomeric excess a lux 3 µm i-Cellulose LC column 150x3 mm (Phenomenex) was used with a 80/20 mix of hexane (0.1 % formic Acid) and IPA (0.1 % formic acid) as eluent at a flowrate of 0.6 ml/min and an injection volume of 1 µm. The method was given on request by Phenomenex and can also be found in their databank.

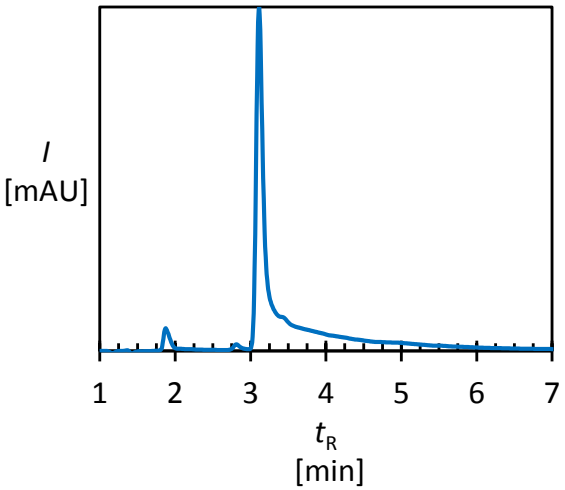

Figure 67: Intensity versus retention time chromatogram of final product in crystallizer 2 measured with chiral HPLC.

Figure 59 shows the chromatogram of the product extracted after the serial mandelic acid experiment. The first peak at a retention time of 1.876 min shows an unknown impurity, which was already present in the procured material and is presumed to be a solvent impurity. The L-MA leaves the column first with a retention time of 2.813 min which can be seen as a small peak prior to the large D-MA peak. As shown in Table 6, the area under the D-MA peak is significantly larger than below the L-MA curve resulting in almost enantiopure D-MA product at the end of the process.

Table 9: Measured areas under the chromatographic peaks with retention times of the peaks for each species identified in the chromatogram.

Species	Ratio of *A* [%]	Retention Time [min]
L-MA	0.76	2.813
D-MA	99.24	3.114

5.8.2 Asparagine Monohydrate

In order to measure the solid purity of ASN a 5 µm Chirobiotic T column from Astec (150_x4.6 mm) was used at 25°C, with a 70/30 v% methanol/water mix as eluent, a flowrate of

0.5 ml/min and an injection volume of 5 µl. The same method was used in a previous publication using ASN as model compound [1].

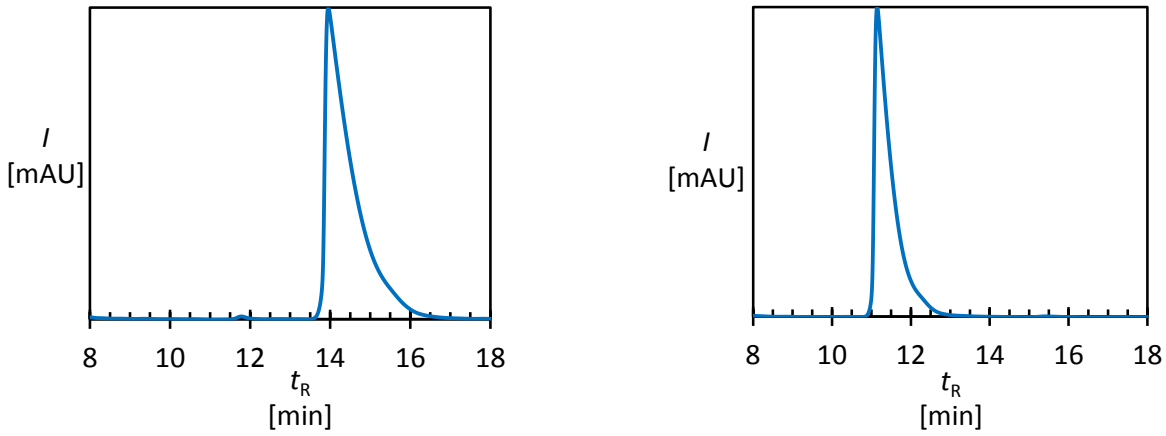

Figure 68: Chromatograms of ASN samples taken from the final product extracted from crystallizer 1 (D-ASN, left) and product crystallizer 2 (L-ASN, right) after the serial ASN experiment.

Figure 60 shows the chromatogram of the produced products extracted from both crystallizers after the serial separation experiment. In crystallizer 1 D ASN is crystallized, while the target product L ASN is produced in crystallizer 2.

Table 10: Measured areas under the chromatographic peaks with retention times of the peaks for each species identified in the chromatogram for product extracted from crystallizer 1 and product crystallizer 2 after the serial ASN experiment.

Species	Ratio of *A* [%]	Retention Time [min]
L ASN (crystallizer 1)	0.04	11.781
D ASN (crystallizer 1)	99.96	13.955
L ASN (crystallizer 2)	100	11.147
D ASN (crystallizer 2)	below detection limit	-

Looking at the chromatogram from the product extracted from crystallizer (Figure 60, left) a small L ASN peak can be observed after 11.781 min retention time prior to the D ASN peak at 13.955 min. However the peak area below the L-ASN peak is very small in comparison to the D ASN peak as shown in Table 7. The product extracted from crystallizer 2 (Figure 60, right) shows only the L ASN peak after 11.147 min retention time, while no D-ASN peak could be observed, which allows to conclude that only enantiopure L-ASN is produced in the second crystallizer.

5.8.3 Clopidogrel-imine

The clopidogrel-imine samples in this work were analysed using a 5 µm Chiralpak IA (250x4.6 mm) column with heptane/ethanol 70/30 v% as eluent, a flowrate of 0.7 ml/min and an injection volume if 4 µL. This method is applied at Syncom B.V. (The Netherlands), where the samples are measured.

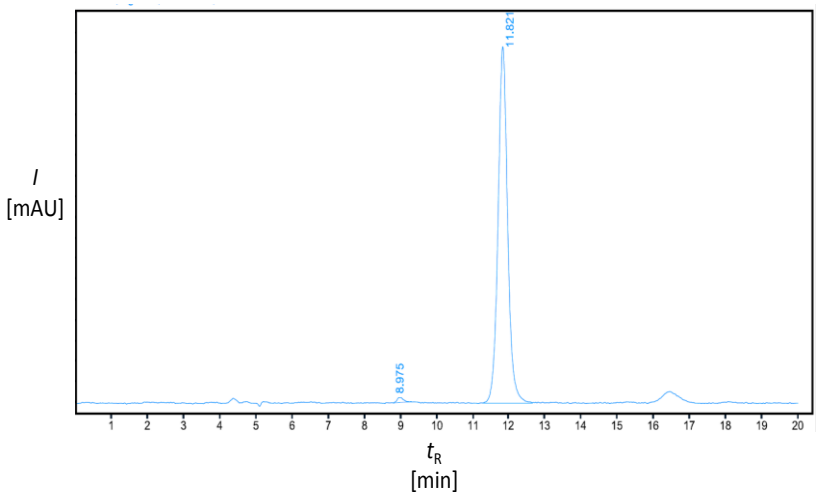

Figure 69: Intensity against retention time chromatogram of final CPG product in crystallizer 2, measured with chiral HPLC

The chromatogram shown in Figure 69 shows the measured peaks of the final product extracted from the crystallizer 2 after the serial CPG separation processes. First the peak of R-CPG appears at an retention time of 8.975 min but with a very small area under the peak in comparison with the S-CPG detected at 11.821 min as shown in Table 11. The enantiomeric excess which can be calculated from the measured areas under the peaks is 98.22%.

Table 11: Measured areas under the chromatographic peaks with retention times of the peaks for each species identified in the chromatogram for product extracted from crystallizer 2 after the serial CPG experiment.

Species	*A* [mAU]	Retention Time [min]
R CPG	0.89	8.975
S CPG	99.11	11.821

5.9 Appendix 2: Raman in-situ Monitoring of Mandelic acid suspension density

As the racemic compound DL-MA and the enantiopure D-MA have different physical properties and crystal structures, they can be distinguished using optical process analytical tools such as Raman spectroscopy [2]. Differences in the spectra and the dependence of the spectra intensity on the suspension density of the solid crystals in the crystallizer can be used to monitor the suspension density of the crystallized solids in-situ during the process. An immersive type Raman probe (RXN2, Kaiser Instruments) was used in the D-MA crystallizer to monitor the suspension density of the D- and DL-MA crystallized and the concentration of the solution during the process. The power of the laser bean was 355 mW and the laser wavelength was 785 nm to reduce fluorescence. In order to quantify the solid composition the Raman probe was calibrated against varying compositions of D- and DL-MA at different suspension density and particle sizes at a crystallization temperature. A partially least squares model was built using the calibrated data for quantification of the solid phase enantiomeric excess. The resulting enantiomeric excess which can be determined was then verified with HPLC, confirming the accuracy of the Raman method at ± 7.5 g/l for the overall measured suspension density.

5.10 Appendix 3: Solubility determination of CPG using crystal 16

For the determination of the solubility, crystal 16 (Technobis, the Netherlands) is used. The crystal 16 consists of 4 independent blocks which can hold four 1.5 ml vials each. The vials are filled with solid and solvent or a solvent mix at a known concentration, where a magnetic or overhead stirrer is added to the vials for agitation. The stirring speed can be adjusted, where 700 rpm are used in this work with magnetic stirrers (6 mm) covered in PTFE. The vials are then placed into the blocks and the desired temperature profile of the solubility experiment is set. In this case each vial underwent 4 temperature cycles, where the vials are heated at a defined rate like 0.3°C/min until a high temperature of 50°C is reached. The vial is held at a high temperature for 30 min to allow all solids to dissolve. Afterwards the vial is cooled at the same rate as it was heated and held at a low temperature of -10°C for recrystallization, after which one cycle is completed. During the cycles, a laser light passes through the vial determining its transmissivity depending on the suspension density. At a transmissivity of 100 all solids have been dissolved, while at the transmissivity 0 no light can pass through the vial to the detector indicating that it is filled with crystals. When the transmissivity reaches 100 at a certain temperature, no more crystals are present in the vial. This temperature is referred to as the clear point temperature and is a good estimation of the saturation temperature of the sample. For each sample of know concentration, 4 temperature cycles are run, leading to 4 clear points temperature measurements. If these clear point temperatures were within ± 3°C margin, an average clear point temperature was determined for the sample, otherwise the run was discarded and a new sample was prepared. During the experiments pure Acetonitrile was used as a solvent. In further experiments the DBU dependent solubility is investigated, where volume fractions of up to 5, 10 and 15 w% of DBU are added to the pure solvent.

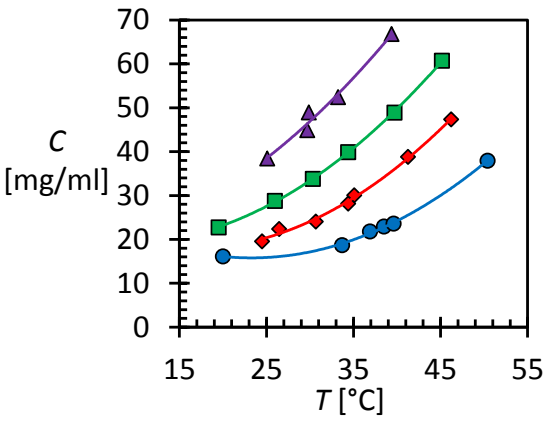

Figure 70: DBU dependent solubility of CPG in Acetonitrile with no DBU (blue), 5 w% DBU (red), 10 w% DBU (green) and 15 w% DBU (purple).

Figure 70 shows the results of the solubility determination in a binary phase diagram. If the DBU fraction in the solvent is increased the solubility increases as well. To prevent errors in the solubility, a low DBU fraction the solvent is chosen as explained in the paper.

5.11 References

1. Dunn, A.S., et al., *Resolution Control in a Continuous Preferential Crystallization Process.* Organic Process Research & Development, 2019. **23**(9): p. 2031-2041.
2. De Beer, T., et al., *Near infrared and Raman spectroscopy for the in-process monitoring of pharmaceutical production processes.* International Journal of Pharmaceutics, 2011. **417**(1): p. 32-47.

6 Process Designs and Approaches towards Continuous Crystallization-based Chiral Resolution, Separation and Deracemization

6.1 Abstract

A large number of new active pharmaceutical ingredients are chiral molecules. Usually, only one enantiomer has the desired effect in the body, while the other can be harmful. As asymmetric synthesis routes for direct production of the preferred handedness are not always available and the racemate is produced instead, a resolution or deracemization is needed. Crystallization-based processes for chiral separation provide a highly selective and efficient method for the separation of enantiomers. However, there is a large variety of such crystallization-based separation technologies, often selected through using trial-and-error methods. The objective of this work is to provide an approach for comparison between the process types and their applicability, and subsequently to provide a support for choosing the suitable crystallization-based resolution or deracemization process.

6.2 Introduction

The majority of pharmaceutical substances are chiral molecules [1], where only one enantiomer has the desired effect in the body, so only one enantiomer is desired for the active pharmaceutical ingredient (API). Asymmetric synthesis [2] during the formulation of the molecule allows for the production of only the desired handedness. However, this route is not always available and a racemic or enriched solution is produced instead. In such cases a resolution process, to separate the enantiomers is needed. There are a number of methods that can be used for chiral separation. Chiral chromatography has shown to be an effective method for chiral separation [3, 4]. Chromatography provides a good enrichment of one enantiomer in one processes step but it challenging to reach full separation through chromatography alone as the enrichment per separation cycle becomes smaller with increasing purity. Also, chirally selective membranes, as shown using mandelic acid [5], or liquid-liquid extraction [6] can be used for the separation of chiral compounds. However, both methods require multiple separations steps to reach acceptable enrichments. Another issue of membrane separation is the scarcity and high cost of selective membranes [4]. A problem for liquid-liquid extractions is the often low selectivity in each stage, requiring a substantial number of stages to reach highly enriched products [4].

Crystallization-based methods have shown to lead to efficient and selective resolution, often in a single process step, and have long been applied in industry [4]. One of the most common crystallization based chiral separation technique is classical resolution [4], where the enantiomers of a racemate are combined with an enantiomerically pure resolving agent resulting in two diastereomeric salts which have, among others, different solubilities. If the solubility difference is sufficiently large, both diastereomers can be directly separated

through crystallization of the low-solubility diastereomer salt. However, the resolving agent has to be removed after the separation to obtain the pure enantiomer and to enable resolving agent recycling. Classical resolution is especially suited for racemic compound forming systems, in which the enantiomers jointly form a crystal, cannot be separated directly by crystallization but need prior enrichment. For the separation of chiral conglomerate forming systems, where the enantiomers form pure crystals, which are physically mixed at an equal ratio at racemic composition, direct preferential crystallization can be applied at the racemic composition as both enantiomers have the same physical properties.

In the pharmaceutical industry, batch processes have been predominating for crystallization processes [7]. This is due to operational simplicity, low annual throughput, a highly regulated environment for production and the need for large degree of flexibility as many compounds are produced with the same equipment after thorough cleaning [8]. They are simple from the equipment design, as they only require one vessel and often no feed and suspension removal. However, with respect to the process conditions, batch processes are dynamic, as process conditions like temperature or antisolvent fraction vary during the process, leading to a changing mass conversion over time. This makes it hard to control and reproduce such processes, leading to changes in the product quality in each batch [7, 8], as well as high running costs. As the produced API is often of high value with strict requirements to purity for chiral compounds as per FDA (Federal Food and Drug Administration) regulations [9, 10], the running costs are often negligible. Due to their simple equipment design, they are highly flexible allowing for the crystallization or production of different products after a thorough cleaning. However, due to their simple design and flexibility, batch processes have lower yields than continuous or semi-batch processes as they are not using a recycle of any kind. Due to the dynamic nature of batch processes the solution can be deprived of the product as much as possible without compromising the overall product. . In cases of low production mass, which needs to be produced, batch processes are often more practical and economical, as continuous processes would often require larger initial investments.

One downside of using batch production is the lack of reproducibility. In addition, batch processes are dynamic processes where one or more control variable such as temperature, stirring speed or others change over time, which makes batch processes harder to control than continuous process, where one steady state is kept at constant conditions. However, there is a drive towards continuous manufacturing due to its many benefits over batch process, such as reproducible product quality, often better productivities and higher yield due to recycling of unused educts. The operating conditions in the crystallizer are constant throughout the process allowing for constant reproducible product production. If high purity product can be produced reproducible, it can reduce the number of post-processing steps and help fulfil the strict requirements on product quality and purity in the heavily regulated pharma environment. As the operating conditions are kept constant, the process can also be controlled and monitored easily in steady-state. Steady-state operation also allows for an easy mathematical description of the process, allowing for the implementation of process models for prediction and process control [8]. As the product in the pharmaceutical industry is of high value, high overall yields are desirable. In continuous processes, the solution with an uncrystallized product is recycled allowing for an overall higher yield than in batch

processes. While continuous processes have a higher initial investment cost, the size required in pharma applications is comparable small so that the investment costs in comparison to the product value might be low. Continuous processes are considered inflexible and only usable for one compound however it was shown in this work (chapter 5) that crystallizer designs can be multi-purposed even though if they are run continuously.

Table 12: Benefits and downsides of continuous and batch processes configurations [7, 8]

	Continous Processes	Batch Processes
Flexibility with regards to products	-	+
Reproducable product quality	+	-
Processcontrol	+	-
Investment costs	-	+

In this work, we aim to present guidelines for the design of batch-wise and continuous crystallization-based separation, resolution and deracemization processes. At first, the benefits of continuous processes over batch are discussed, followed by a review of the current state of the art regarding crystallization-based separation, resolution and deracemization of chiral compounds. Afterwards productivity, yield and product enantiopurity are discussed and exemplified for a number of processes. Finally, a guideline is presented, detailing choices that must be made to arrive at a suitable crystallization-based separation, resolution or deracemization process.

6.3 Towards Continuous

Batch-wise crystallization is still the most common process mode applied in the pharmaceutical industry due to the comparably low annual production rates and heavily regulated production environment. A simple batch crystallization process schematic is shown in Figure 71 (left). During a batch process, the starting solution is prepared in a single vessel and the crystallization is started by inducing the supersaturation for instance through cooling or evaporative crystallization. In chapter 3 a fed-batch process was performed, where a starting solution is prepared in a vessel and antisolvent was added over time at a constant rate to induce supersaturation, leading to crystallization. In such processes still nothing is removed from the vessel until the end of the processes but a constant feed is used to run the process. Instead of adding a solution or antisolvent in a fed-batch process, a process by Xiouras [11] used addition of racemic solids, which then underwent a transformation and subsequent ripening to produce pure solid enantiomer. At the end of the process, all slurry is removed, filtered and washed to obtain the final product. During a batch process usually, no product or solution is removed from the vessel, but addition can occur especially in the case of antisolvent crystallization, where the antisolvent needs to be added during the process. The largest benefit of batch processes are their operational simplicity despite their complexity due to dynamic operation. Batch processes can be used for separation, resolution or deracemization processes alike and many examples can be found in the cited literature in the next section 6.4. Especially deracemization processes such as Viedma ripening and

temperature cycling are often performed batch wise, due to their scalability and dynamic nature. For the production of enantiopure clopidogrel-imine seeds, as explained in chapter 5, a batch deracemization was used reducing the temperature stepwise after a constant holding period. When performing small scale processes or processes requiring dynamic changes of processes variables, batch processes provide an ideal configuration.

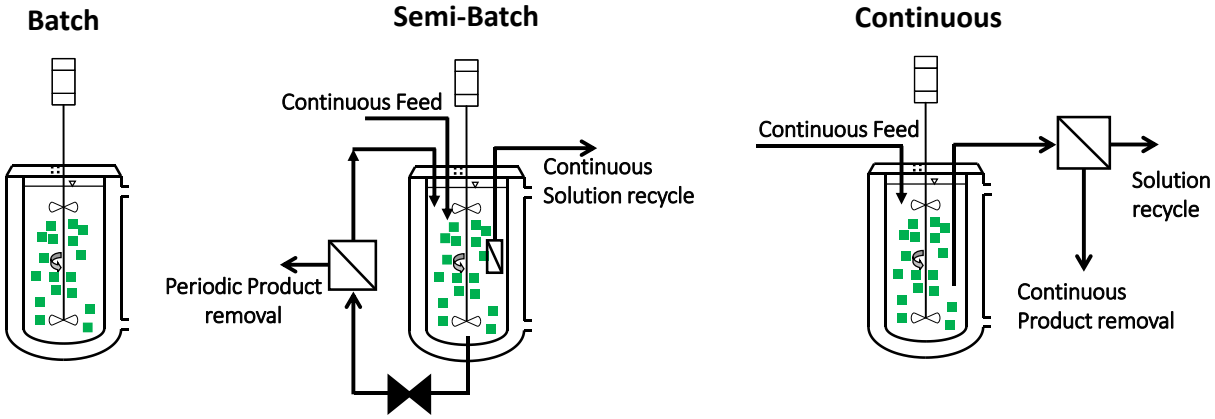

Figure 71: Schematic of (left) a batch crystallization process, (middle) semi-batch processes with a continuous feed and solution recycle and an optional periodic product removal, and (right) a continuous process with a continuous feed and continuous product removal.

Figure 71 (middle) shows a schematic of a semi-batch process which is a compromise between batch and continuous process. Semi-batch crystallization processes have a feed stream over a period of process time, as well as an outlet for recycle. They run at constant operating conditions such as crystallization temperature and solution residence time. In comparison to continuous processes, semi-batch processes have a periodic product removal, or the product is removed at the end of the processes similar to batch, which makes them more flexible than continuous processes but allows for a higher product reproducibility than a batch process due to the constant operating conditions. However their yields are lower than a continuous process and the product has to be extracted periodically which interrupts the processes and only a temporary steady state can be achieved. Similar to batch processes they offer higher flexibility and can be used at product throughput lower than that of continuous processes. However, they have larger initial investment costs than batch processes and repeated start-up phases with shorter steady states than continuous processes. In this work semi-batch processes are used for the separation of mandelic acid (chapter 4), where a feed solution was constantly feed into a crystallizer, cooled and the depleted solution recycled back into the feed. Semi-batch operation is also frequently performed in resolution processes for conglomerates as shown in section 6.4. As semi-batch processes are less operationally complex than continuous processes, especially at lower throughputs, they can often be obtained by batch process modifications. In this work a semi-batch processes was also used for deracemization of clopidogrel-imine in chapter 5, providing a different approach then other deracemization techniques such as temperature cycling or Viedma ripening.

Continuous processes have been applied for a long time in the chemical industry as large product quantities have to be produced. While in pharma significantly smaller throughputs are required, continuous processes may not seem to be a necessity but they offer many benefits especially with regards to product purity which is of high importance in the

pharmaceutical industry. In a continuous process as shown in Figure 71 (right) a continuous feed flow is going into a crystallizer where the supersaturation is induced and the product crystallized. At the same time, the suspension is removed from the crystallizer at the same ratio as the feed flow. After extraction, the solid product is separated from the solution and the solution is recycled. Continuous processes are often complex with regards to operational complexity, as many unit operations are required at the same time. But as they operate at a steady state at constant process conditions, they are easy to run once they reach steady state. In this work a continuous process has been used for a continuous antisolvent deracemization in chapter 3. There different steady state operation for the process where tested and compared. But continuous crystallization processes have also been applied for resolution processes [12]. They can also be applied for deracemization processes, such as the serial deracemization, which will be developed in the future. In this case the semi-batch process can be used as bases for further modification into a true continuous process.

As product quality and purity are of very high importance in the pharmaceutical industry, there is a drive towards continuous manufacturing for newly developed products. Once the configuration of the process is decided on, a suitable separation process depending on the compound type needs to be chosen.

6.4 Crystallization-based Resolution and Deracemization

Table 13 shows an overview of publications, where separation processes suitable for the crystallization-based separation of chiral compounds with respect to the compound type are described.

Table 13: Overview of crystallization-based resolution processes, their specifications and suitability with regards to the compound type, with conglomerate forming systems (CFS) and racemic compound forming systems (RCFS)

Process Configuration	**Suitable Compounds and Process specifications**	**Reference**
Resolution Processes		
Serial Crystallization	**Resolution of CFS/ *P* = 3.5 g/lh/ *Y* = 55%/ *E* > 98%**	**Chapter 5**
Continuous Parallel preferential crystallization	Resolution of CFS/ *P* = 6…8 g/lh/ *E* > 98%	[13]
Continuous/Batch Coupled parallel preferential crystallization	CFS/ *P* = 3…13 g/lh	[12, 14, 15]
Fluidized bed crystallizer	Shown to work for conglomerate forming systems, can be adopted for racemizing conglomerates/ *P* >13 g/lh/ *Y* = 35%/ *E* > 98%	[16]

Continuous MSMPR with nucleation control	CFS/ P = 1…5 g/lh/ Y = 20%/ E > 98%	[17]
Deracemization Processes		
Continuous antisolvent deracemization	**Racemizing conglomerate forming systems with fast racemization kinetic**	**Chapter 3**
Serial Deracemization	**Racemizing CFS/ P = 2.5 g/lh/ Y = 65%/ E > 98%**	**Chapter 5**
Viedma Ripening	Racemizing CFS/ E > 98%	[18-20]
Batch Temperature Cycling	Racemizing CFS/ P = 0.5…2.5 g/lh/ E > 98%	[21-24]
Semi Batch Temperature Cycling	Racemizing CFS/ P = 0.1…0.9 g/lh/ E > 98%	[25]
Viedma ripening Hybrid process	Racemic compounds forming a racemizable metastable Conglomerate	[11]
Ultrasound induced deracemization	Racemizing CFS	[26]
Enzymatically catalyzed deracemization	Conglomerates racemizable with an enzyme	[27, 28]
Second Order Asymmetric Transformation	Racemizing CFS with fast racemization kinetic/ P = 69 g/lh/ E > 98%	[29, 30]
Hybrid and Separation Processes for Racemic compound forming Systems		
Serial Crystallization	**Separation of conglomerate and racemic compound forming systems at eutectic composition**	**Chapter 5**
Classical Resolution	CFS/ RCFS	[4]
Membrane separation with coupled batch crystallization	CFS/ RCFS/ P = 7.6 g/lh/ Y = 1.8%/ E > 96%	[5]
Chromatography with preferential crystallization	CFS/ RCFS/ P = 33.3 g/lh/ Y = 56.5%/ E > 98%	[31-33]
Chromatography with antisolvent crystallization	CFS/ RCFS/ P > 100 g/lh/ Y > 70%/ E > 98%	[34]

6.4.1 Hybrid and Crystallization-based Separation Processes for Racemic Compound Forming systems

The most common process for the separation of racemic compound forming systems (RCS) is classical resolution, where the enantiomers of the racemic compound form two diastereomeric salts with different solubilities allowing for the direct separation of the diastereomeric salts.

In the case of RCS, both enantiomers form a racemic compound at the racemic composition with molecules of both handednesses being incorporated in the crystal lattice. This results in different physical properties of the racemic compound from its pure enantiomers and the formation of two eutectic points, where the solution is saturated with regards to one pure enantiomer and the racemic compound. Therefore RCS cannot be preferentially crystallized directly at the racemic composition, like conglomerates, but require enrichment to the eutectic composition by a second primary separation technique such as membrane or chromatographic separation. Once enriched to the eutectic composition, the triphasic domain can be accessed which allows for the stable enantiomer and racemic compound to be separated. In such hybrid processes, combining a primary separation technique with a crystallization based separation, the primary method only needs to be used until a sufficient enrichment is achieved as they usually have multiple separation stages, while crystallization can be done in one stage. Furthermore, the racemic compound byproduct can be recycled to the primary separation method while the pure enantiomer product is obtained, increasing the overall yield of the hybrid process. While primary separation methods are often more efficient using racemic starting material [3, 4, 35], crystallization is more efficient in enriched starting solutions. Combining a primary separation method and preferential crystallization can, therefore, result in higher overall productivity and yield, as well as lower running costs.

A membrane separation followed by a preferential crystallization in a coupled batch crystallizer has been shown to work for mandelic acid by Gou [5], resulting in an enantiomerically high purity product. Also combining chiral chromatography with preferential batch crystallization has been shown to work efficiently in a number of publications [31, 33, 34, 36]. However as the crystallization steps in the published work have been batch processes, a serial crystallizer is used to separate an enriched starting solution in chapter 4 of this work, in a semi-batch configuration. This process allowed for high productivity of at least 13 g/lh and yields of over 74 %. The separated racemic compound can be recycled for the primary separation process.

6.4.2 Conglomerate Resolution

There are a number of crystallization based chiral separation method which can be used to separate chiral compounds. Which process, or combination of processes to use, strongly depends on the compound type and specific properties of the material to be separated. Some of the presented processes, such as the serial crystallizer configuration in chapter 5, can be used for a number of compound types with varying physical properties. Once a process has been decided, the feasibility of the process can be investigated using equations to describe productivity as a function of the demands on the process and information on the compound. The enantiomers of conglomerates systems at racemic composition form a single eutectic point with a solvent at a certain temperature in equilibrium, allowing for a direct separation at the racemic composition using preferential crystallization. In this thesis chapter 4 a semi-batch parallel process configuration was presented which is here used for the separation of a racemic compound forming system enriched to eutectic composition, however, it can also be used for the separation of conglomerate forming systems. Parallel separation process configurations where both enantiomers are crystallized simultaneously, while the solutions from both crystallizers are mixed in a feed vessel, to ensure racemic composition in solution,

have been shown to work in a CSTR configuration [13]. Ensuring racemic composition in solution prevents primary nucleation as no enantiomer enriches. Parallel separation processes have also been shown to work in a fluidized bed, plug flow type crystallizer [16]. Such plug flow type crystallizers in continuous operation can reach productivities up to 20 g/lh as shown in a soon to be published book by Niman and Zoltan (chapter 12). In a special case, the solutions of both crystallizers can also be exchanged, using the enrichment of counter enantiomer in solution, to be crystallized in the respective other crystallizer. This keeps the solutions in both crystallizers close to the racemic composition and allows to prolong the process duration, as shown by Lorenz, Seebach and Temmel [12, 14, 15]. Cyclic batch processes have shown to reach productivities around 12-13 g/lh using threonine as model compound (Soon to be published book by Niman and Zoltan, chapter 12). Alternatively, innovative control strategies in continuous preferential crystallization processes can be used to control the nucleation of the counter enantiomer as shown by Dunn [17].

In chapter 5 a serial process is used for the resolution of conglomerates in a semi-batch process, where the solution is continuously pumped from a feed into a crystallizer where the undesired enantiomer is crystallized first, while the counter enantiomer is enriched in solution and served as feed for the second crystallizer, where the target enantiomer is crystallized. This way the primary nucleation of the counter enantiomer in the target product crystallizer can be prevented. Afterwards the solution is cycled back to the feed where a solid excess equal to the racemic composition is dissolved over time. In a review paper by Rougeot [37], a similar serial process for the separation of conglomerates and other process configurations are shown.

Most of the preferential crystallization processes shown in the literature use cooling crystallization which allows for the processes to be applied in continuous or semi-batch configurations by alternating the temperatures between feed and crystallizer vessels.

6.4.3 Conglomerate Deracemization

In some cases, conglomerate forming systems can be racemized at crystallization conditions, allowing for a racemic composition to be maintained in the solution during the crystallization process, preventing primary nucleation of the undesired handedness. This allows for the application of new deracemization processes such as Viedma ripening or temperature cycling to be applied. During Viedma ripening [38], a slightly enantiomerically enriched suspension is isothermally ground using glass beads, resulting in pure enantiomer after a certain time. This method has been applied a number of times on small scale batches [18, 19], but has also been scaled up successfully [20]. Another method which is much faster than Viedma ripening and does not require milling is temperature cycling, where a slightly enriched suspension is repeatedly heated and cooled, dissolving and recrystallizing a fraction of its suspension has been shown to work in small scale in batch [21-23] and semi-batch processes [25]. While scale-up of Viedma ripening processes is challenging especially due to the grinding involved, temperature cycling allows for an easier scale up but mixing effects and dissolution, as well as growth kinetics, have to be considered.

If racemization at crystallization conditions is possible, a preferential cooling crystallization can be applied directly using a feed saturated at a higher and crystallizer operating at a lower

temperature as done in chapter 5 using CPG as a model compound. This process can be applied in a semi-batch or continuous manner and allows for an efficient separation at high product purities. The racemization rate in solution for such a process must be fast enough to prevent any enrichment of the counter enantiomer as this can lead to primary nucleation event of the undesired handedness after a certain time. Such processes are also referred to as second order asymmetric transformation (SOAT) as they allow for the production of only the desired pure enantiomer similar to asymmetric synthesis and have also been shown to work by Oketani [29, 30]. The major difference between serial deracemization performed in chapter 5 and SOAT lies in the approach and scalability. Both processes perform a preferential crystallization at racemization conditions, but SOAT transforms all present racemate immediately. While SOAT requires fast racemization rates and crystallizes from solution, serial crystallization can use solid racemate in a feed tank, which dissolved and pumped to a crystallizer with enantiopure seeds. The flowrate of solution in a serial crystallization can be scaled to match the racemization rates, which allows access to a larger range of compounds and racemization catalysts.

In cases of a fast racemization rate, antisolvent deracemization can also be applied for the chiral separation as shown in chapter 3. This process allows for high yields and can be applied in a continuous process configuration.

While the above mentioned processes can be applied if the racemization occurs at crystallization conditions in some cases the racemization requires high temperatures, ph or other specific conditions to take place at an ample rate. In such cases, the racemization reaction can be decoupled from the crystallization as shown for an enzymatically catalyzed preferential crystallization process [28].

There are a number of processes that allow for the separation of a racemizing conglomerate depending on the compound specifications. However, conglomerates make up only a small fraction of chiral compounds with the majority being racemic compound forming systems, which are more difficult to separate.

6.5 Basic Process design: Predicted and realistic Productivity

After deciding on a suitable separation process and its configuration, the crystallizers need to be designed based on the desired specifications, desired turnover, enantiomeric excess, product loss. . The process specifications can be viewed as product or process demands, which include for a chiral separation process a high enantiopurity of the produced crystalline product, high productivity and yield. The enantiopurity defines the amount of pure enantiomer in the total product mass and should be no lower than 98 %. The yield expresses the percentage of target compound which crystallizes out from amount that could crystallize out. Therefore the loss of product can be described as the percentage of target compound which can crystallize out but does not do so. Productivity defines how much mass of product can be produced per unit time and volume. In this case, the product mass is the overall product-mass produced in a crystallizer, the time is measured in hours and the volume of solution in a crystallizer is used, which does not change during the process. For productivity, values between 10-20 g/lh [13, 39] should be targeted as a reasonable productivity. However defining productivity depends on many factors and can therefore not easily generalised. For

the productivity value, the solubility of the compound, as well as the growth rate of a compound in a solvent have a large influence. If the compound has a low growth rate, productivity will be lower as the process takes longer. At the same time low solubilities could make extreme conditions such as large temperature differences necessary, where also the stability of the compound against temperature fluctuations can be an issue. But also a certain process types have different effects on the productivity. Antisolvent crystallization for example causes a fast growth of the compound from the solution, while cooling crystallization can take much longer. Also continuous processes often have a higher productivity than batch processes, as down and preparation times are shorter in continuous process in comparison to production time. In a soon to be published book by Niman and Zoltan (chapter 12) the productivities of batch and continuous processes are compared showing the continuous process to be the once with higher productivity in general. There are some cases where cyclic process have shown to be more productive than continuous process however. In literature other ways to define the product mass, time and volume can be found. In a study by Oketani [29] where SOAT was used for the deracemization of an Atropisomeric Naphthamide, only the pure enantiomer was considered as product mass, including the enantiomeric excess into the equation. It is therefore very important that productivities and its variables are defined clearly so the productivity values remain comparable.

To determine if set values for the process demands can be realized with a compound, equations can be defined for the process demands (specifications). After defining the equations for the specifications of the process, they can be combined in an equation for the productivity. These specifications can be determined based on information of the compound to be separated like the phase diagram of the compound in a solvent, the compound type (conglomerate or racemic compound forming system), as well as the crystallization and dissolution kinetics and information about the racemizability, as well as the racemization kinetics of the compound. This information is needed to design any crystallization processes and is obtained through preliminary investigations. Through the phase diagram the solubility of the compound in a solvent at any given temperature or antisolvent fraction can be determined, which allows for the starting- and end concentration (C_i and C^*), as well as the supersaturation $S = C/C^*$ for the process to be chosen, where C is a concentration of a compound measured in solution during the crystallization process. While the solubility is needed in all cases, the crystallization kinetics k_G and growth rate G is essential to determine the processes time, seed material and supersaturation to be used for the processes and are of special interest in preferential crystallization as they can impose limitations on the processes design (S.S Dependence of productivity on system properties). In the case of a racemizable compound, a recycling route for the undesired handedness or different process design (Table 13) can be implemented. If a racemization reaction of the compound occurs in solution, the racemization kinetics k_R can be a limiting factor for the production of the pure enantiomer. Based on the information available of the compound, the crystallization process can be designed accordingly to fulfill the specifications of the process.

Table 14: Compound specific information needed for the design of the crystallization process and determination of the process conditions.

Compound Information	Units	Definition
C_F	g/l	Feed concentration of the target enantiomer
C	g/l	Target enantiomer concentration in the crystallizer solution
C^*	g/l	Solubility of the target enantiomer under conditions in the crystallizer
z	˚C/K	Depended variable for supersaturation induction (temperature, AS fraction)
ρ_E	g/l	Solid density of the enantiomer of a compound
$k_{D,E}$	m^2/s	Dissolution kinetic constant of an enantiomer in a solvent
$k_{G,E}$	m^2/s	Growth kinetic constant of an enantiomer in a solvent
k_R	g/s	Racemization kinetic of enantiomers is a solvent
D_E	l/m^2s	Dissolution rate of a compound in a solvent
G_E	l/m^2s	Growth rate of a compound in a solvent
c_A	m^2	Surface area dependent shape factor of an enantiomer crystal ($A_{cr} = c_A L_2$)
c_v	m^3	Volume dependent shape factor of an enantiomer crystal ($V_{cr} = c_v L_3$)
m_2	m^2	Second moment (Total surface area)
m_3	m^3	Third moment (Total Volume)
$L_{2,3}$	m	Specific average Size (m_3/m_2)
P	g/lh	Productivty
Y	-	Yield
E	-	Enantiomeric excess

Table 14 provides some important compound specific information relating to thermodynamic and kinetic properties of the compound which can be used to determine crystallizer dimensions and process conditions, as well as limitations of the process.

Producing a pure product is the main goal of a purification process, for which the productivity and yield have to be adjusted in order to achieve this goal. The overall yield $Y = m_P/m_{th}$ can be described as the total mass of product achieved m_P over the theoretical mass of product m_{th} which could be produced under ideal conditions. The overall yield of a process strongly depends on the process design and parameters. Usually, there is a practical limitation of how much of the target product can be produced due to thermodynamics and the way the crystallizer is designed and run. However, recycling uncrystallized product or using multistage crystallizers can increase the overall yield of a process in such cases. The last specification is the productivity P which is defined as the mass of product produced during the processes,

divided by the process time and Volume of the crystallizer. The productivity is a set value that is to be achieved for a crystallization process, where the mass of product, crystallizer volume and process time are connected to the yield and enantiomeric excess.

6.5.1 Connecting Productivity with Yield and Enantiomeric Excess

The major specifications for a crystallization process are enantiomeric excess *E*, describing the purity of the obtained crystalline product. The second specification is the yield *Y* which provides information on how much product was crystallized with regards to what could have been crystallized under ideal conditions. Besides the yield, the loss of product has be considered. The loss $L = C/t*V$ can be represented by the remaining solid concentration *C*, leaving the crystallizer over process time *t* and volume of the vessel *V*. The loss depends on the operating window of the process but also on recycle of educts. The loss of product will be discussed separately in section 6.5.5. A third specification is the productivity *P*, which relates the produced product mass over process time and crystallizer volume.

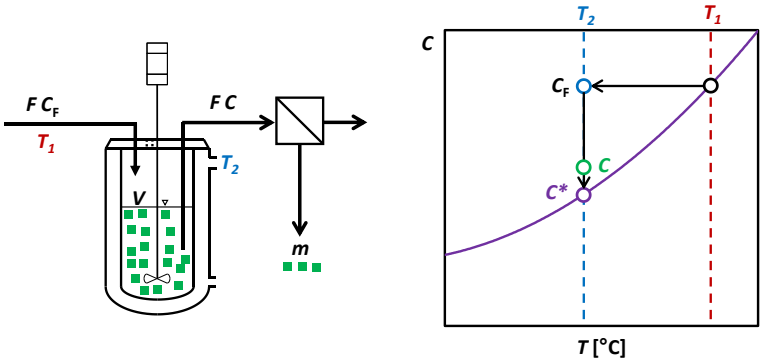

Figure 72: Illustration of a continuous preferential cooling crystallization process (left) with flowrate *F*, inlet concentration C_F and outlet concentration *C*, as well as the schematic of a binary phase diagram (right) detailing the dependence of the concentrations to the crystallization and feed temperature.

Here we define the experimentally measurable productivity *P* as the amount of crystalline material produced per unit of volume and process time.

$$P = \frac{m(V,t)}{Vt} \tag{20}$$

With $m(V,t)$ the amount of produced crystalline material within a certain volume *V*, usually the crystallizer volume, and a characteristic time *t* in which the process to produce the product mass *m* takes place. Note that the purity of the crystalline material is not accounted for in our definition of the experimentally measurable productivity *P*.

For a continuous process with a continuous product stream, $\mathrm{d}m/\mathrm{d}t$ the experimentally measurable productivity becomes:

$$P = \frac{1}{V}\frac{\mathrm{d}m}{\mathrm{d}t} \tag{21}$$

The theoretically maximum achievable product stream $\mathrm{d}m_0/\mathrm{d}t = F(C\text{-}C^*)$ of a pure product depends on the feed flow rate *F* and the difference between the feed concentration and the solubility under conditions in the crystallizer as illustrated in Figure 72. We can, therefore, define a theoretical productivity P_0:

$$P_0 = \frac{F(C_F - C^*)}{V} \tag{22}$$

The productivity for preferential crystallization processes are usually between 10 to 20 g/lh [29]. The overall yield of the process can be described as the produced mass of product over the theoretical producible mass, which is depending on the difference between feed concentration and solubility.

$$Y = \frac{m}{m_0} \tag{23}$$

As the goal of a crystallization process is to crystallize the pure target enantiomer, the yield is defined specifically for one enantiomer and related to the solubility of one enantiomer C^*_E which depends on a variable describing the dependence of the solubility on the temperature, antisolvent fraction or other means of inducing supersaturation.

$$Y_E = \frac{m_E}{m_0} = \frac{C_{F,E} - C_E}{C_F - C^*} \tag{24}$$

The mass of pure enantiomer crystallized m_E can be determined by the difference of concentration between initial pure enantiomer in solution $C_{F,E}$ and the solubility of the enantiomer C_E*. Combining equations 3 and 5 allows for the determination of the yield dependent productivity for one enantiomer P_E.

$$P_E = P_0 Y_E = \frac{F(C_F - C^*) * Y_E}{V} \tag{25}$$

The purity of a chiral compound can be expressed as enantiomeric excess *E*, which describes the excess ($m_{E1} - m_{E2}$) of one enantiomer in the total product ($m_{E1} + m_{E2}$).

$$E = \frac{m_{E1} - m_{E2}}{m_{E1} + m_{E2}} \tag{26}$$

The value of the enantiomeric excess spreads from -1 to 1, where 1 or -1 are enantiomerically pure products and 0 is the racemic mix or compound. The enantiomeric excess relates the mass fractions $x_{E1}=m_{E1}/(m_{E1}+m_{E2})$ and $x_{E2}=m_{E2}/(m_{E1}+m_{E2})$ of the produced enantiomers respectively.

$$E = \frac{m_{E1}}{m_{E1} + m_{E2}} - \frac{m_{E2}}{m_{E1} + m_{E2}} = x_{E1} - x_{E2} \tag{27}$$

With the sum of the mass fractions of both enantiomers $x_{E1} + x_{E2} = |1|$ in the binary product, the mass fraction of one enantiomer can be described with the other $x_{E2} = 1 - x_{E1}$.

$$E = x_{E1} - (1 - x_{E1}) = 2x_{E1} - 1 \tag{28}$$

By using equation 8 the mass fraction of one enantiomer x_E can be described as a function of the enantiomeric excess.

$$x_E = \frac{E - 1}{2} \tag{29}$$

The overall productivity of a process can be expressed by dividing the productivity of one enantiomer by the mass fraction of one enantiomer.

$$P = \frac{P_E}{x_E} \tag{30}$$

If equation 11 is now combined with equations 10 and 6, the overall productivity of a process can be expressed as a function of the yield and enantiomeric excess of one enantiomer.

$$P = \frac{P_{th} X_E}{x_E} = \frac{2F(C_F - C^*)Y_E}{V(E+1)} = \frac{2(C_F - C^*)Y_E}{(E+1)\tau} \tag{31}$$

By defining productivity which is a function of the yield and enantiomeric excess, the equation combines all specifications of the process into one equation.

If the yield, productivity and enantiomeric excess are seen as defined specifications desired for the process, the residence time and driving force, defined by the concentration difference, can be modified to achieve the desired productivity with respect to yield and product purity. Using set values for the enantiopurity, productivity and yield, the process parameters such as concentration difference and its dependent variables like temperature or antisolvent fraction, as well as the residence time can be calculated. Also, the residence time and concentration difference can be varied, in order to minimize the concentration difference and maximize the residence time. By minimizing the concentration difference the risk of primary nucleating the undesired enantiomer is also reduced. The productivity equation can also be used to determine if the process can be run at feasible process conditions. This equation can be used for semi-batch and continuous processes, however, in the case of batch processes, the flowrate would have to be substituted with the crystallizer volume, leaving only the concentration difference.

As examples for the feasibility investigation, the mandelic acid experiments, described in chapter four, can be used. In the case of racemic compound mandelic acid, the eutectic composition contains unequal amounts of each enantiomer in solution. Equation 12 allows determining the needed concentration difference in order to achieve target productivity at given specifications and crystallizer volume. This also allows for initial feasibility investigations of the desired specifications with regards to the solubility of the compound and volume of the crystallizer. The results can be found in Table 15, along with other experiments conducted in this work, where the calculated values for productivity are compared with the experimental once. While productivity defined in equation 12 allows determining the constraints and degrees of freedom with regards to the specifications and process conditions, the productivity can also be defined as a function of the system properties allowing to define the constrains based on information of the compound.

6.5.2 Dependence of productivity on system properties

The dependency of the process productivity on the system properties can be illustrated in the serial preferential crystallization process as shown in Figure 73. There are two types of processes that are performed during the serial process: a preferential crystallization where the desired enantiomers are crystallized sequentially in each crystallizer respectively (MA, ASN) and deracemization processes where only one crystallizer was needed, as the counter enantiomer is racemized in solution.

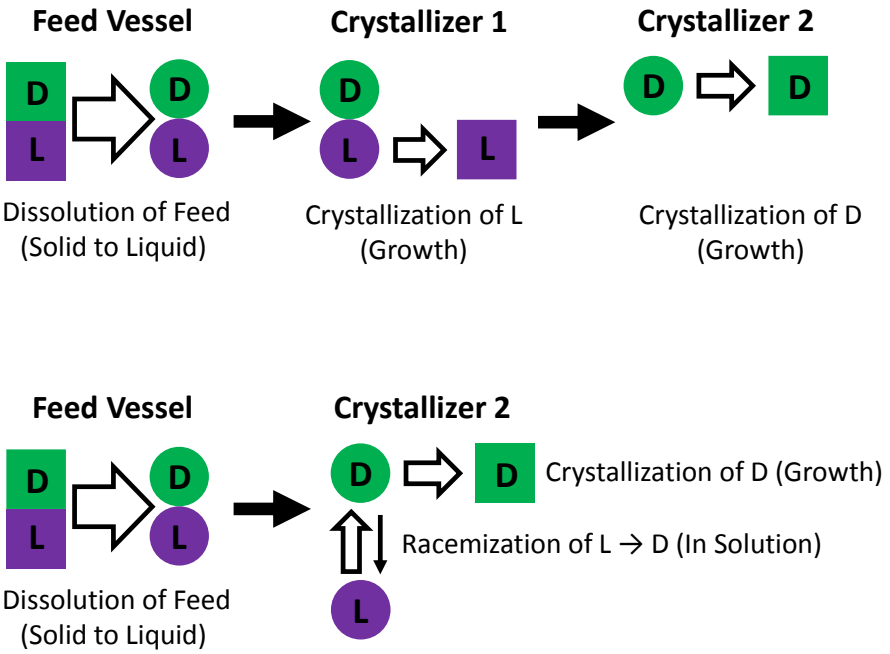

Figure 73: Schematic illustration of the dissolution, growth and racemization processes occurring during the serial crystallization in the case of preferentially crystallizing MA and ASN (top) and the deracemization of CPG (bottom).

In the case of a preferential crystallization, the productivity can be defined as function the dissolution rate *D* of the solid enantiomers in the feed, resulting in a dissolution dependent productivity for each enantiomer.

$$P_E = \rho_E \frac{A_E}{V} D = \frac{M_E}{V} \tag{32}$$

This productivity is specific for each enantiomer present in the feed vessel as in the case of racemic compound forming systems the dissolution rate of the pure enantiomer and the racemic compound are different. The equation puts the solid density of the enantiomer ρ_E, surface area of the solid A_E and the dissolution rate constant *D* into relation with the liquid volume of the crystallizer. The dissolved mass is then available for crystallization and can be defined as a mass flow M_E of each enantiomer. The solid density and dissolution rate are constants, allowing for the alteration of the surface area and crystallizer volume. If the mass of the solid remains constant different surface areas can be achieved depending on the particle size, where smaller particles dissolve faster. Using the equation it can be calculated if the desired productivity can be achieved under feasible conditions. Each enantiomer has to be looked at individually as in the case of racemic compound forming systems the dissolution rates and densities can differ between pure enantiomer and racemic compound. In the cases of the model compounds used for the serial experiments, the dissolution rate has not shown to be an issue as it outperforms the growth rate. In most cases, the dissolution is faster than the growth of crystals however in a case where this would be reversed the serial crystallizer would not be able to use a solid excess but a saturated solution would have to be provided for the feed in a different way.

After the dissolution, the solution is transported to the crystallizers for the target enantiomers to be crystallized. The crystallization of the target enantiomer depends on one hand side by

concentration difference provided with respect to feed and crystallizer concentrations as shown by equation 12. On the other hand side independent of the supersaturation supplied to be crystallized, the enantiomer is limited by a specific growth rate G_E and growth kinetic $k_{G,E}$, which limits how much mass can be crystallized.

$$P_E = \rho_E \frac{A_E}{V} G_E = \frac{M_E}{V} = \frac{C_{F,E} - C_E}{\tau} \tag{33}$$

Using equation 14 the growth rate can be described as:

$$G_E = \frac{M_E}{A_E \rho_E} \tag{34}$$

The mass flow M can be described as mass m over relative time $M = m/t$, where the mass can be expressed by the third moment m_3 and a volume based shape factor c_V and the surface area through the second moment m_2 and the surface based shape factor c_A, which specific to the compound in a solvent and the relative time as residence time τ.

$$\frac{M_E}{A_E} = \frac{\rho_E c_V m_3}{c_A m_2} \frac{1}{\tau} \tag{35}$$

The volume based shape factor with the third moment and surface based shape factor by the second moment can be combined to a characteristic average size $L_{2,3}$ of the solid crystals produced. By combining equations 15 and 16 the growth rate can be described as a function of the characteristic average size of the produced crystals and the residence time.

$$G_E = \frac{c_V m_3}{c_A m_2} \frac{1}{\tau} = L_{2,3} \frac{1}{\tau} \tag{36}$$

The growth rate is described by the growth kinetic and concentration difference [40]:

$$G_E = k_{G,E}\left(C_{F,E} - C_E^*\right) \tag{37}$$

Combining equations 14, 17 and 18 allows for the productivity to be described as a function of the growth kinetic, characteristic average size of the produced crystals and residence time.

$$P_E = \frac{L_{2,3}}{2\tau k_{G,E}} \tag{38}$$

Equation 18 allows describing the crystal growth rate depended on productivity for one enantiomer by variables that can be easily determined experimentally for a compound in a solvent. The characteristic average crystal size can be calculated through the produced product mass which is a function of the flow rate and concentration difference, where the feed and crystallizer concentration can be measured. The surface area can easily be calculated through the volume based mean particle size distribution, which can be estimated by in-situ measurements like FBRM. The growth kinetic is system specific and can only be determined experimentally. Alternatively, a linear deposition rate, describing a linear quantitative increase of solid mass or suspension density in the crystallizer, can be used instead of a growth kinetic as it can be measured in-situ during an experiment. While the growth rate kinetic is constant, the characteristic average size depends on the process conditions. Equation 19 allows determining growth rate limitations on the productivity in dependence on the concentration difference provided. If a more supersaturated solution is provided then can be

crystallized through the given surface area and growth kinetic, the additionally provided supersaturation will remain in the solution, leading to a concentration difference with respect to equilibrium conditions in the crystallizer and provided excess material. This accumulation can lead to an undesired primary nucleation event as shown in chapter 4 or an inert material that has to be recycled.

For the case of deracemization processes, the productivity can be defined as a function of the racemization rate constant k_R and the difference in the solution concentrations of both enantiomers C_{E1} - C_{E2} present, as the undesired enantiomer in solution has to undergo a transformation to the desired handedness to be crystallized first.

$$P_E = k_R(C_{E1} - C_{E2}) = \frac{M_E}{V} \tag{39}$$

The racemization rate for one enantiomer in a solvent is system dependent but can also depend on the racemization mechanism. Some compounds are auto racemizing in certain solvents [24], others need catalysts like in the case of CPG, where DBU was used, enzymes that transform the undesired handedness [27]. Process conditions like temperature and solubility also influence the racemization kinetic. For deracemization processes very fast almost immediate racemization is preferred as no enrichment of the counter enantiomer can occur, allowing for higher concentration differences and shorter residence times to be used to maximize productivity.

The productivity can be described as a function of the process specifications but also of the system properties. Both are necessary to determine the limitations and feasibility of the process design and parameters.

6.5.3 Application of Productivity Prediction

To validate the equation 12 which allows calculating the productivity based on the process specifications, the solubilities, yields, residence times and product purities from the experiments of this thesis are used to show that using the same process parameters as in the experiments similar productivities can be determined, as reached in the experiments.

For the starting concentrations C_F the feed concentrations are used depending on the experiment. For the serial MA experiments, the theoretical concentration of the solution coming from the first crystallizer is used. If all DL-MA acid is crystallized din the first crystallizer and only D-MA remains, a solution with a concentration of 243 g/l would be transported to the second crystallizer. In the case of a changing temperature difference, this value changes as the overall concentration difference between feed and crystallizers would also change. For the serial CPG experiment the solubilities from the feed are used and the mixing point on the dilution line for the antisolvent experiment. The end concentrations C^* are the equilibrium concentrations in the crystallizers at crystallization conditions. The yields and residence times used in the calculation (Table 15) are the same as in the respective experiments. For easier comparison, the enantiomeric excess for all cases was set to 98 % (Table 15) for easier comparison.

The estimated productivities calculated P_{Cal} using equation 12 shown in Table 15 are quite close to the experimentally achieved productivities. This indicates that the equation allows for a good prediction thought the calculated productivities are higher as ideal concentrations

are used for the calculations. The prediction can be used to test suitable residence times, concentration differences and yields with regards to the desired process productivity. After that, the found values for productivity can be evaluated with the equations for the compound information.

Table 15: Process conditions and calculated productivity in comparison with the experimental productivity of the serial mandelic acid and CPG experiments as well as one continuous antisolvent experiment.

Process	C_F [g/l]	C [g/l]	Y [-]	E [-]	τ [h]	P_{Exp} [g/lh]	P_{Cal} [g/lh]
Serial MA (S1)	243	225	0.75	0.98	1	13.3	13.6
Serial MA (S2)	243	225	0.63	0.98	0.5	22.4	22.9
Serial MA (S3)	219	186	0.75	0.98	1	24.4	25
Serial CPG	19.8	15	0.60	0.98	1.16	2.42	2.49
Antisolvent Exp 1 (continuous)	171	20	0.88	0.98	0.43	310.8	312.1

6.5.4 Combining system properties and process specifications through the productivity

Using productivity as a function of process specifications, productivity can be described in dependence of process conditions such as residence time, concentration difference, target purity and yield. On the other hand, defining productivity as a function of system properties allows investigating the limitations of the dissolution, growth and racemization kinetics with regards to the concentration difference and residence time. If both equations are combined, each process, or system parameter can be made a function of one another, allowing calculations on how the parameters need to be balanced to fulfil the equation. This way it can be predicted if the chosen values for the variables are feasible with regards to the given values of the compound properties.

$$P = \frac{2(C_F - C^*)X_E}{(E+1)\tau} = \rho\frac{A}{V}D = \frac{L_{2,3}}{2\tau k_G} = k_R(C_{E1} - C_{E2}) \tag{40}$$

This can be illustrated in the example of a growth rate limitation. If equation 21 is used and applied to this specific case, the productivity can be written as:

$$P = \frac{2(C_F - C^*)Y_E}{(E+1)\tau} = \frac{L_{2,3}}{2\tau k_{G,E}} \tag{41}$$

Now the equation can be changed to determine what growth rate constant is needed, to achieve the desired productivity, which can be compared to a real growth rate kinetic constant for the compound to see if such productivity can be achieved.

As an example of this, the continuous antisolvent experiment 1 detailed in chapter 3 can be used. The calculated value of the productivity based on the process specifications can be

found in Table 15 P = 312.1 g/lh. Using this productivity the growth rate needed for this productivity can be calculated using equation 14, where the density of sodium bromate is ρ = 3360 g/l, and the surface is of the bulk in the suspension A can be determined through the suspension density ρ_S in the crystallizer which is constant in a continuous process and is measured as 149.5 g/l, the middle volume based particle size d_{50} = 341 µm (Masterziser, Malvern), and the assumption of cubic particles.

$$A = \frac{6\rho_s V}{d_{50}\rho} \tag{42}$$

Using equation 23 the growth rate can be calculated to G = 4.4*10^{-7} m/s. Using the growth rate in equation 17 the growth rate kinetic constant can be determined as the concentration in the crystallizer during the experiment is measured (29.5 g/l) and the solubility is known (20 g/l), resulting in k_G = 4.6815*10^{-8} m l/s g. If this value is compared to literature [41], where the growth rate was measured in aqueous solution at different supersaturations, a growth rate constant of k_G = 1.1447*10^{-8} m l/s g can be determined. Using this growth rate constant productivity of 75.5 g/lh is calculated using equation 13 and 17 with the same concentration difference as the previous growth rate constant. This productivity is much lower than the one achieved during the process (310 g/lh), which might be due to a solvent mixture used instead of water. This example illustrates how the limitations of such a process with respect to the compound properties can be determined and compared to the process specifications.

6.5.5 Minimising Product Loss

While designing crystallization processes the loss of product L needs to be considered. The loss L can be considered a productivity and is representing the amount of uncrystallized material per time and unit volume leaving the crystallizer with the solution. As shown in chapter 3, where the product loss was analysed in more detail for a continuous antisolvent process, the operating window with regards to solubility has to be considered to minimise the loss. While high productivities can be achieved at certain concentration differences as shown in chapter 3, a low end concentration of solid in the solution should be targeted. In cases where a number of crystallizations are performed in series or recycle is used, the overall loss of the process needs to be considered and crystallization units have to be designed individually to minimise overall product loss. While loss of product is a very important criteria for process design, this has to be considered while choosing the operating conditions and therefore the productivity.

In order to design feasible crystallization processes and determine the process conditions, the specifications of the process need to be determined with regards to system properties. To that end, equations for productivity as a function of the process specifications and system properties can be defined. As the productivities are equal these equations allow investigating the dependence of the specifications on the properties, as well as the limitations of the process. Furthermore, optimal process conditions can be determined for crystallization by using the system properties to define concentration differences and residence times. While the serial process was shown as a specific example, the equations can also be applied to other preferential crystallization or deracemization processes.

6.6 Conclusions

The design of crystallization process is a complex procedure which involves many steps from choosing the process type based on the compound; batch, semi-batch or continuous configuration based on the economy and regulations, to designing the actual processes based on mathematical equations involving both the specifications of the process and properties of the compound to be crystallized. While batch processes have been predominantly used in the pharmaceutical industry for crystallization, there is a trend towards continuous as it has many benefits over the batch processes. In this work, it was shown how processes can be designed towards a continuous approach while preserving the benefit of the flexibility of batch processes. It was also shown how continuous processes can be designed for a specific application on the example of preferential antisolvent deracemization. By using the processes in this work as well as the steps which have been discussed in this chapter, a guideline can be drawn on how to design batch and continuous crystallization process for chiral separation, resolution, and deracemization as shown in Figure 74.

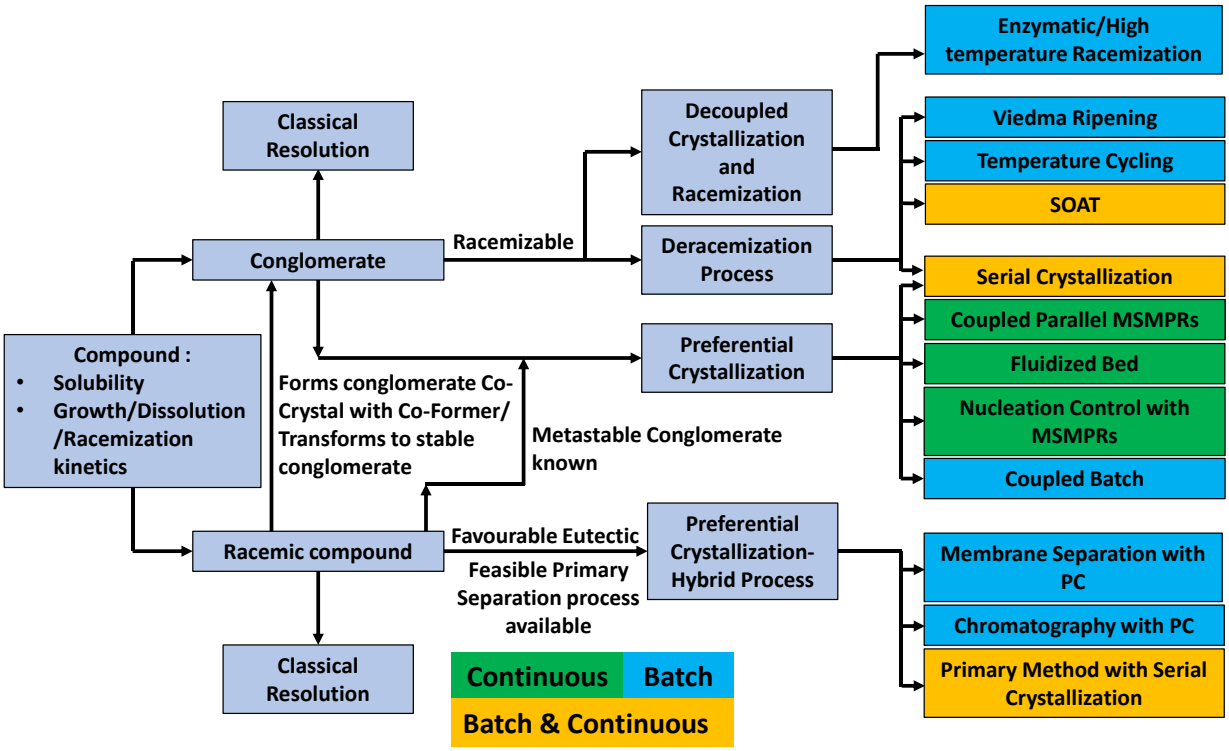

Figure 74: Guideline for the design of a continuous and batch crystallization process for chiral separation, resolution and deracemization.

The guideline in Figure 74 begins with the compound information, where the following steps can be chosen based on the compound type, racemizabiltiy, solubility and growth kinetics. Two major routes can be distinguished depending on the compound type. If the compound is a racemic compound forming system there are three different routes for crystallization based separation that can be taken as shown in Figure 74. In case a stable conglomerate of a racemic compound forming system can be found under certain process conditions, the compound can be separated like a conglomerate forming system as shown by Xiouras [11]. In some cases a compound can be found, which forms a conglomerate co-crystal with the racemic compound,

or a metal stable conglomerate exist at certain processes conditions, also allowing for separation like a conglomerate forming system. Another alternative for the separation of a racemic compound forming system is through a primary method like chromatography, which can be combined with a preferential crystallization process for separation if a favorable eutectic, as discussed in chapter 4, for the compound can be found in a solvent system. There are a number of hybrid processes that have been discussed in 6.4.1. In case no other route is feasible, classical resolution, which has been applied in industry for a long time, can be used for the separation of the racemic compound forming system.

In the case of a conglomerate forming system, which can be racemized at crystallization conditions, deracemization processes can be applied. In this work, deracemization in a serial process configuration has been conducted but there are also other processes, which have been discussed in 6.4.3, for deracemization. In case the racemization and crystallization conditions are different, the racemization process can be decoupled from the crystallization to achieve enantiopure product. If no racemization process can be found, preferential crystallization provides a well-proven process with a large number of process configurations, for the resolution of racemic conglomerates, as shown in 0. The configuration and process used for the separations depend on compound-specific information but also on the desired quantities at which the compound is to be produced.

6.7 References

[1] J. Chen, B. Sarma, J.M.B. Evans, A.S. Myerson, Pharmaceutical Crystallization, Crystal Growth & Design 11(4) (2011) 887-895.

[2] I.R. Baxendale, R.D. Braatz, B.K. Hodnett, K.F. Jensen, M.D. Johnson, P. Sharratt, J.-P. Sherlock, A.J. Florence, Achieving Continuous Manufacturing: Technologies and Approaches for Synthesis, Workup, and Isolation of Drug Substance May 20–21, 2014 Continuous Manufacturing Symposium, Journal of Pharmaceutical Sciences 104(3) (2015) 781-791.

[3] C.M. P. Franco, Chiral Separation Techniques (Ed.: G.

Subramanian), 2nd ed., Wiley-VCH, Weinheim, 2001.

[4] H. Lorenz, A. Seidel-Morgenstern, Processes to separate enantiomers, Angew Chem Int Ed Engl 53(5) (2014) 1218-50.

[5] L. Gou, S. Robl, K. Leonhard, H. Lorenz, M. Sordo, A. Butka, S. Kesselheim, M. Wolff, A. Seidel-Morgenstern, K. Schaber, A hybrid process for chiral separation of compound-forming systems, Chirality 23(2) (2011) 118-27.

[6] J.D. Thornton, Science and Practice of Liquid – Liquid Extraction, Clarendon, Oxford, 1992.

[7] S.L. Lee, T.F. O'Connor, X. Yang, C.N. Cruz, S. Chatterjee, R.D. Madurawe, C.M.V. Moore, L.X. Yu, J. Woodcock, Modernizing Pharmaceutical Manufacturing: from Batch to Continuous Production, Journal of Pharmaceutical Innovation 10(3) (2015) 191-199.

[8] K. Plumb, Continuous Processing in the Pharmaceutical Industry: Changing the Mind Set, Chemical Engineering Research and Design 83(6) (2005) 730-738.

[9] W.H. De Camp, The FDA perspective on the development of stereoisomers, Chirality 1(1) (1989) 2-6.

[10] W.H. De Camp, Chiral drugs: The FDA perspective on manufacturing and control, Journal of Pharmaceutical and Biomedical Analysis 11(11) (1993) 1167-1172.

[11] C. Xiouras, E. Van Cleemput, A. Kumpen, J.H. Ter Horst, T. Van Gerven, G.D. Stefanidis, Towards Deracemization in the Absence of Grinding through Crystal Transformation, Ripening, and Racemization, Crystal Growth & Design 17(2) (2016) 882-890.

[12] H. Lorenz, A. Perlberg, D. Sapoundjiev, M.P. Elsner, A. Seidel-Morgenstern, Crystallization of enantiomers, Chemical Engineering and Processing: Process Intensification 45(10) (2006) 863-873.

[13] K. Galan, M.J. Eicke, M.P. Elsner, H. Lorenz, A. Seidel-Morgenstern, Continuous Preferential Crystallization of Chiral Molecules in Single and Coupled Mixed-Suspension Mixed-Product-Removal Crystallizers, Crystal Growth & Design 15(4) (2015) 1808-1818.

[14] K. Petruševska-Seebach, A. Seidel-Morgenstern, M.P. Elsner, Preferential Crystallization of l-Asparagine in Water, Crystal Growth & Design 11(6) (2011) 2149-2163.

[15] E. Temmel, M.J. Eicke, F. Cascella, A. Seidel-Morgenstern, H. Lorenz, Resolution of Racemic Guaifenesin Applying a Coupled Preferential Crystallization-Selective Dissolution Process: Rational Process Development, Crystal Growth & Design 19(6) (2019) 3148-3157.

[16] D. Binev, A. Seidel-Morgenstern, H. Lorenz, Continuous Separation of Isomers in Fluidized Bed Crystallizers, Crystal Growth & Design 16(3) (2016) 1409-1419.

[17] A.S. Dunn, V. Svoboda, J. Sefcik, J.H. ter Horst, Resolution Control in a Continuous Preferential Crystallization Process, Org. Process Res. Dev. 23(9) (2019) 2031-2041.

[18] M.L. Maarten W. van der Meijden, Edith Gelens, Wim L. Noorduin, Hugo Meekes, Willem J. P. van Enckevort, Bernard Kaptein, Elias Vlieg and Richard M. Kellogg, Attrition-Enhanced Deracemization in the Synthesis of Clopidogre l - A Practical Application of a New Discovery, Org. Process Res. Dev. 13(6) (2009) 1195-1198.

[19] W.L. Noorduin, B. Kaptein, H. Meekes, W.J.P. van Enckevort, R.M. Kellogg, E. Vlieg, Fast Attrition-Enhanced Deracemization of Naproxen by a Gradual In Situ Feed, Angewandte Chemie International Edition 48(25) (2009) 4581-4583.

[20] W.L. Noorduin, P. van der Asdonk, A.A.C. Bode, H. Meekes, W.J.P. van Enckevort, E. Vlieg, B. Kaptein, M.W. van der Meijden, R.M. Kellogg, G. Deroover, Scaling Up Attrition-Enhanced Deracemization by Use of an Industrial Bead Mill in a Route to Clopidogrel (Plavix), Org. Process Res. Dev. 14(4) (2010) 908-911.

[21] W.W. Li, L. Spix, S.C.A. de Reus, H. Meekes, H.J.M. Kramer, E. Vlieg, J.H. ter Horst, Deracemization of a Racemic Compound via Its Conglomerate-Forming Salt Using Temperature Cycling, Crystal Growth & Design 16(9) (2016) 5563-5570.

[22] F. Breveglieri, G.M. Maggioni, M. Mazzotti, Deracemization of NMPA via Temperature Cycles, Crystal Growth & Design 18(3) (2018) 1873-1881.

[23] G.M. Maggioni, M.P. Fernández-Ronco, M.W. van der Meijden, R.M. Kellogg, M. Mazzotti, Solid state deracemisation of two imine-derivatives of phenylglycine derivatives via high-pressure homogenisation and temperature cycles, CrystEngComm 20(27) (2018) 3828-3838.

[24] R.R. Steendam, M.C. Brouwer, E.M. Huijs, M.W. Kulka, H. Meekes, W.J. van Enckevort, J. Raap, F.P. Rutjes, E. Vlieg, Enantiopure isoindolinones through Viedma ripening, Chemistry 20(42) (2014) 13527-30.

[25] K. Suwannasang, A.E. Flood, G. Coquerel, A Novel Design Approach To Scale Up the Temperature Cycle Enhanced Deracemization Process: Coupled Mixed-Suspension Vessels, Crystal Growth & Design 16(11) (2016) 6461-6467.

[26] C. Xiouras, J. Van Aeken, J. Panis, J.H. Ter Horst, T. Van Gerven, G.D. Stefanidis, Attrition-Enhanced Deracemization of NaClO3: Comparison between Ultrasonic and Abrasive Grinding, Crystal Growth & Design 15(11) (2015) 5476-5484.

[27] T. Carneiro, S. Bhandari, E. Temmel, H. Lorenz, A. Seidel-Morgenstern, Shortcut Model for Describing Isothermal Batch Preferential Crystallization of Conglomerates and Estimating the Productivity, Crystal Growth & Design 19(9) (2019) 5189-5203.

[28] K. Wurges, K. Petrusevska-Seebach, M.P. Elsner, S. Lutz, Enzyme-assisted physicochemical enantioseparation processes-Part III: Overcoming yield limitations by dynamic kinetic resolution of asparagine via preferential crystallization and enzymatic racemization, Biotechnol Bioeng 104(6) (2009) 1235-9.

[29] R. Oketani, M. Hoquante, C. Brandel, P. Cardinael, G. Coquerel, Resolution of an Atropisomeric Naphthamide by Second-Order Asymmetric Transformation: A Highly Productive Technique, Org. Process Res. Dev. 23(6) (2019) 1197-1203.

[30] R. Oketani, F. Marin, P. Tinnemans, M. Hoquante, A. Laurent, C. Brandel, P. Cardinael, H. Meekes, E. Vlieg, Y. Geerts, G. Coquerel, Deracemization in a Complex Quaternary System with a Second-Order Asymmetric Transformation by Using Phase Diagram Studies, Chemistry – A European Journal 25(61) (2019) 13890-13898.

[31] M.D.D. Heike Lorenz, E.D.L.K. Polenske, M.D. Andreas, M.D. Seidel-Morgenstern, METHOD FOR SEPARATION OF RACEMIC COMPOUND-FORMING CHIRAL SUBSTANCES BYA CYCLIC CRYSTALLIZATION PROCESS AND A CRYSTALLIZATION DEVICE, in: U.P. Office (Ed.) United States, 2012.

[32] H. Lorenz, D. Polenske, A. Seidel-Morgenstern, Application of preferential crystallization to resolve racemic compounds in a hybrid process, Chirality 18(10) (2006) 828-40.

[33] D. Polenske, H. Lorenz, A. Seidel-Morgenstern, Potential of different techniques of preferential crystallization for enantioseparation of racemic compound forming systems, Chirality 21(8) (2009) 728-737.

[34] H. Kaemmerer, Z. Horvath, J.W. Lee, M. Kaspereit, R. Arnell, M. Hedberg, B. Herschend, M.J. Jones, K. Larson, H. Lorenz, A. Seidel-Morgensten, Separation of Racemic Bicalutamide by an Optimized Combination of Continuous Chromatography and Selective Crystallization, Org. Process Res. Dev. 16(2) (2012) 331-342.

[35] K.G. Feitsma, B.F.H. Drenth, Chromatographic separation of enantiomers, Pharmaceutisch Weekblad 10(1) (1988) 1-11.

[36] H. Lorenz, D. Polenske, A. Seidel-Morgenstern, Application of preferential crystallization to resolve racemic compounds in a hybrid process, Chirality 18(10) (2006) 828-840.

[37] C. Rougeot, J.E. Hein, Application of Continuous Preferential Crystallization to Efficiently Access Enantiopure Chemicals, Org. Process Res. Dev. 19(12) (2015) 1809-1819.

[38] C. Viedma, Selective Chiral Symmetry Breaking during Crystallization: Parity Violation or Cryptochiral Environment in Control?, Crystal Growth & Design 7(3) (2007) 553-556.

[39] M.J. Eicke, G. Levilain, A. Seidel-Morgenstern, Efficient Resolution of Enantiomers by Coupling Preferential Crystallization and Dissolution. Part 2: A Parametric Simulation Study to Identify Suitable Process Conditions, Crystal Growth & Design 13(4) (2013) 1638-1648.

[40] A.S. Myerson, Handbook of Industrial Crystallization, in: A.S.E.D.L.A.Y. Myerson (Ed.), Handbook of Industrial Crystallization (Third Edition), Cambridge University Press, Woburn, 2019, p. xi.

[41] V. Surender, K. Kishan Rao, Growth mechanism of NaBrO3 crystals from aqueous solutions, Bulletin of Materials Science 18(3) (1995) 289-299.

7 Conclusion and Outlook

This work aimed to develop and demonstrate new crystallization-based separation and resolution processes, performed in one serial semi-batch configuration and deracemization processes, conducted in the serial configuration, as well as an antisolvent deracemization, for chiral compounds, which can easily be adapted to continuous operation. Therefore, new crystallization processes towards continuous separation, allowing for a highly enantiopure product, were investigated with regards to their productivity, yield, and applicability. The newly developed separation, resolution, and deracemization processes together with other novel process designs for crystallization-based chiral separation, from other research groups, were compared regarding their range of applicability to present a guideline that allows choosing a suitable process design and determine its feasibility.

In chapter 3 we investigated antisolvent deracemization as a new continuous deracemization process configuration. It was shown that, with racemization in solution, the control over chirality in an antisolvent crystallization has been maintained, despite the high supersaturation which typically occurs in antisolvent crystallization. By controlling the residence time and antisolvent fraction, antisolvent deracemization was conducted in a continuous fashion allowing for high yields and productivities to be achieved. The control over chirality further has important implications for the understanding of such crystallization processes in general: It is conventionally thought that primary nucleation is the dominant mechanism in antisolvent crystallization processes, due to the high local supersaturations at the mixing points. However, the investigation revealed that enantioselective secondary rather than aselective primary nucleation was the dominating nucleation mechanism even at the high local supersaturation occurring during antisolvent crystallization. This dominance of secondary over primary nucleation may well also be true in general for crystallization processes involving high local supersaturations. The prevalence of secondary rather than primary nucleation would have important implications for the design and operation of such industrial crystallization processes since the key controlling factors for primary and secondary nucleation differ.

In chapter 4 a parallel and serial crystallizer configuration was investigated and compared, regarding their suitability for separating the racemic compound forming system mandelic acid (MA) at the eutectic composition. Therefore, the obtained product purity, productivity, yield and reliability of both process configurations were investigated at varying process conditions. As mandelic acid can be monitored in situ due to the racemic compound and its pure enantiomer having different physical properties, the parallel and serial process could be investigated in detail using this compound. The investigation revealed that during the parallel separation process a high supersaturation for the racemic compound prevails in the solution of the crystallizer producing the pure enantiomer. This caused the racemic compound to primary nucleate, shortening the process duration, which resulted in lower productivities and yields. It was not possible to increase the yield or productivity by using milder process conditions. Additionally, the process proved to be sensitive for temperature fluctuations, allowing only for a prolonged separation of D-MA and DL-MA at very low-temperature differences. In comparison, the serial separation process first removed the racemic

compound from the solution in a first crystallizer, while the target D-MA was remaining in solution but not nucleating. In a second crystallizer, the D-MA was then crystallized, with a low risk of DL-MA nucleating as it was already removed from the solution. This led to higher robustness of the process against changes in temperature and residence time, which was demonstrated in experiments. This lead to an increased production time during which the racemic compound and pure enantiomer were separated, as well as higher yields and productivities than in the parallel process. As no primary nucleation of the DL-MA occurred in the D-crystallizer during any of the experiments, all the product produced was enantiopure. The results of the mandelic acid experiments show that the serial process configuration allows to robustly separate a racemic compound forming system at the eutectic at high product purities and yields. In addition, the by-product can be used for recycling into a primary purification method to produce eutectic feed for the process.

The information from chapter 4 was applied in chapter 5 where the serial process configuration was used to resolve the conglomerate forming systems asparagine monohydrate and to deracemize clopidogrel-imine. The objective was to show that one crystallizer design can be used for the separation of racemic compound forming systems, as well as conglomerates in the presence and absence of racemization in solution. The investigation revealed that all model compounds were obtained at high enantiopurities, productivities, and yields. The productivities were similar or higher to specific crystallization processes used to separate the respective compounds.

In a final review chapter 6, the information gathered in chapters 3-5 as well as in literature were used to provide a guideline for choosing a suitable process depending on the model compound and test the initial feasibility of a possible process. Therefore, an overview of processes, including batch, semi-batch, and continuous configurations, together with their suitable compound types was given. To test the initial feasibility a set of equations is used to combine specification of the processes such as productivity, purity, and yield with the compound specific properties such as racemization kinetics, solubility, and growth rate. These equations can be used to determine process conditions such as concentration difference and residence time, to reach a given set of process specifications. In addition, the specifications and process conditions can then be compared to compound properties to determine if the process is feasible. The chapter culminates in a guideline, which can be used to choose a suitable chiral separation, resolution or deracemization process depending on the compound information and type.

7.1 Outlook

To expand the scope of application for the developed processes, more experiments need to be conducted. As the continuous antisolvent crystallization process was conducted using sodium bromate as a model compound which as achiral in solution, the process needs to be adapted to organic compounds. One compound which self racemizes in the presence of ethanol is Isoindolineone. This compound would be ideal to verify the method for an organic compound as it is somewhat comparable to sodium bromate. Another compound for which this process can be applied for separation is clopidogrel-imine. Initial experiments have shown, that clopidogrel-imine could be separated using the same method in a small scale

batch experiment. By showing that secondary rather than primary nucleation is the dominating mechanism in the process, continuous preferential antisolvent crystallization could also be suitable for polymorphism control by seeding with the target polymorph. This application needs to be investigated but holds great potential as polymorphism control is a very important aspect in the pharmaceutical industry.

The serial process configuration as shown in chapters 4 and 5 to be flexible and robust processes for separation, resolution, and deracemization of chiral compounds. To show that the serial process configuration is truly versatile, the process can be used to separate more conglomerate and racemic compound forming systems. In the next step, the process can be extended into a true continuous process by adding a suspension removal, eutectic feed and purge stream. It can then be used for the continuous deracemization of clopidogrel-imine, presenting a continuous alternative for Viedma ripening and temperature cycling. Also, other compounds that racemize in solution can be deracemized using this process. Following that, optimal process parameters for deracemization and resolution processes can be investigated, maximizing yield and productivity. In addition, a model of the process should be designed, to simulate the separation of compounds, where the data is available. This in addition to experiments, to verify the model, can be used to investigate the general applicability and laminations of the process configuration. Another possible application for this process could also be to increase the efficiency of classical resolution. Two diastereomeric salts have different solubilities, so one can be crystallized while the other remains in solution. If two or more crystallizers at different process conditions are used in series, more target compounds could be separated out. In addition, a solution recycle would be added, allowing for an overall higher yield of the process. As classical resolution is a widely applied process, investigations into increasing its yield could be interesting for industrial applications.